Doctoral Thesis

Study on Wireless Detection Techniques of Temperature and Position for Hyperthermia using Magnetic Particles with Low Curie Temperature

ハイパーサーミアのための低キュリー点の感温磁性微粒子を利用した位置および温度のワイヤレス検知技術に関する研究

Field of Mathematical Science and Electrical-Electronic-Computer Engineering
Department of Integrated Engineering Science
Graduate School of Engineering Science, Akita University

Ton That Loi

Supervisor
Professor Kazutaka Mitobe

2019

Abstract

Cancer is the second leading cause of death globally behind ischemic heart disease and stroke, accounting for an estimated 9.6 million deaths in 2018 according to World Health Organization. Magnetic hyperthermia is a promising cancer therapy which has been gaining more attention in recent years owing to fewer side effects compared to chemotherapy and less invasive than surgical therapy. This therapy utilizes the fact that the antitumor effect occurs when the tumor is heated continuously within the therapeutic temperature range of 40–45°C. Heat generation in magnetic hyperthermia mainly ascribes to hysteresis and/or relaxation loss from magnetic particles subjected to a high-frequency magnetic field.

To date, magnetic hyperthermia applications capable of heating the affected part at a constant temperature while being minimally invasive in detecting the temperature and position of heating element are not established, thus the development of such systems are needed. So far, we are aiming to develop an induction heating system while monitoring the temperature and position of heating element. In previous studies, Mitobe *et al*. succeeded in developing a microsize thermosensitive ferromagnetic implant with low Curie temperature (FILCT) as a self-controlled heating element. FILCT was then coated with gold to improve its heating efficiency (Au-FILCT). Furthermore, a wireless temperature measurement method has been proposed to monitor the temperature of the tumor during treatment by using the implant as a thermal probe.

The results obtained in this study are listed below.

(1) Development of hyperthermia implant with high heating efficiency and high permeability

The previously developed Au-FILCT improved significantly the heating efficiency of FILCT (8 times), but part of the applied magnetic field was shielded ascribed to the conductive coating around FILCT. As a result, the change in the detected voltage induced in pickup coil (hereafter pickup voltage) was reduced by half, thereby the accuracy of our wireless thermometry was significantly lowered compared to that of FILCT. As an alternative approach to the gold coating, we proposed to mix FILCT with a high heating-efficient magnetic nanofluid. In the case of using a commercial nanofluid named Resovist® (MRI contrast agent), the heating efficiency of the proposed mixture of micro/nano-magnetic particles was improved 4.3 times, and the accuracy of the thermometry was improved 1.3 times compared to that of FILCT under a magnetic field of 500 kHz, 4.95 kA/m. A similar tendency was obtained when using a lab-made nanofluid.

(2) Development of localization technique of hyperthermia implant

The implant in the tumor cannot be seen from the body surface. When the implant deviates from the central axis of the magnetic field supply and detection unit composed of drive coil and pickup coil (MFSD unit), the magnetic flux density applied on the implant decreases, resulting in a decrease in its heating efficiency and the thermometry accuracy. To solve this problem, we devised a position adjustment method

in which the central axis is aligned directly above the implant by referring to three voltages induced in three pickup coils symmetrically installed inside drive coil. Using the constructed position adjustment system, it was possible to automatically locate the position of the implant with accuracy below 1 mm by operating MFSD unit in two modes of coarse adjustment (rotary scanning) and fine adjustment (linear scanning).

(3) Development of rotary scanning technique of body motion artifact reduction method

It is considered that the relative position between MFSD unit and the implant is fluctuated due to the periodic physiological motions such as respiration and heartbeat induced artifact during treatment. Therefore, we cannot distinguish whether the change in pickup voltage is caused by the change in temperature of the implant around the therapeutic temperature, or by the change in distance between MFSD unit and the implant by the artifact. To overcome this problem, we proposed a body motion artifact reduction method by using rotary scanning technique on MFSD unit in a different period cycle from the periodic respiration and heartbeat. Using the difference in the frequency domain of spectral component of rotary scanning (signal) and that of the artifact (noise), only the target signal is extracted. Using the constructed verification system, we confirmed that regardless of the presence of the artifact, the change of the extracted power around the Curie point is sufficiently large to detect whether the temperature of the implant has reached the therapeutic temperature. In particular, in the case with the artifact the SN ratio for temperature measurement was –3.1 dB, whereas the SN ratio after reducing the artifact using the proposed method was enhanced significantly 38.7 dB.

The thesis is composed of six chapters. In Chapter 1, we introduced the background and purpose of the research. Chapter 2 introduced the principle of hyperthermia such as its biological effects with respect to temperature, and heating methods used in hyperthermia. We then introduced the heating method used in this study named magnetic hyperthermia, and summarized the previous studies such as development of self-controlled heating mediator, wireless temperature measurement technique, and heating system for clinical application using the proposed wireless temperature measurement technique. In Chapter 3 to Chapter 5, we introduced the development and the obtained results from the evaluation experiments of (1) development of the implant of micro/nanomagnetic particles, (2) development of the automatic implant localization technique, and (3) development of the rotary scanning technique, respectively. Finally, we concluded the important results in this study and outlined future work in Chapter 6.

Contents

Chapter 1

Introduction

1.1 Background

Cancer is the second leading cause of death globally behind ischemic heart disease and stroke, accounting for an estimated 9.6 million deaths in 2018 according to World Health Organization [1]. In Japan, cancer is the largest cause of death since 1981, and accounts for 27.8% (373,178 deaths) of all deaths in 2017 as shown in Fig. 1 [2]. Therefore, it is of paramount importance to pursue effective cancer treatment. Currently, the most common treatments are surgery, chemotherapy, and radiation therapy. In recent years, hyperthermia (also called thermotherapy) has gained great interest as a possible method for cancer treatment. This therapy is less invasive than surgery and has fewer side effects compared to chemotherapy. It utilizes the fact that cancer cells are more sensitive to heat than healthy cells, and antitumor effect occurs when the tumor is heated within the therapeutic temperature range of 40–45°C for 30 to 60 minutes [3]. It can also be used in combination with chemotherapy, radiotherapy, and immunotherapy to enhance its effects.

There are several heating techniques to induce hyperthermia such as radio frequency, microwave, and ultrasound heating method. In recent years, magnetic hyperthermia has been gaining more attention as a

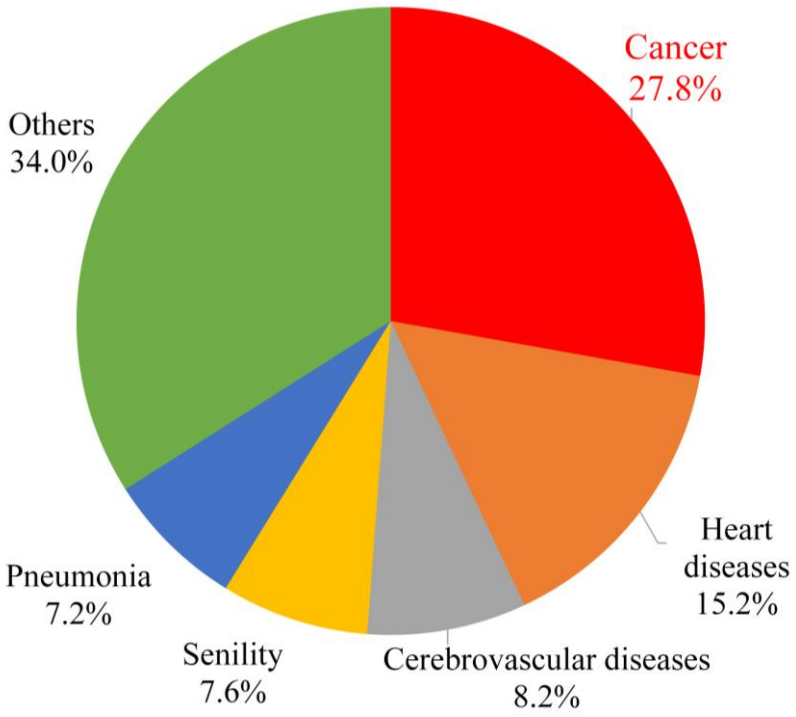

Fig. 1 Proportion of major causes of death in Japan in 2017 [2].

promising heating method. In this method, heat generation mainly ascribes to hysteresis and/or relaxation loss from a magnetic material subjected to a high-frequency magnetic field. Based on this method, Matsuki *et al*. also proposed a soft heating method in which magnetic materials are self-controlled heating mediators with low Curie point adjusted close to therapeutic temperature [4].

Since the pioneering work on hyperthermia by Gilchrist *et al*. in 1957 [5], to date clinical applications capable of heating affected parts at a constant temperature while being minimally invasive in detecting the temperature of heating elements are not established, thus the development of such systems are of paramount importance. So far, we aim to develop an induction heating system while monitoring the temperature of heating elements. In previous studies, we succeeded in developing a microsize thermosensitive ferromagnetic implant with low Curie temperature (FILCT) as a self-controlled heating element [6]. The antitumor effect could be enhanced and the survival rate of the rat improved in a melanoma model when using FILCT combined with a heat shock protein 90 inhibitor [7, 8]. Then, FILCT was coated with gold to improve its heating efficiency (Au-FILCT) [9]. Furthermore, a wireless temperature measurement method has been proposed for monitoring the temperature of the tumor during treatment by using the implant as a thermal probe [10].

In this study, we focus on the following three problems which are listed below.

(1) The previously developed Au-FILCT improved significantly the heating efficiency of FILCT, but part of the applied magnetic field was shielded ascribed to the conductive coating around FILCT due to the gold layer. As a result, the change in the detected pickup voltage induced in pickup coil (pickup voltage) was reduced by half, thereby the accuracy of the proposed wireless temperature measurement was significantly lowered compared to that of FILCT. Therefore, it is necessary to develop a hyperthermia implant with high heating efficiency and high permeability.

(2) When the implant which cannot be seen from the body surface of the patient deviates from the central axis of the magnetic field supply and detection unit composed of drive coil and pickup coil (MFSD unit), the magnetic flux density applied on the implant decreases, resulting in a decrease in its heating efficiency as well as the accuracy of the proposed wireless temperature measurement. Currently, to localize the position of the implant during treatment, techniques such as X-ray CT and ultrasonography are used, but this leads to an increase in the cost for hyperthermia treatment. Thus, it is also important to improve the cost performance by localizing the implant with an inexpensive technique.

(3) The relative position between MFSD unit and the implant is considered to fluctuate due to the periodic physiological motions such as respiration and heartbeat (artifact) during treatment. When the fluctuation of the implant is large, it cannot distinguish whether the change in pickup voltage is caused by the change in the temperature of the implant around therapeutic temperature, or by the change in distance between MFSD unit and the implant by the artifact. It is thus of paramount importance to reduce the artifact to make the approach of wireless temperature measurement feasible in clinical settings.

1.2 Purpose

In this study, we solve the three problems aforementioned in the previous section. Firstly, as an alternative approach to the gold coating, we mixed FILCT with a high heating-efficient magnetic nanofluid for developing hyperthermia implant with high heating efficiency and high permeability. Secondly, to localize the position of the implant we devised a position adjustment method for MFSD unit in which the central axis of MFSD unit is aligned directly above the implant by referring to the three voltages induced in three pickup coils symmetrically installed inside drive coil. Finally, we developed a rotary scanning technique of reducing periodic physiological motions by using rotary scanning technique on MFSD unit in a different period cycle from the periodic respiration and heartbeat and extracting only the target signal by utilizing the difference in the frequency domain of spectral component of rotary scanning (signal) and that of the artifact (noise).

1.3 Thesis organization

In this thesis, (1) development of the implant of micro/nano magnetic particles with high heating efficiency and high permeability, (2) development of the automatic localization technique of the implant, and (3) development of the rotary scanning technique of reducing the artifact will be explained in detail.

This thesis is composed of six chapters. In Chapter 1, we introduced the background and purpose of the research. Chapter 2 introduced the principle of hyperthermia such as its biological effects with respect to temperature, and heating methods used in hyperthermia. We then introduced the heating method used in this study named magnetic hyperthermia, and summarized the previous studies such as development of self-controlled heating mediator, wireless temperature measurement technique, and heating system for clinical application using the proposed wireless temperature measurement technique. In Chapter 3 to Chapter 5, we introduced the development and the obtained results from the evaluation experiments of (1) development of the implant of micro/nanomagnetic particles, (2) development of the automatic implant localization technique, and (3) development of the rotary scanning technique, respectively. Finally, we concluded the important results in this study and outlined some future works in Chapter 6.

Chapter 2

Hyperthermia principle and previous research

2.1 Introduction

In this chapter, we describe the principle of hyperthermia such as its biological effects and heating methods to induce hyperthermia. We then introduce the heating method used in this study, magnetic hyperthermia, especially focusing on the property of magnetic materials as well as heating mechanism under magnetic field. Later, we describe the previous studies such as development of self-controlled heating mediators, principle of proposed wireless temperature measurement technique, and development of heating system for clinical application using the proposed wireless temperature measurement technique.

2.2 Biological effects of hyperthermia

Cancer cells have high thermal sensitivity compared to normal cells. When cancer cells are heated up to 40–45°C, they are shrunk whereas normal cells are not affected due to the difference in heat dissipation mechanism between them. Figure 2-1 shows their heat dissipation mechanism against temperature rise. When normal cells and cancer cells are heated respectively, normal cells can release heat due to an increase in blood flow accompanying vasodilation due to temperature rise of tissues and it is possible to prevent a sudden

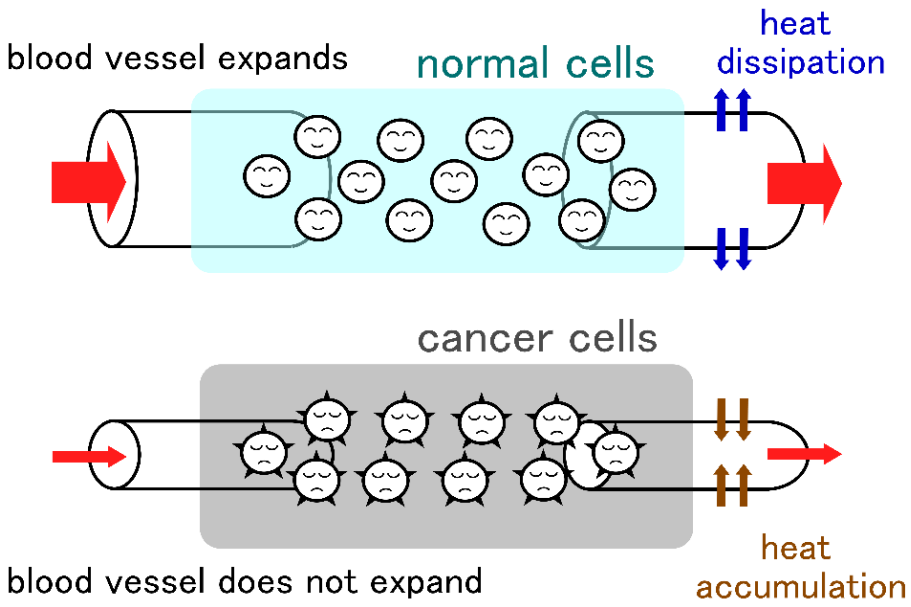

Fig. 2-1 Heat dissipation mechanisms of cancer cells and normal cells [11].

temperature rise. In contrast, cancer cells do not have a heat dissipation mechanism associated with vasodilation like normal cells, thereby they cannot deal with temperature rise. As such, it is possible to locally heat only cancer cells [11].

In general, the heating temperature range used in hyperthermia is set to 40–45°C at which cancer cells are shrunk to obtain a sufficient therapeutic effect. However, more cancer cells are shrunk when temperature is higher. Figure 2-2 shows the rate of cancer cells killed with respect to the temperature. The rate of cancer cells killed increases exponentially with temperature. Even though normal cells have a heat dissipation mechanism function, their function is also limited. The limit temperature for magnetic hyperthermia which can be heated for clinical settings is below 50°C. If the temperature is exceeded, such protein denaturation also affects normal cells.

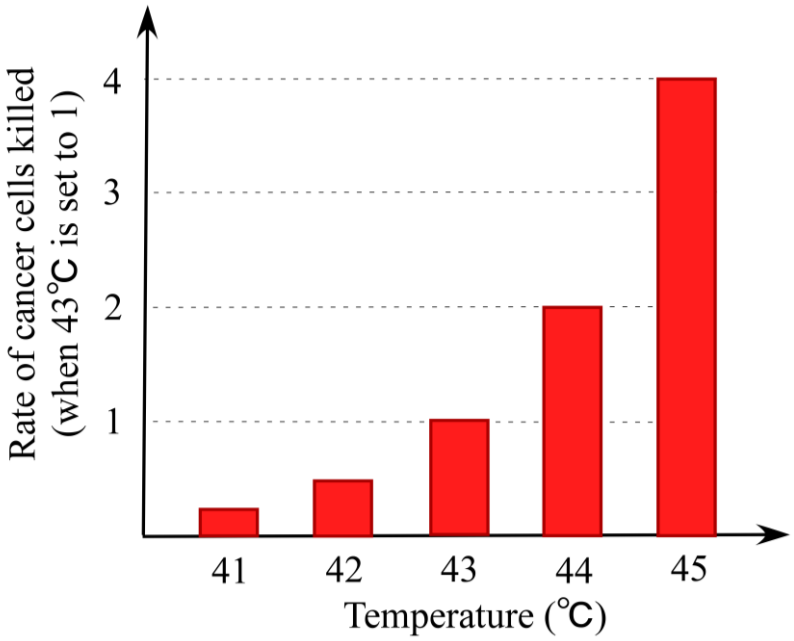

Fig. 2-2 Rate of cancer cells killed against temperature [11].

➢ Thermal tolerance

As described above, heating cancer cells to 40–45°C promotes their death. However, the therapeutic effect obtained is decreased after heating consecutively as there is another mechanism provided to try to reduce the damage due to heat. When cancer cells are heated, the proteins such as heat shock protein 70 which protect and repair cancer cells from heat (thermal tolerance) are denatured. This means that when the heat shock proteins are present, sufficient hyperthermia effect cannot be obtained even if hyperthermia is repeated immediately. For this reason, hyperthermia is generally performed at about twice per week with 30–60 minutes at a time. Although heat shock proteins have been regarded as disadvantageous for hyperthermia in order to have thermal tolerance to cancer cells, the importance of heat shock protein in terms of immunology have also been reported [12].

2.3 Heating methods of hyperthermia

It is difficult to locally heat cancer tissues at a constant temperature (40–45°C) for a certain time (30–60 minutes). At present, hyperthermia adopts various heating methods, each having advantages and disadvantages, and to date a prominent heating method does not exist yet. Typical heating methods are described in detail below [11].

➢ Radiofrequency (RF) capacitive heating

The principle of RF capacitive heating is shown in Fig. 2-3. The tumor tissues are heated by the electric current flowing from one electrode to the other one by applying a high frequency electric field of 8 to 13 MHz. It is the most adopted heating method in Japan and the heating systems based on this method are simple and are also capable of heating deep-seated tumors.

However, it also has drawbacks such as hot spot and overheating near the electrodes. Thus, in clinical settings, the boluses (flexible bags containing saline solution) are placed across the human body to cool the body surface. Furthermore, another problem is that it cannot confirm whether the affected area is really heated or not. Thus, the invasive temperature measurement techniques such as optical fiber thermometers is generally used to monitor the temperature of the tumor during treatment.

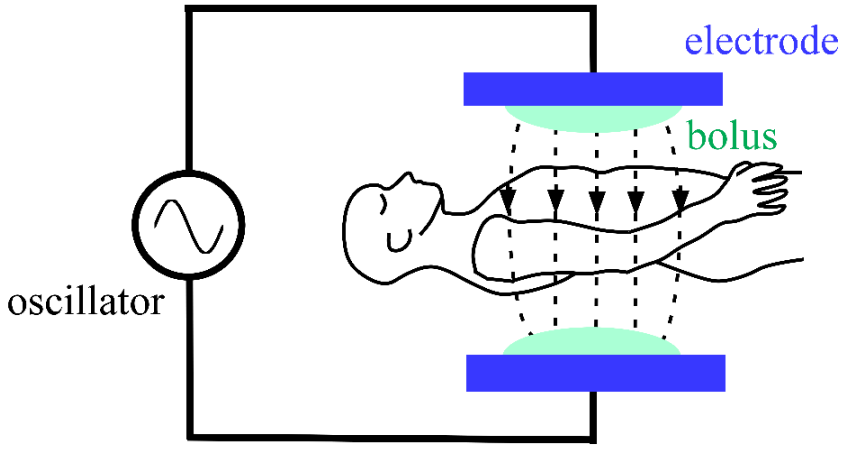

Fig. 2-3 Principle of radiofrequency capacitive heating.

➢ Microwave heating

This is a heating method using microwave of 300 MHz–300 GHz. In the RF capacitive heating, at least two electrodes are required because the tumor is heated by the electric current flowing from one electrode to the other one. In contrast, in the microwave heating method, electromagnetic waves generated from the antenna of heating energy sources, propagate through living tissues. Thus, it is possible to heat the tumor with one antenna.

This method has excellent characteristics such as wide range heating, non-contact heating, and high

heating efficiency. However, heating deep parts is difficult as the electromagnetic energy incident on living tissue attenuates to the square of the depth. In addition, the external heating by microwave energy may cause overheating body surface near antenna (hot spot), thereby it is required to cool the body surface. Also, it has many risks such as high operating frequency and difficulty in measuring temperature.

➢ Ultrasound heating

At present, ultrasound imaging is widely known in diagnostic field to visualize internal body structures. So far, attempts to utilize ultrasound for cancer treatment have been made since 1950s. Ultrasonic waves have been found to have antitumor effects by converting ultrasound energy into thermal energy. The advantage of ultrasound heating is the easiness to locally heat deep-seated tumors. However, due to the influence of reflection in the body tissues, accurate irradiation and scanning techniques are of paramount importance.

➢ Inductive heating (magnetic hyperthermia)

There are two ways of heating living body by electromagnetic waves. The first one is capacitive heating method mentioned above in which the electrical current with electromagnetic wave between 300 MHz and 300 GHz is applied to living body and heat is induced by the resistance loss of the tissue. The second one is inductive heating method (also called magnetic hyperthermia). As shown in Fig. 2-4, heat is induced from the loss of magnetic material such as hysteresis loss or relaxation loss occurred when the material subjected to an applied magnetic field with electromagnetic wave of several tens of kHz to several hundreds of kHz. One of the advantages of the inductive heating method is that it can heat selectively the tumor region without damaging normal tissues around.

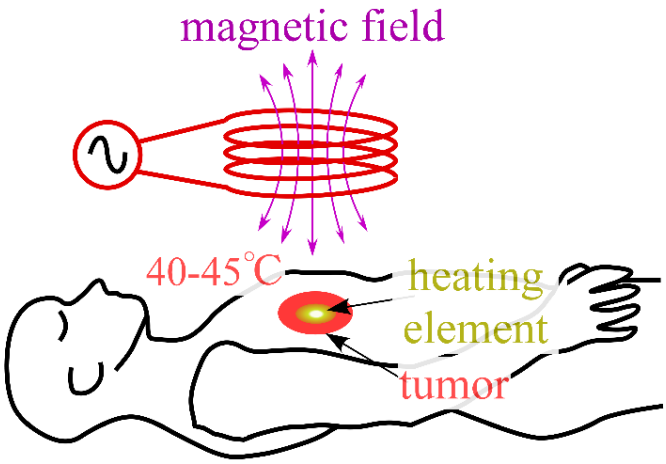

Fig. 2-4 Principle of inductive heating.

2.4 Magnetic hyperthermia

2.4.1 Magnetic particle properties

Figure 2-5 shows the schematic illustrating the arrangements of magnetic dipoles for common types of magnetic materials in the absence or presence of applied magnetic field [13]. When a magnetic field is applied to magnetic material, magnetic moment is generated inside it. As most materials have the property of making pairs and canceling each other out, the total spin becomes zero. Such materials are called non-magnetic

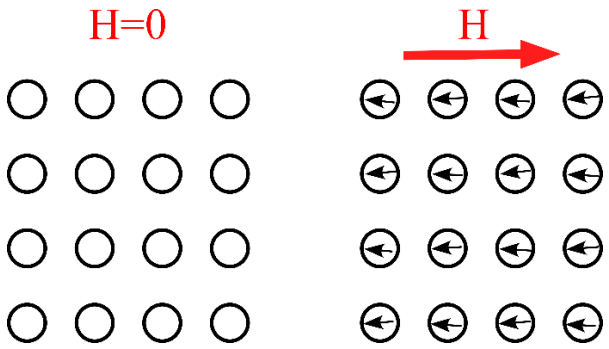

(a) Diamagnetic material

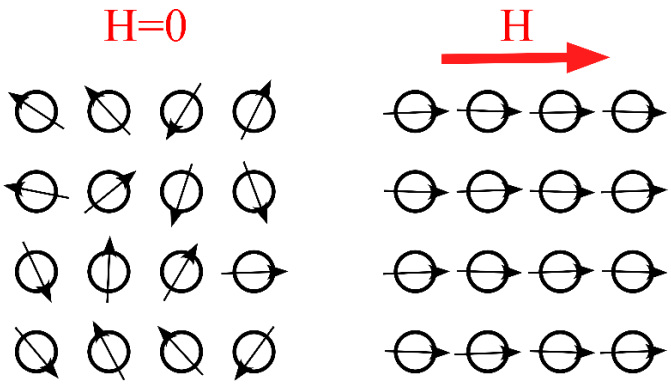

(b) Paramagnetic material

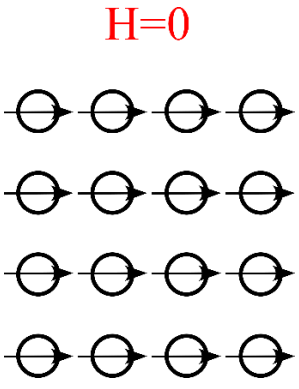

(c) Ferromagnetic material

Fig. 2-5 Schematic illustrating the arrangements of magnetic dipoles for common types of magnetic materials in the absence or presence of applied magnetic field [13].

materials. However, as shown in Fig. 2-5(a) when a magnetic field is applied, magnetization in the direction opposite to the magnetic field is generated. Such materials are called diamagnetic materials.

As shown in Fig. 2-5(b), for the materials with unpaired electrons, the electron spins do not cancel each other out and each atom has a magnetic moment. Generally, macroscopic magnetization by thermal motion does not appear in the materials. However, when a magnetic field is applied, magnetic moment slightly inclines in the direction of the applied magnetic field and macroscopic magnetization appears. Such materials are called paramagnetic materials.

However, when the spins are ordered without the applied magnetic field, macroscopic magnetization appears spontaneously (spontaneous magnetization) as shown in Fig. 2-5(c). Such materials are called ferromagnetic materials. When the temperature of the ferromagnetic material rises above a certain temperature, the fluctuation of the magnetic moments becomes larger, its spontaneous magnetization disappears and becomes paramagnetic material. This temperature is called Curie point.

Figure 2-6 shows the typical magnetization curves for magnetic materials under applied magnetic field. Note that the higher the area of hysteresis loop, the higher the heat generation that can be obtained from hysteresis loss of magnetic materials. In Fig. 2-6, the maximum magnetization possible is called saturation magnetization, whereas remanent magnetization is magnetization remaining after removing the applied magnetic field. The coercivity is the magnetic field strength required to force the magnetization to zero.

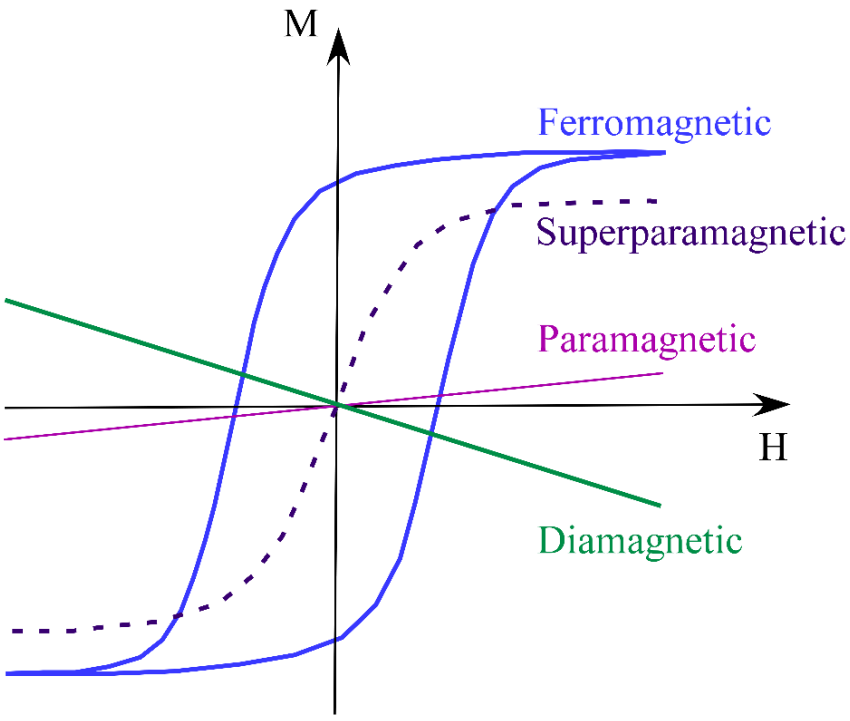

Fig. 2-6 Magnetic behavior of typical magnetic materials under applied magnetic field.

2.4.2 Heating mechanisms of magnetic particles

Heat generation in magnetic material under applied magnetic field can be divided mainly into three different mechanisms: (1) eddy current loss in bulk magnetic materials, (2) hysteresis loss in bulk and multi-domain magnetic materials, and (3) relaxation loss in superparamagnetic, single-domain nanoparticles.

➢ Eddy current loss

Figure 2-7 shows the diagram of eddy current loss. When a magnetic material is subjected to an alternating magnetic field, an electromotive force is induced in the material itself. As the magnetic material is conductor material, electromotive force circulates currents within the material (eddy current), resulting in resistive heating. Only for bulk magnetic materials (e.g. above 1 mm for magnetite), significant eddy current heating effects are observed, whereas for iron oxide nanoparticles (below 100 nm), eddy current effects can be neglected [14]. The eddy current loss in a magnetic material can be estimated by the following equation.

$$P_e = K_e B_m{}^2 f^2 t V$$

where K_e is the coefficient of eddy current depending on magnetic material, B_m is the maximum of magnetic flux density, f is the frequency of magnetic field, t is the thickness of material, and V is the volume of material.

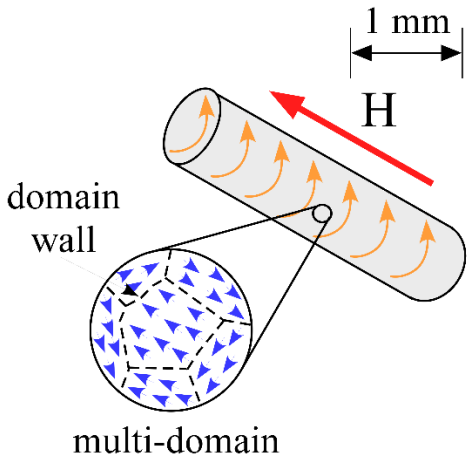

Fig. 2-7 Eddy current loss in bulk magnetic materials [14].

➢ Hysteresis loss

Figure 2-8 shows the diagram of hysteresis loss. When ferromagnetic or ferrimagnetic material is placed in an alternating magnetic field, it produces heat due to hysteresis loss occurring in multi domain materials. Magnetic moments in the materials tend to align in the direction of applied magnetic field, i.e. domain walls can move in the presence of applied magnetic field such that many single domains combine and create larger domains. This domain displacement continues until the material reaches saturated point.

Hysteresis loss can be estimated by the following empirical formula proposed by Charles Steinmetz.

$$P_h = K_h B_m{}^n f$$

where K_h is the coefficient depending on the magnetic material, B_m is the maximum of magnetic flux density, f is the frequency of applied magnetic field, and n is known as Steinmetz hysteresis exponent varying from 1.5 to 2.5 depending on the material (e.g. for iron n may be taken as 1.6).

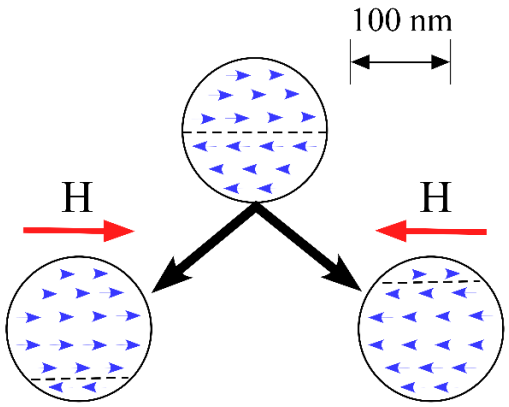

Fig. 2-8 Hysteresis loss in magnetic materials [14].

➢ Relaxation loss

In superparamagnetic nanoparticles (≤ 10–20 nm), although remanent magnetization and hysteresis behavior are eliminated, significant loss can still occur via magnetic moment relaxation mechanisms: Brownian relaxation and Neel relaxation [15]. Figure 2-9 shows the diagrams of these two relaxation mechanisms. Brownian relaxation represents the rotational friction component in a suspending medium resulting in heat generation, when the whole particle oscillates toward the direction of applied magnetic field. On the other hand, Neel relaxation represents the rotation of each magnetic moment towards to the magnetic field.

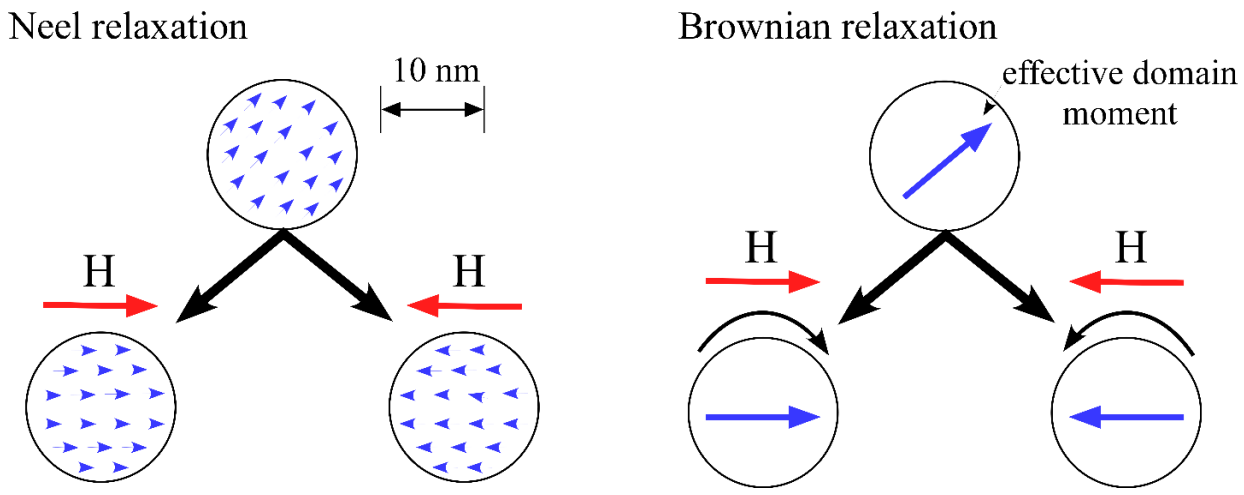

Fig. 2-9 Relaxation loss in nanomagnetic materials [14].

2.5 Previous research

So far, we aim to develop an induction heating system while wirelessly monitoring the temperature and position of heating element. In this section, we describe the previously-developed implant (ferromagnetic implant with low Curie temperature and its gold coating). In addition, a wireless temperature measurement method for monitoring the temperature of the tumor during treatment by utilizing the implant as a thermal probe is also described. Finally, we describe our developed system for hyperthermia.

2.5.1 Development of ferromagnetic particles with low Curie point and its gold coating

The heating method used in our study is soft-heating method using self-controlled heating mediators with low Curie point. Figure 2-10 shows the image and size distribution of ferromagnetic implant with low Curie point. The image was captured by an optical microscopy (Eclipse L150, Nikon). The FILCT had a particle size of 50–120 μm. The red solid line represents the fitting curve constructed from log-normal function.

$$F(d) = \frac{1}{\sqrt{2\pi}d\sigma}\exp\left(-\frac{(\ln d / d_0)^2}{2\sigma^2}\right)$$

where d is the diameter of the particle, d_0 is the median diameter, and σ is the polydispersity index.

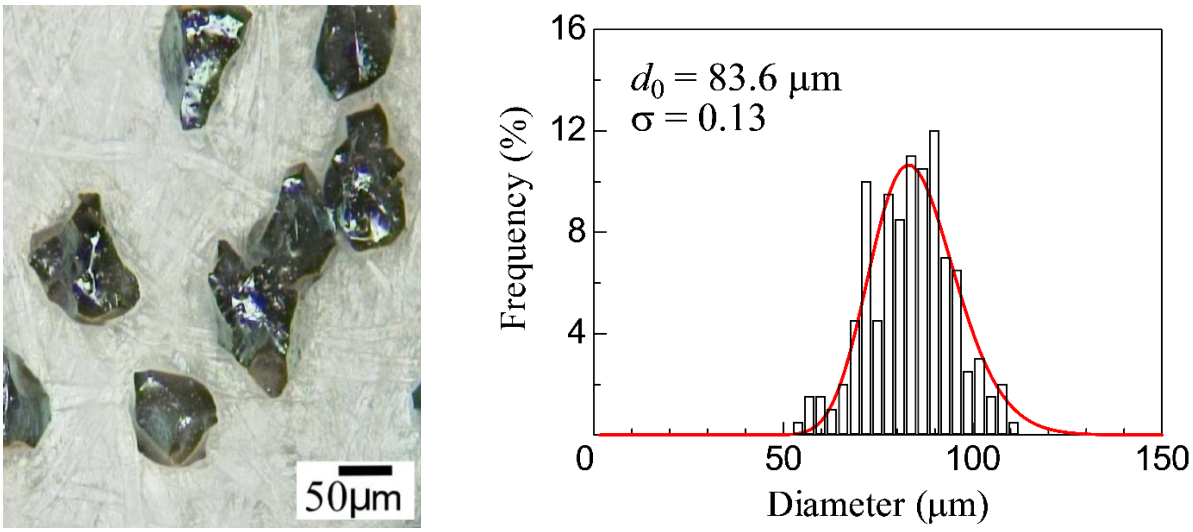

Fig. 2-10 Ferromagnetic implant with Low Curie point (left) and its size distribution (right).

The FILCT was composed of Fe_2O_3:CuO:ZnO:MgO = 49:7:30:14 mol%. Its Curie point was adjusted by changing the ratio of (Mg, Zn) without any surface modification on it. Figure 2-11 shows the magnetic behavior of FILCT around its Curie point when it is subjected to magnetic field. Figure 2-12 shows the temperature dependence and magnetic field frequency dependence of its permeability. The permeability decreased significantly when the temperature of FILCT exceeded 45°C. This means that its Curie point was 45°C. As shown in Fig. 2-12, FILCT had low coercivity, indicating that it was a soft magnetic material.

FILCT had large electrical resistivity (> 10^5 Ω·m) and heat generation due to eddy current loss was small. In short, in the case that FILCT is inductively heated, its temperature rise stops when its temperature reaches its Curie point (45°C). With this characteristic, the tumor can be heated at a constant temperature.

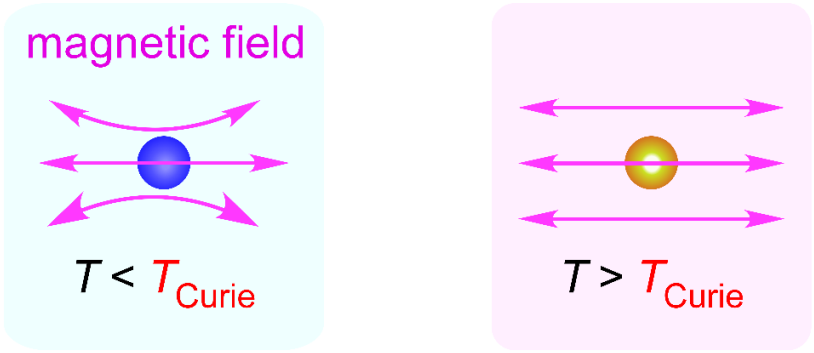

Fig. 2-11 Magnetic behavior of FILCT around its Curie point when it is subjected to magnetic field.

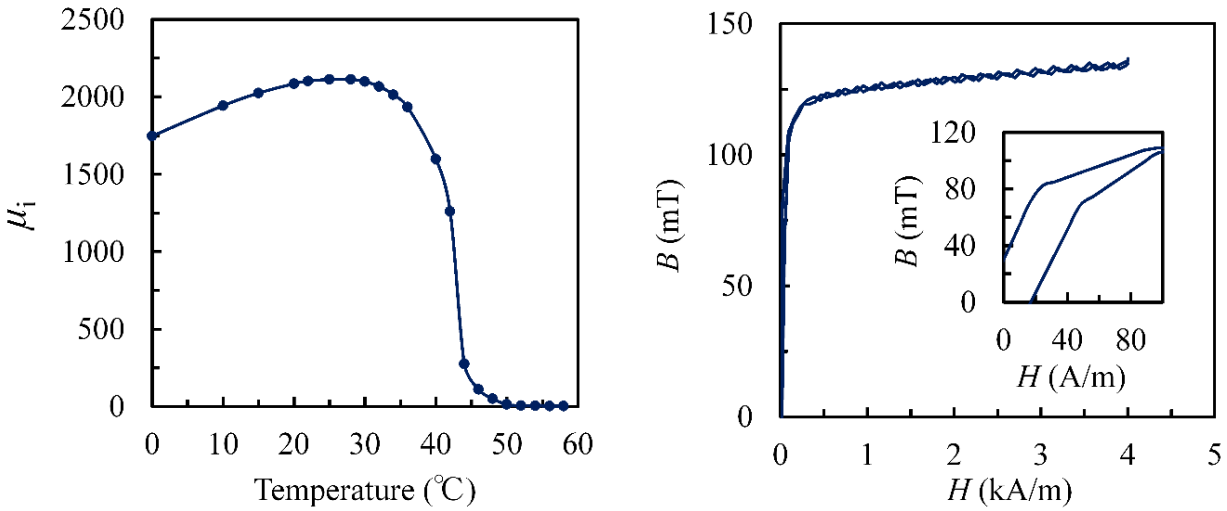

Fig. 2-12 Temperature characteristics (left) and DC magnetization (right) of FILCT provided from TDK.

➢ Gold coating ferromagnetic implant with low Curie point (Au-FILCT)

As can be seen from Fig. 2-12, the area of hysteresis loop is small (i.e. its heat generation is small). It was difficult to heat up to therapeutic temperature when targeting human body, thereby the improvement of its heat efficiency was required. Therefore, FILCT was coated with gold to improve its heating efficiency. Figure 2-13 shows the image of Au-FILCT. The thickness of gold coating layer was 80–130 nm. Figure 2-14 shows the temporal change in temperature of Au-FILCT and FILCT when subjected them to magnetic field. Heat generation mainly ascribes to hysteresis loss for FILCT, whereas for Au-FILCT it mainly ascribes to eddy current loss generated by the gold, resulting in significant improvement in heating efficiency (8-fold). However, even if the temperature of Au-FILCT exceeds therapeutic temperature, heat generation due to eddy current loss does not stop, thereby there is also adverse effect that requires temperature monitoring and controlling.

Fig. 2-13 Image of Au-coated FILCT (the thickness of gold was 100 nm).

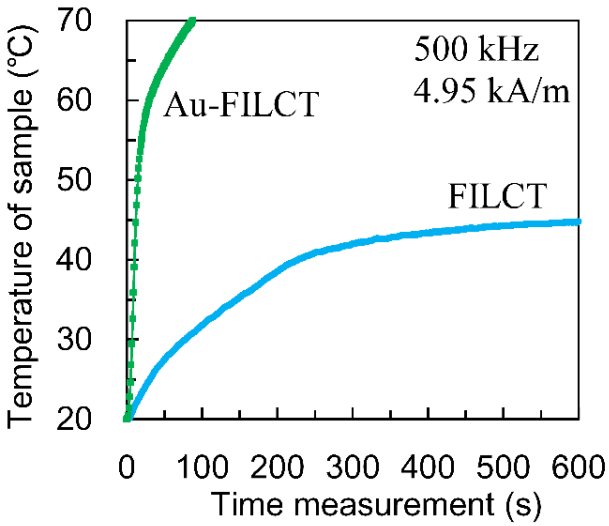

Fig. 2-14 Temporal change in the temperature of Au-FILCT and FILCT.

2.5.2 Principle of wireless temperature measurement method

In magnetic hyperthermia, heat generation from heating element that continues to increase even after its temperature exceeds therapeutic temperature may damage surrounding healthy tissue. To monitor the temperature of heating element we proposed a wireless temperature measurement using thermosensitive ferromagnetic implant as shown in Fig. 2-15. A ferromagnetic material with high magnetic permeability attracts magnetic flux density around the material. If the temperature of ferromagnetic material exceeds its Curie point, then its magnetic permeability will significantly decrease. As a result, the material cannot attract magnetic flux density around it. The shift in the magnetic flux density vector can be measured by the induced voltage in a pickup coil located orthogonally in drive coil.

A key advantage of this thermometry is that it can noninvasively determine whether the target temperature

has reached the Curie point without inserting invasively the optical fiber used in the traditional method. This approach contributes to an ability to have minimally invasive wireless temperature measurement for various types of hyperthermia.

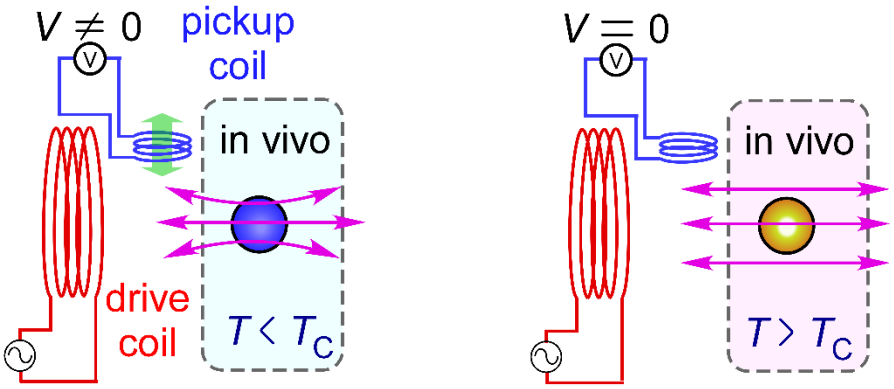

(a) Below Curie point (b) Above Curie point

Fig. 2-15 Fundamental concept of wireless temperature measurement using thermosensitive ferromagnetic implant with low Curie point.

2.5.3 Development of wireless temperature measurement and heating system

Using the proposed wireless temperature measurement method, we are also developing a heating system enabling the monitoring of the temperature of the implant [16–19]. Figure 2-16 shows the configuration of the wireless temperature measurement and heating system for clinical settings. Here, a high frequency magnetic field is applied from induction heating power supply EKOHEAT (30/100 ES CE, Ameritherm) through solenoid drive coil (outer diameter 103.3 mm, inner diameter 95.9 mm, thickness 54.0 mm, turn to turn distance 15.5 mm, number of turns 4). A DC inverter chiller (RKE2200B-V, Orion Machinery) is used to maintain the temperature and pressure of cooling water inside drive coil as well as the resonance circuit of heating power supply. To measure the signal (superimposed voltage) that depends on the temperature of the implant, an analog circuit is used to reduce the bias as well as drift induced in pickup coils before inputting these pickup voltages to lock-in amplifier [16]. The signal detected by the lock-in amplifier is recorded in real-time on a PC through an automatic measurement program made by LabVIEW (National Instruments). At the same time, the temperature of the sample is measured using a fiber optic thermometer (AMOTH FL-2000, Anritsu Meter).

Figure 2-17 shows the results obtained using the constructed system above. The frequency of applied magnetic field frequency was at 129 kHz, the magnetic flux density applied at 1, 2, 3, 4, 5, and 6 cm from the surface of drive coil were 13.7, 10.9, 8.6, 6.4, 4.4, 2.2, and 1.2 mT, respectively. The sample used consisted of 1.0 g of FILCT dispersed in 1.0 mL of Resovist® which was purchased from Fuji Film RI Pharma. The results indicate that it was possible to heat the sample up to therapeutic temperature and monitoring its temperature via the proposed wireless temperature measurement up to 5 cm [19].

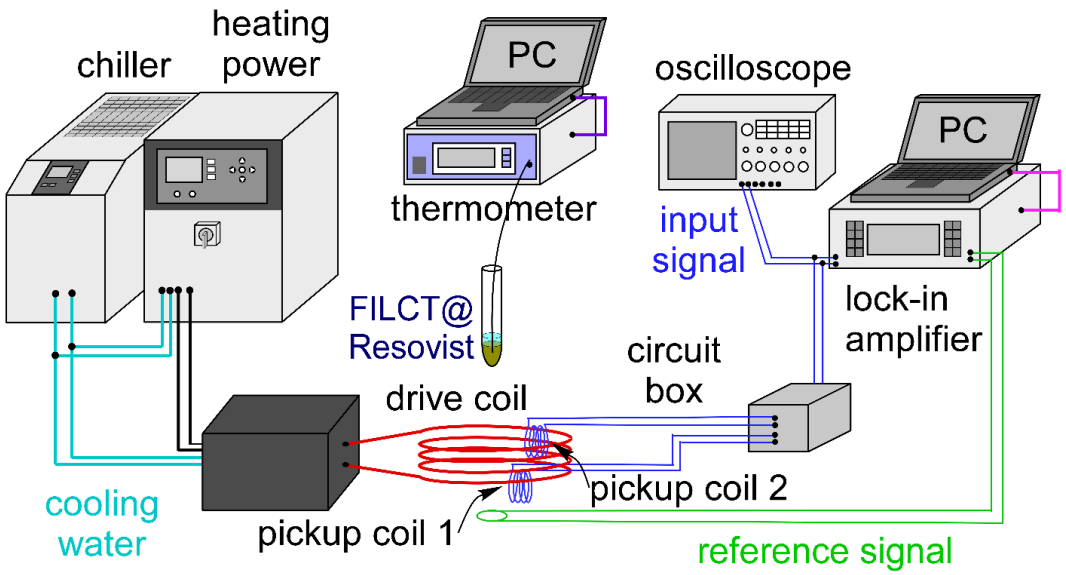

Fig. 2-16 Block diagram of wireless temperature measurement and induction heating system [19].

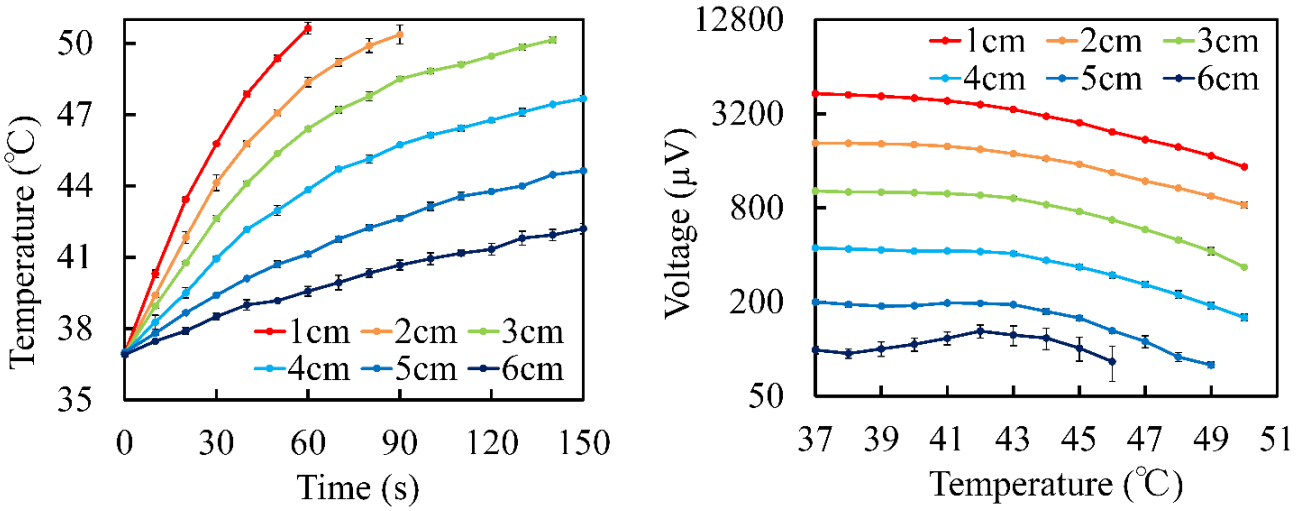

(a) Temporal change in sample temperature (b) Relationship between voltage and sample temperature

Fig. 2-17 Sample temperature and relationship between its temperature and voltage when there was a change in distance between the sample (FILCT mixed with Resovist®) and drive coil [19].

2.6 Summary

In this chapter, we described the principle of hyperthermia such as its biological effects, heating methods to induce it, focusing on magnetic hyperthermia. Later, we described the previous studies such as development of self-controlled heating mediators, principle of proposed wireless temperature measurement technique, and development of heating system for clinical application using the wireless thermometry so far.

Chapter 3

Development of hyperthermia implant with high heating efficiency and permeability

3.1 Introduction

In previous studies, we succeeded in developing a micro-size thermosensitive ferromagnetic implant with low Curie temperature (FILCT). We then coated the surface of FILCT with gold (Au-FILCT) to improve its heating efficiency. Subsequently, we also developed an orientable pickup coil system for contactless temperature measurement by using the implant as a thermal probe. Note that the larger the change in the magnetic flux density around the Curie point resulting from the permeability of the implant detected, the higher the accuracy that can be obtained from the proposed thermometry method. However, part of magnetic field was shielded ascribed to the conductive coating around FILCT. As a result, the amount of change detected decreased compared to FILCT.

In this chapter, we describe the development of micro/nanomagnetic particles as hyperthermia implant with high heating efficiency and considerable permeability change around therapeutic temperature. Although hyperthermia has been known for several decades, to the best of our knowledge, there have been no reports on the mixture of magnetic micro/nanoparticles as a thermosensitive implant for hyperthermia.

3.2 Proposed materials

Among magnetic materials for biomedical applications, superparamagnetic nanoparticles have been gaining more attention due to their potential as not only therapeutic agents for magnetic hyperthermia but also as diagnostic agents for magnetic particle imaging [20]. In this study, we attempted to use nano-magnetic particles with high heating efficiency instead of gold coating. In particular, we mixed FILCT with a commercial Resovist® consisting of maghemite nanoparticles or a lab-made nanoparticles (Fe_3O_4 Nps).

Figure 3-1 shows the images and the size distributions of FILCT and nano-ferrofluids used. Resovist®, a MRI contrast agent which is clinically approved for human use has been widely used to evaluate magnetic hyperthermia and/or magnetic particle imaging applications [21–25]. It consists mainly of maghemite (γ-Fe_2O_3) coated with carboxydextran in which maghemite has a Curie point of 675°C. The lab-made Fe_3O_4 Nps were synthesized based on the one-pot synthesis procedure [27], and the oleic acid modified on the surface of Fe_3O_4 Nps was then replaced with dimercaptosuccinic acid so that the surface shifts from

hydrophobic to hydrophilic [28], Fe_3O_4 Nps was finally dispersed in pure water. The concentration of magnetic nanoparticles were 39.9 mg/mL. The size distribution histograms were constructed by counting over 200 particles. The average diameter of micro-magnetic particles (83.6 μm) of FILCT was significantly different in size compared to that of nano-magnetic particles in Resovist® (3.6 nm) and Fe_3O_4 Nps (13.9 nm).

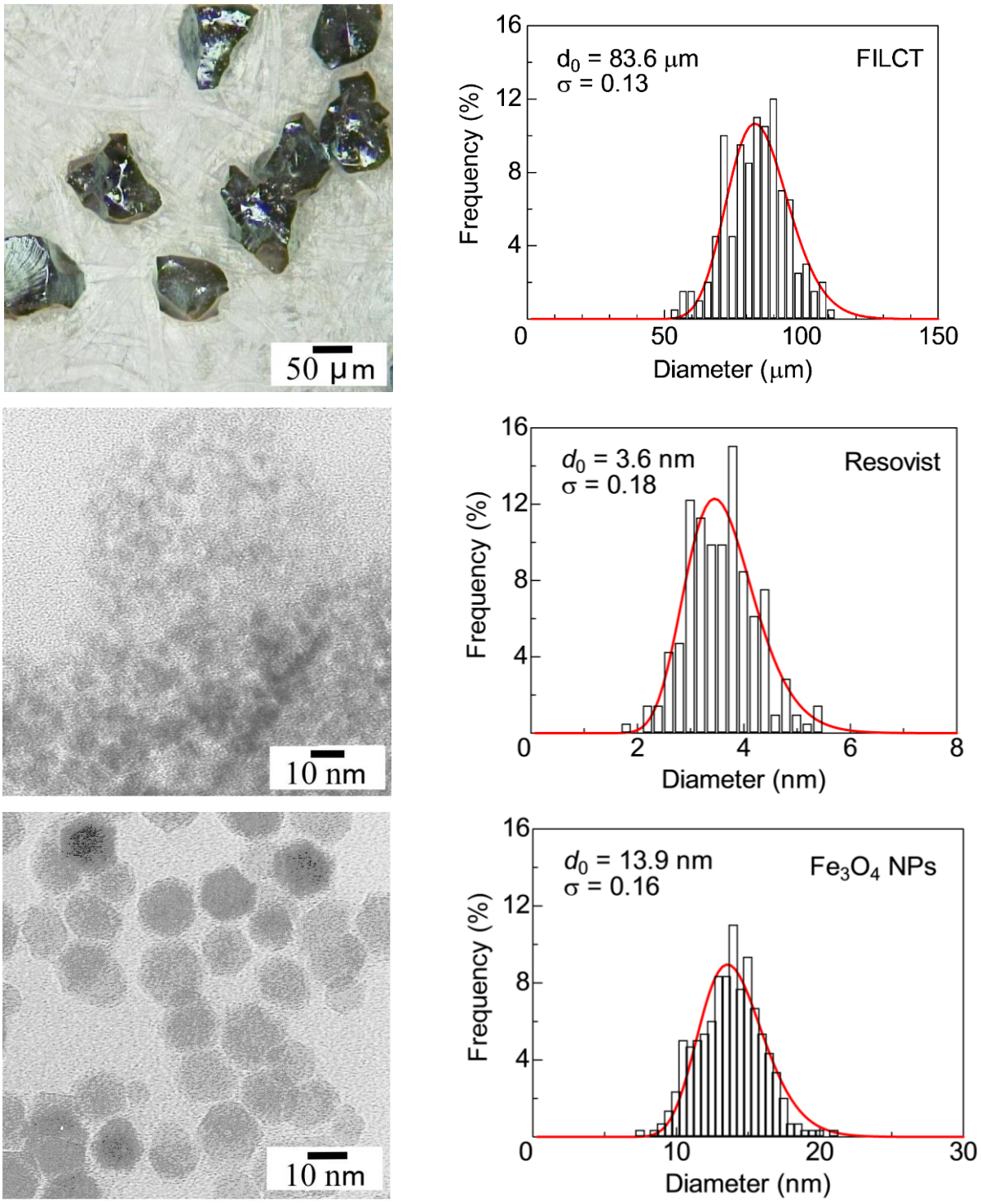

Fig. 3-1 Magnetic particles used to develop the mixture of micro/nanoparticles. Ferromagnetic implant with low Curie point (above), commercial Resovist® (middle), and lab-made Fe_3O_4 Nps (below).

3.3 Experimental method

Firstly, we examined its preferred volume fraction in the proposed mixture of micro/nanomagnetic particles. Then we compared the thermal and permeability properties of the proposed mixture compared to the traditional FILCT and Au-FILCT. Finally, we examined its magnetic field dependence of the properties under a high frequency magnetic field.

➢ Experimental setup

Magnetic heating experiments under magnetic field were performed using lab-made equipment as shown in Fig. 3-2 [29, 30]. Our measurement system was designed similar to pickup coil systems for measuring the ac magnetization of magnetic particles in the literature [31–36]. In all the experiments below, the product of frequency and field strength was determined under a criterion of 5×10^9 $Am^{-1}s^{-1}$ to prevent unwanted damage to the surrounding healthy tissue [20]. The drive coil was connected to a high frequency power supply (T162-5524A, Thamway) through a matching box (T020-5523B, Thamway). The drive coil had a height of 70.0 mm, an external diameter of 46.0 mm, an internal diameter of 36.0 mm, and a turn number of 14 turns.

The change in the magnetic flux density around the sample was measured by a pickup coil which was connected to a compensation coil. These two coils had an external diameter of 12.2 mm, an internal diameter

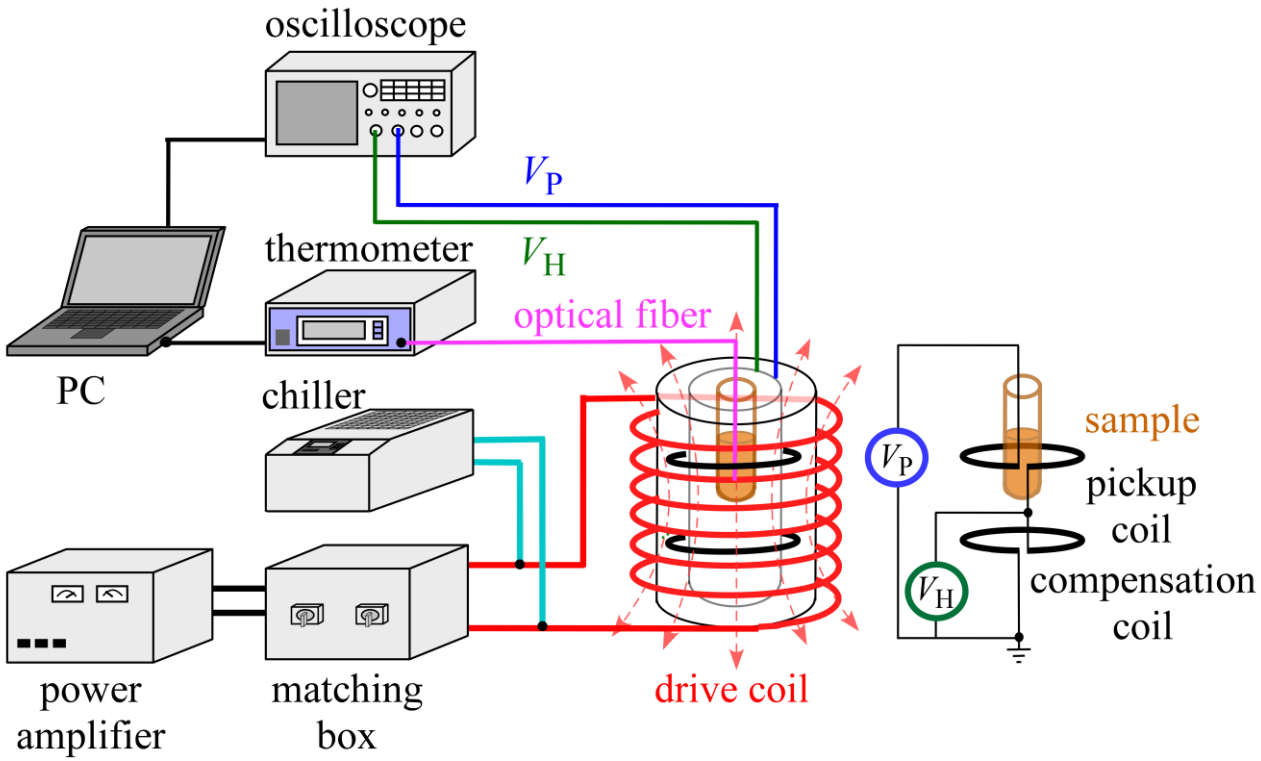

Fig. 3-2 Block diagram of the experimental setup for evaluating the thermal and permeability properties of the material subjected to high frequency magnetic field (f = 500 kHz, H = 4.95 kA/m).

of 12.0 mm, and a turn number of 1 turn. These upper and lower coils were wound in opposite directions and fixed at a distance of 25 mm. Here, the voltage V_H detected from the lower coil was used to obtain the field strength, whereas the voltage V_P (pickup voltage) was used to evaluate the permeability of the sample. Furthermore, a probe of an optical fiber thermometer (FL-2000, Anritsu) was simultaneously inserted into the central part of the sample during induction heating.

3.4 Results and discussion

➢ Examination of preferred volume fraction of magnetic nanoparticles

Firstly, we attempted to find the preferred range of the volume fraction of nanoparticles in the mixture using the samples shown in Table 1 (without adding water to sample, that is, water only came from the added Resovist®), assuming the density of maghemite nanoparticles was about 4.6 g/cm^3. A magnetic field from a drive coil with a frequency of 500 kHz and strength of 4.95 kA/m was applied on the samples.

Table 1 Samples prepared for examining the preferred range of mixing rate.

	S1	S2	S3	S4	S5	S6	S7
Micro-particles in FILCT (g)	1.0	0.9	0.7	0.5	0.3	0.1	0.0
Resovist® in mixture (mL)	0.0	0.1	0.3	0.5	0.7	0.9	1.0
Nano-particles in Resovist® (mg)	0.0	4.0	12.0	19.9	27.9	35.9	39.9
Mass rate of nano/microparticles (%)	0.0	0.4	1.7	3.8	8.5	26.4	100.0
Total sample volume (mL)	0.33	0.40	0.53	0.67	0.80	0.93	1.00
Volume fraction of nanoparticles (%)	0.00	0.22	0.49	0.65	0.76	0.84	0.87

Figure 3-3 shows the temporal change in the temperature of the samples when there was a change in the mixing rate of micro/nano magnetic particles. In general, the specific absorption rate (SAR) is used for evaluating the heating efficiency of magnetic particles [37]. Thus, the SAR in W/g was calculated based on the calorimetric method which is most commonly adapted [38].

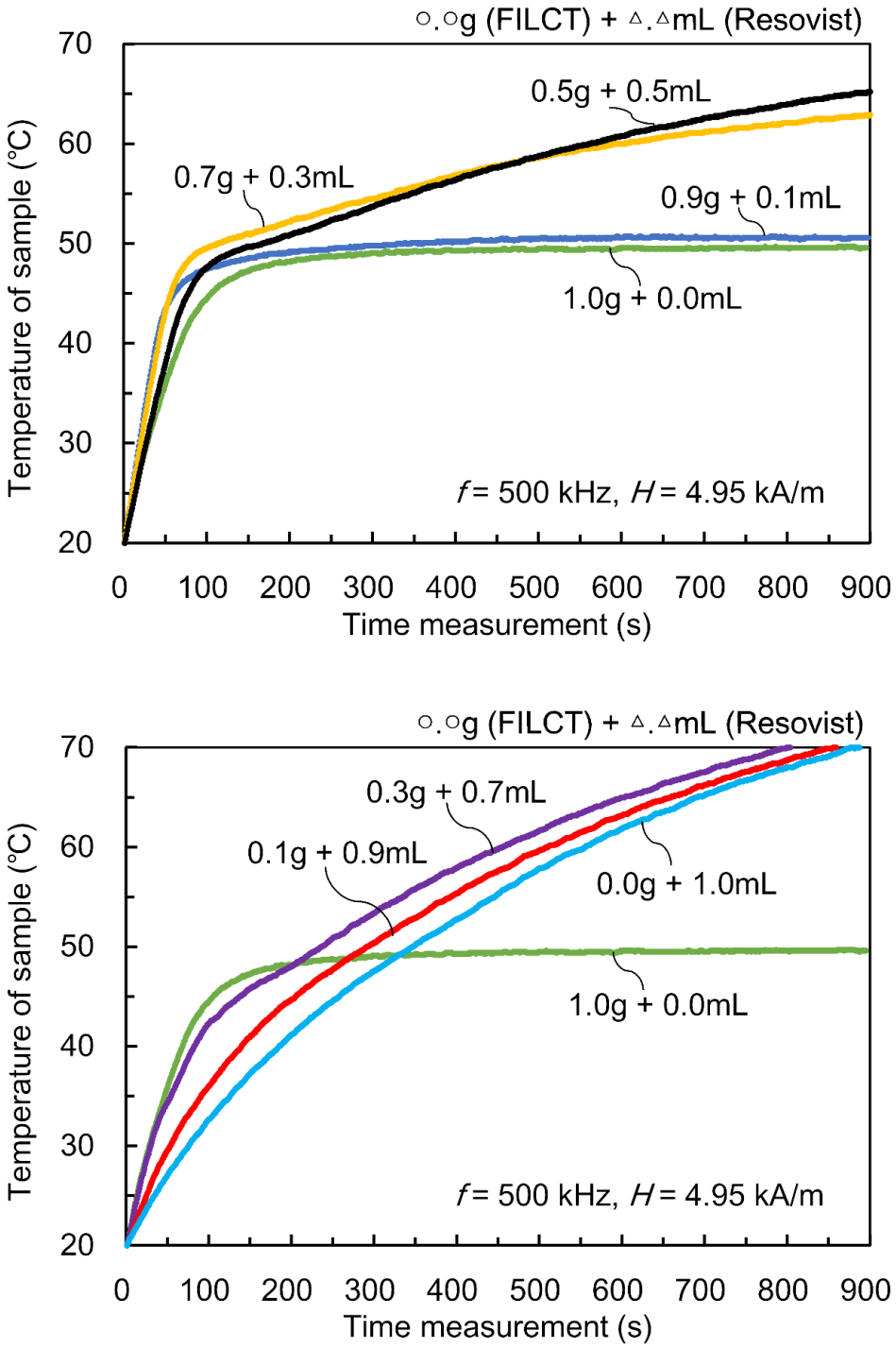

Fig. 3-3 Temporal change in the sample temperature when there was a change in mixing rate of micro/nanoparticles.

$$SAR = \frac{\sum_i c_i m_i}{m_{MP}} \frac{\Delta T}{\Delta t}$$

where c_i is the specific heat capacity (4.185 J/(g·K) for water, 0.7 J/(g·K) for FILCT or Au-FILCT), m_i is the mass of each substance (water or magnetic particles), m_{MP} is the total mass of magnetic micro/nanoparticles and $\Delta T/\Delta t$ is the initial slope of the change in temperature versus time curve (heating rate fitted with temperature data up to 30s). In this study, the product $c_i m_i$ of superparamagnetic nanoparticles was considerably small compared to that of water or microparticles, thus it was neglected. In terms of the ease of controlling the implant around the therapeutic temperature, the SAR of the sample was calculated both in the pre-stage regime (20–42.5°C) and in the post-stage regime (≥45°C) using the temperature data presented in Fig. 3-3. Here, the upper limits of the post-stage regime for Samples 1 and 2 were 49.5°C and 50.5°C respectively, whereas it was 60°C for Samples 3–7.

As shown in Table 2, the SAR tended to be faster in both regimes as the volume fraction of nanoparticles increases. Furthermore, the decrease in the SAR of the post-stage regime compared to the pre-stage regime of Samples 2–4 was approximately equivalent to Sample 1; however, it was considerably larger than that of Samples 5–7. This means that it is easier to control Samples 2–4 around the therapeutic temperature compared to Samples 5–7.

Figure 3-4 shows the relationship between the magnetic flux density calculated from pickup voltage and the temperature of the sample. Here, we calculated the change in magnetic flux density around the sample

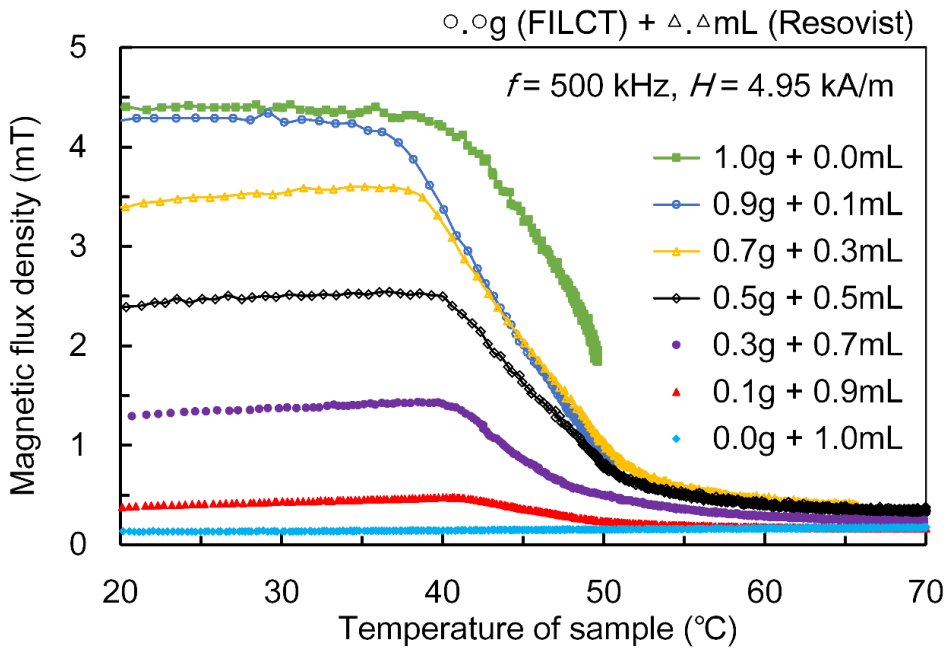

Fig. 3-4 Relationship between magnetic flux density calculated from voltage and the sample temperature.

from the pickup voltage measured according to the following equation.

$$B_P = \frac{V_P}{2\pi nfS}$$

where f is the frequency of magnetic field, n is the number of turns and S is the cross-sectional area of pickup coil.

As shown in Fig. 3-4, the magnetic flux density of sample which contained FILCT (Samples 1–6) clearly changed around the therapeutic temperature. It was also confirmed that the green curve (Sample 1) had a shift of several degrees Celsius compared to the others. This comes about because the liquid part of Resovist® enables good thermal contact with the optical fiber probe compared to the air filled between FILCT particles. In Table II, the magnetic flux density per gram of the magnetic particles at 20°C of Samples 2–4 is considerably larger than that of Samples 5–7. For this reason, the change in magnetic flux density per gram of the magnetic particles in 37–50°C of Samples 2–4 was considerably larger than that of Samples 5–7. In brief, the above results indicate that Samples 2–4 are more superior as a thermosensitive ferromagnetic implant for hyperthermia compared to Samples 1, 5–7.

Table 2 Change in magnetic flux density and heating efficiency depending on mixing rate.

Volume fraction of nanoparticles (%)	S1 (0.00)	S2 (0.22)	S3 (0.49)	S4 (0.65)	S5 (0.76)	S6 (0.84)	S7 (0.87)
SAR in pre-stage regime (20–42.5°C) (W/g)	0.25	0.16	1.21	1.82	3.32	6.02	16.45
SAR in post-stage regime (≥45°C) (W/g)	0.008	0.004	0.069	0.145	0.454	1.398	5.250
Decrease rate in SAR in post-stage regime compared to its pre-stage (%)	96.8	97.7	94.3	92.0	86.3	76.8	68.1
Magnetic flux density per gram of magnetic particles at 20°C (mT)	4.40	4.72	4.77	4.60	3.91	2.80	3.42
Change in magnetic flux density per gram of particles in 37–50°C (mT)	2.46	3.46	3.60	3.36	2.83	1.66	–0.35

The tendency of (1) the change in magnetic flux density within 37–50°C and (2) the SAR depending on the volume fraction of nanoparticles are plotted in Fig. 3-5 using the results in Table 2. The result suggests that the preferred volume fraction of nanoparticles is approximately 0.5%. The mixture in this preferred range has not only high heating efficiency and considerable permeability change around the Curie point, it is also easily controllable around the therapeutic temperature.

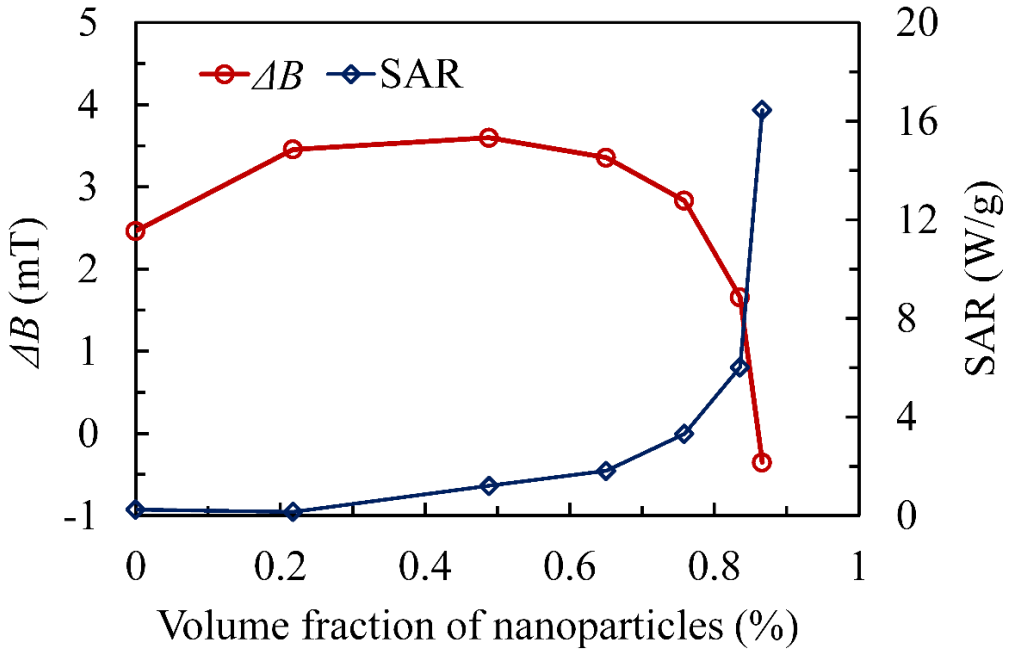

Fig. 3-5 Change in magnetic flux density within 37–50°C and the SAR within 20–42.5°C depending on the volume fraction of nanoparticles in the mixture (using the results of the second and last rows of Table 2).

➢ Proposed mixture compared to traditional implants

Next, we evaluated the thermal and permeability properties of the proposed mixture compared to the traditional implants. The four samples prepared were (1) 1.0 g of FILCT dispersed in 0.5 mL of deionized water; (2) 1.0 g of Au-FILCT dispersed in 0.5 mL of deionized water; (3) 1.0 g of FILCT dispersed in 0.5 mL of Resovist® which contained 0.02 g of nanoparticles; and (4) 0.5 mL of Resovist®. The total volume in sample (1), (2) and (3) was kept constant at about 0.83 mL (the measured density of FILCT was about 3.017 g/cm^3).

Figure 3-6 shows the temporal change in the temperature of four samples above. The SAR of FILCT, Au-FILCT, mixture and Resovist® were 0.48 W/g, 3.71 W/g, 2.06 W/g and 21.33 W/g, respectively. The result indicates that the heating efficiency of the mixture was considerably higher than that of FILCT (4.3 times). More importantly, as shown in Fig. 3-6 the mixture is likely to be superior to Au-FILCT for temperature control during treatment. Owing to the fact that the temperature rising rate after reaching the therapeutic temperature of the mixture decreases significantly compared to that of Au-FILCT, the mixture becomes easier to control around the therapeutic temperature. The SAR of the proposed mixture was slightly smaller compared to that of La-Sr-Mn-Cu perovskite bulk with Curie point around 35–37°C (about 5 W/g) [39] and that of magnetic nanoparticles (about 20–30 W/g) under a similar magnetic field [24], [29, 30].

The SAR of Resovist® was much larger than the theoretically calculated value of maghemite nanoparticles with a similar diameter (almost does not generate heat) [15]. Since the conductivity of Resovist® measured

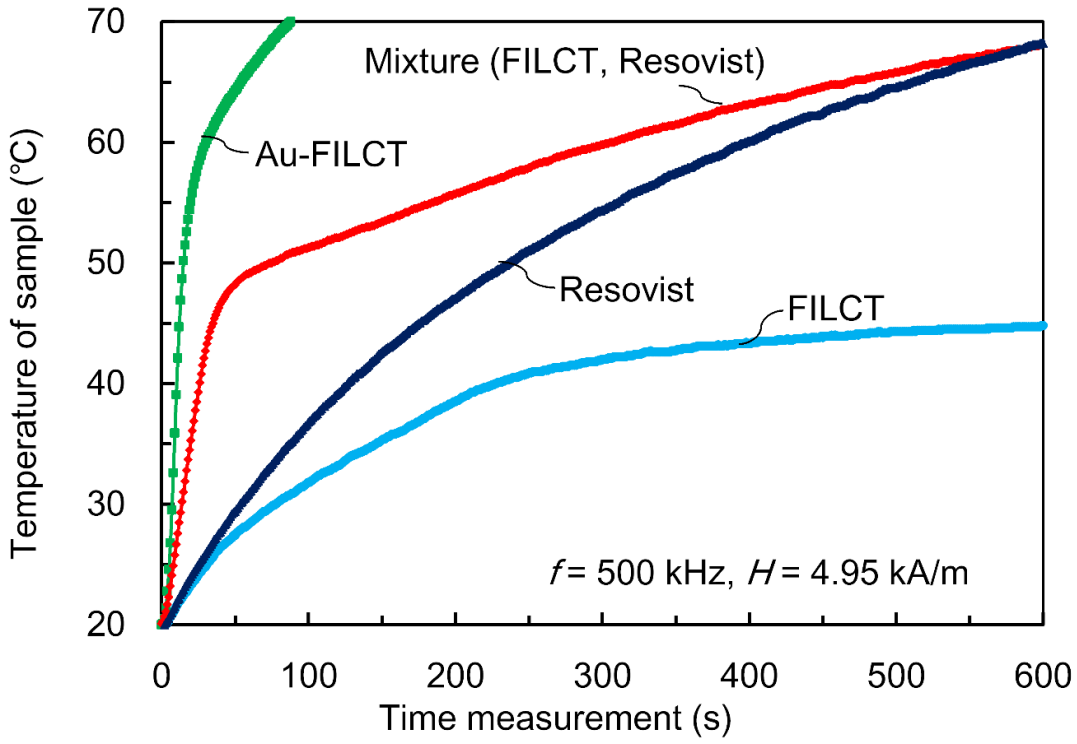

Fig. 3-6 Temporal change in sample temperature measured by fiber optic probe during induction heating.

using a water quality analyzer (LAQUAtwin, B-771, HORIBA) was smaller (2.1 mS/cm at 24°C) than for phosphate-buffered saline (20 mS/cm at 25°C), the heating generation caused by eddy current loss was considerably smaller than that of the relaxation and hysteresis loss of magnetic nanoparticles in it. We assume that the superparamagnetic nanoparticles aggregated and formed nano-assemblies such as chains and clusters under the magnetic field applied. Thus, it behaved like large particles, leading to an enhancement in heating efficiency of the nanoparticles [37].

Figure 3-7 shows the relationship between the magnetic flux density change in pickup coil and the temperature of the sample. It can be seen that the magnetic flux density at 20°C of the mixture (5.56 mT) was significantly enhanced compared to that of Au-FILCT (2.88 mT) and FILCT (4.40 mT). Furthermore, the magnetic flux density of the mixture clearly changed around the therapeutic temperature, whereas that of Au-FILCT changed slightly. This means that it is easier to detect if the implant has reached the therapeutic temperature when using the mixture compared to Au-FILCT and FILCT.

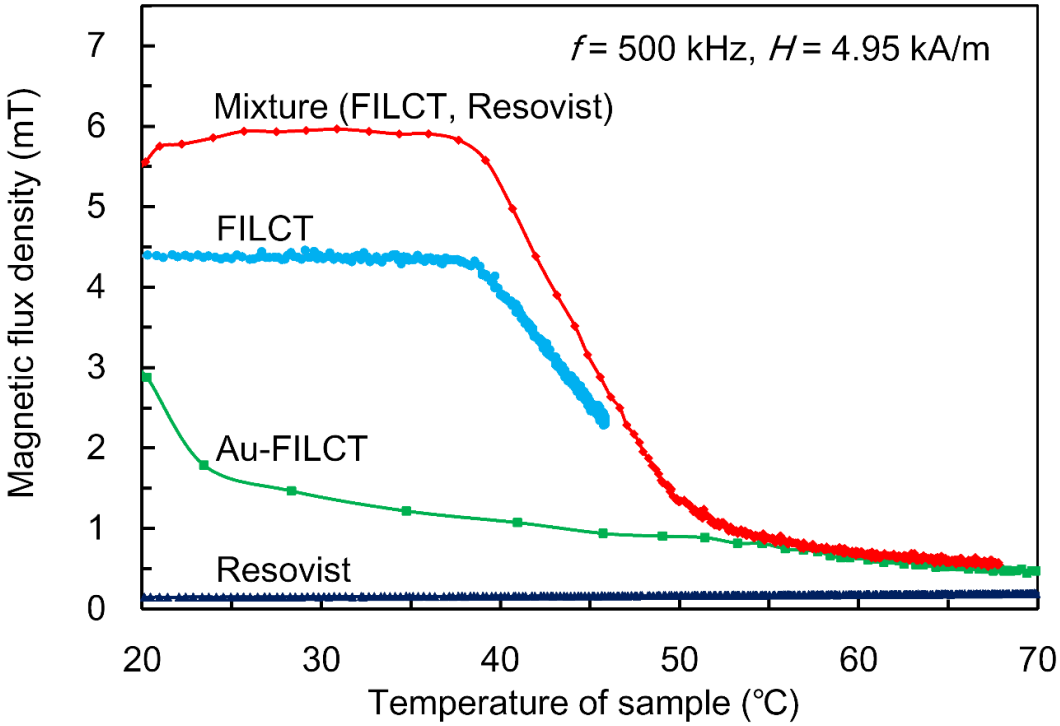

Fig. 3-7 Relationship between magnetic flux density calculated from the pickup voltage and the measured temperature of the sample.

➢ Postulated mechanism in the proposed mixture of micro/nanomagnetic particles

The ac magnetic hysteresis curves of the samples in the first series experiment were examined as shown in Fig. 3-8. Here, we used the magnetization and field strength calculated from V_H and V_P obtained at 20°C under a magnetic field of 500 kHz and 4.95 kA/m. The results indicate that the magnetization of the proposed mixture was larger than that of FILCT and Au-FILCT. The magnetization curve of Resovist® also shows the superparamagnetic behavior.

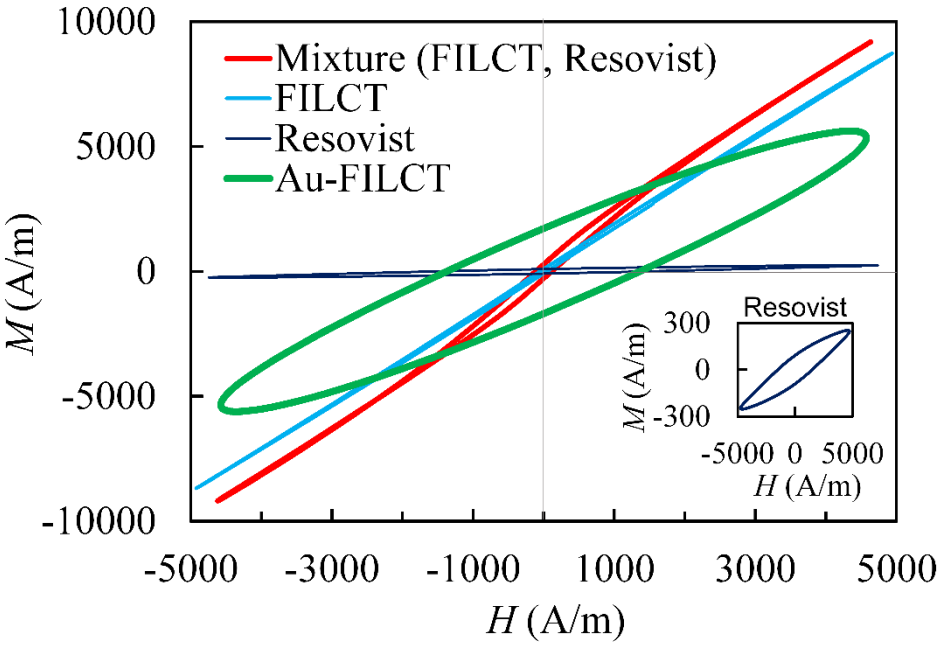

Fig. 3-8 AC hysteresis curves of the samples at 20°C under applied magnetic field frequency of 500 kHz.

To explain the improvement in permeability of the proposed mixture, we hypothesized a mechanism described below. Figure 3-9 shows schematic diagram illustrating the magnetic coupling of microparticles by the capillary bridges of nanoparticles (i.e. decreasing the demagnetizing factor of microparticles). When it is composed only of FILCT particles, there are gaps between particles filled by air, resulting in greater demagnetizing field effect of the particles. For this reason, the permeability of FILCT is lower than that of the original ferromagnetic material forming the FILCT particles.

In contrast, in the mixture, magnetic nanoparticles dispersed in water in Resovist® are disposed to fill the gaps between magnetic microparticles in FILCT. The nanoparticles can make capillary bridges binding microparticles together. The magnetic moments of micro/nanoparticles were aligned in the direction of magnetic field. Thus, it is possible to magnetically couple FILCT particles, thereby reducing the demagnetizing field effect of FILCT particles. As a result, the ferromagnetic material recovers its original permeability.

Our hypothesized mechanism also agrees with the finding of Shimada *et al.* where they developed electromagnetic noise absorbers using ferromagnetic particles [41]. They reported that the initial permeability of a composite consisting of Fe (average diameter of 1 μm) and Fe_3O_4 (10 nm) particles was improved by combining them at an appropriate mixing rate.

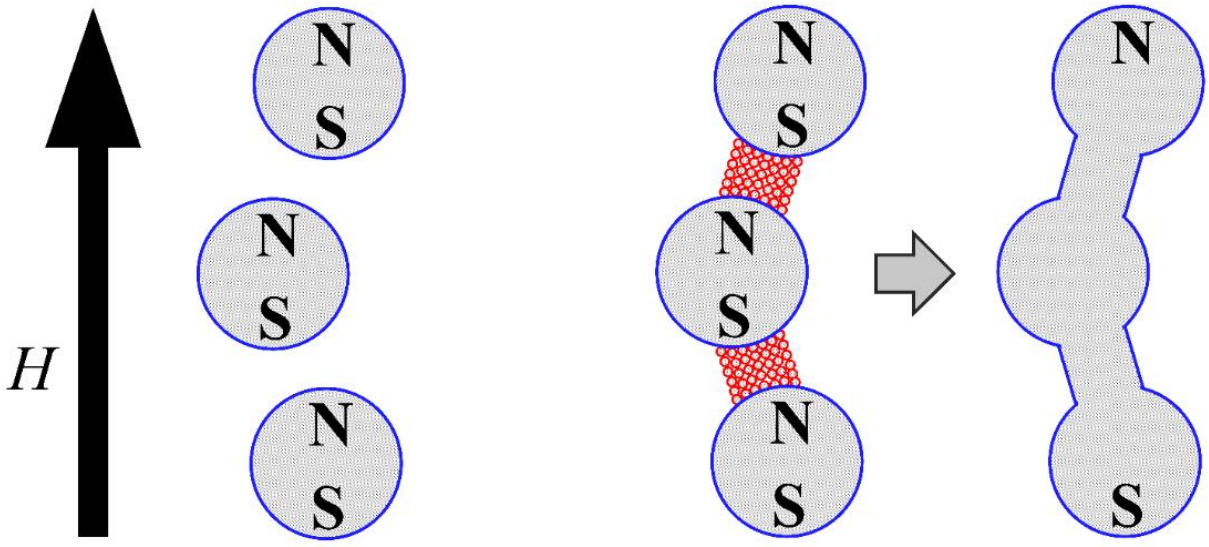

(a) With only microparticles (b) With micro/nanoparticles

Fig. 3-9 Schematic diagram illustrating the magnetic coupling of microparticles by the capillary bridges of nanoparticles (i.e. decreasing the demagnetizing factor of microparticles).

➢ Magnetic field dependence of hyperthermia implant (Resovist®)

The heating property of magnetic particles strongly depends on e.g. their magnetic properties, size, shape, coating materials, and solvent viscosity. Next, we examined the amplitude dependence of heating property, magnetic field with a fixed frequency f = 500 kHz and amplitudes H = 1.8–7.1 kA/m were applied to the sample (0.3 mL of Resovist® consisting 0.012 g nanoparticles). Then, magnetic field with a fixed amplitude H = 4.8 kA/m and frequencies f = 200–1000 kHz were applied to examine its frequency dependence. In all the experiments, magnetic field at a desirable value was applied after the sample was stable at 19°C for more than

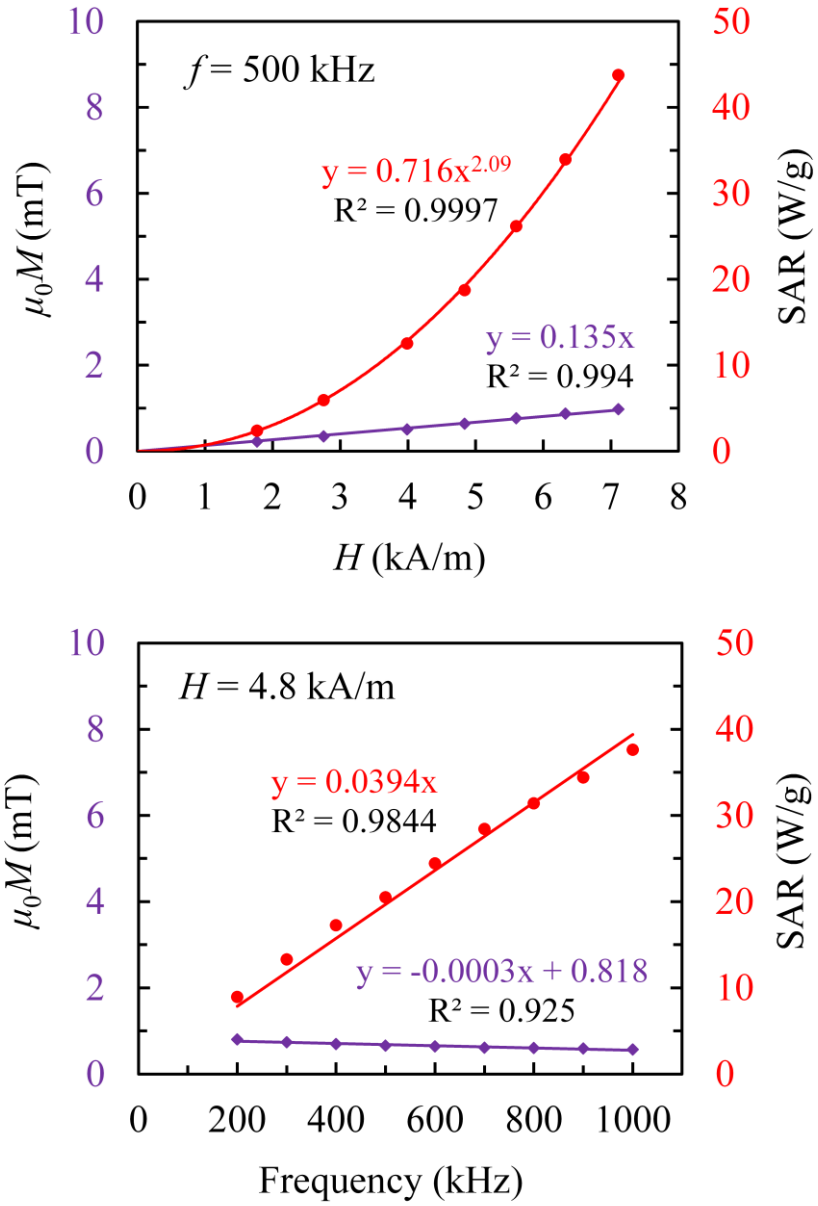

Fig. 3-10 Magnetic field amplitude (above) and frequency (below) dependence of permeability and heating properties of Resovist®.

100s. Figure 3-10 shows the magnetic field dependence of heating property of Resovist® for hyperthermia examined. As shown in Fig. 3-10, the SAR of Resovist® is linearly proportional to the applied magnetic field amplitude square and frequency. Figure 3-11 shows the magnetic field square dependence of heating property of Resovist®. Our finding matches with the results of linear response theory for superparamagnetic regime (SAR $\propto H^2$) in which heating generation mainly ascribes to relaxation loss [15].

In addition, the SAR was 44 W/g at H = 7.1 kA/m, f = 500 kHz, which was sufficient to heat the tumor for hyperthermia (assuming the concentration of the nanoparticles in tumor is 10 mg/mL and the tumor diameter is 15–20 mm, the SAR needed for hyperthermia is at least 10–20 W/g [24]).

The results obtained here may enable us to find the optimal conditions of the applied magnetic field or the amount of Resovist® required for hyperthermia under the specific condition of the applied magnetic field [42].

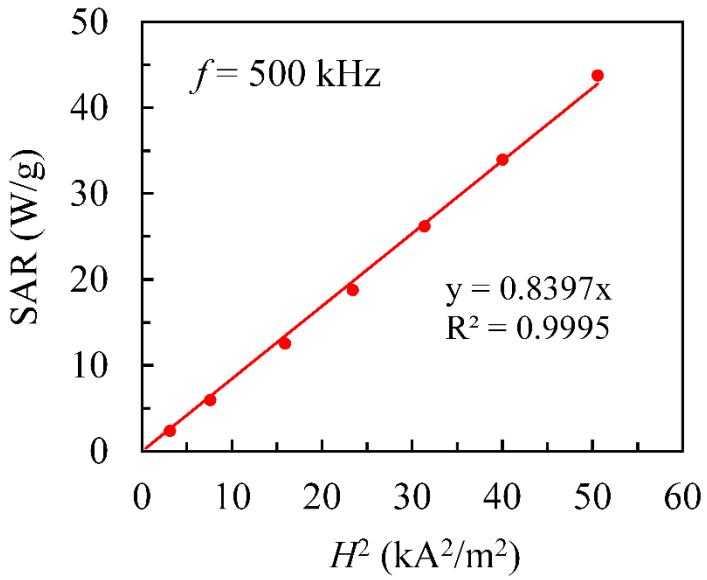

Fig. 3-11 Magnetic field amplitude square dependence of heating properties of Resovist®.

➢ Magnetic field dependence of the proposed mixture compared to FILCT

The magnetic field dependence of the permeability and heating properties of the proposed mixture compared to the traditional implant was also examined. The mixture used consisted of 0.7 g of FILCT which was mixed with 0.3 mL of Resovist® at a preferred mixing rate (volume fraction of nanoparticles of 0.5%) compared to 0.7 g of FILCT. Figures 3-12 and 3-13 show magnetic field strength and frequency dependence, respectively. Here, $\mu_0 M$ was the intensity of magnetization resulting from the sample at 20°C. Note that the larger the magnetization, the higher the accuracy that can be obtained from wireless temperature measurement. The

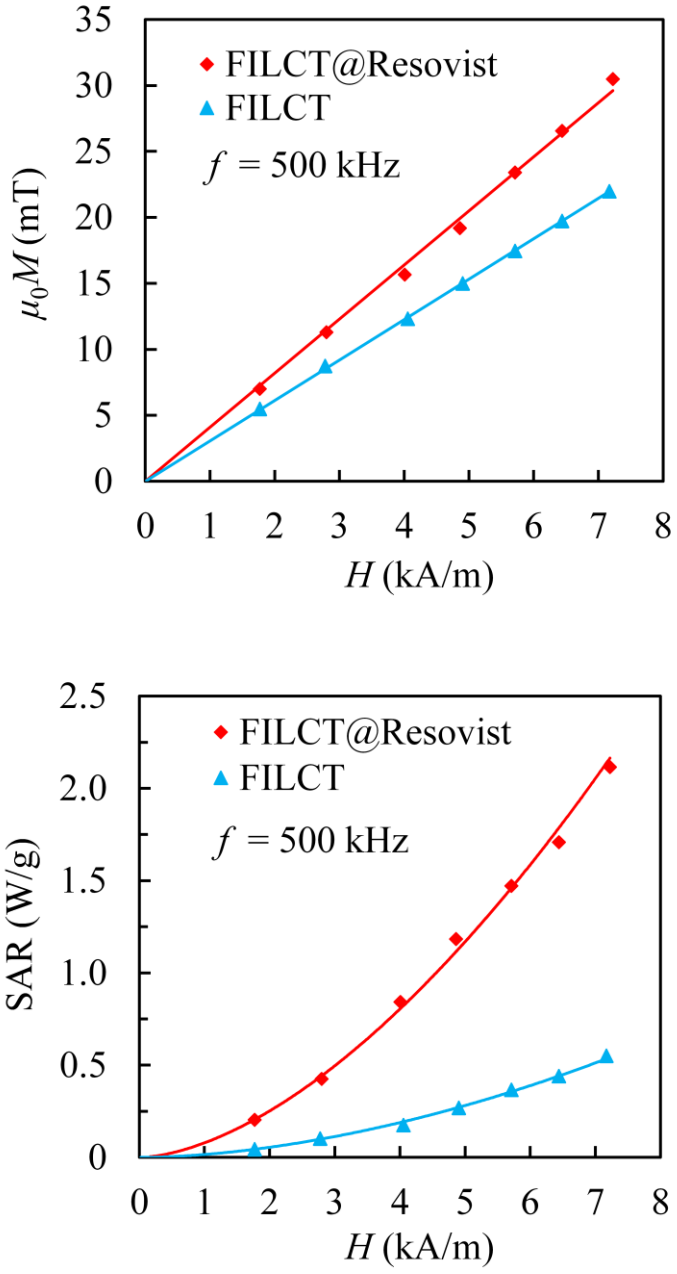

Fig. 3-12 Magnetic field amplitude dependence of magnetization and heating properties of the proposed mixture and traditional implant FILCT.

result obtained indicates that with an extremely small amount of nanoparticles at 0.012 g (0.3 mL of Resovist®) mixed, the magnetization and the SAR can be enhanced compared to FILCT.

Furthermore, the intensity of magnetization was linearly proportional to the magnetic field amplitude, whereas it remained almost unchanged with the frequency. We confirmed that the SAR of Resovist® was linearly proportional to the applied magnetic field amplitude square and frequency, whereas the SAR of the mixture and FILCT do not obey the square of magnetic field amplitude.

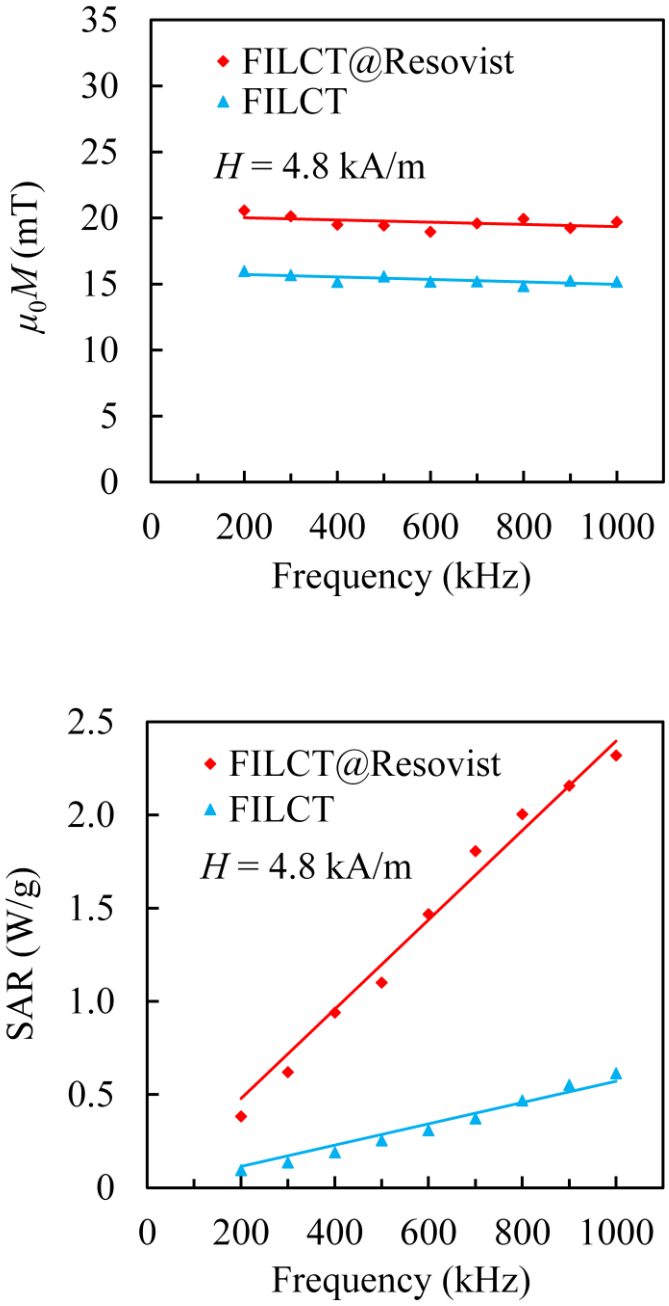

Fig. 3-13 Magnetic field frequency dependence of magnetization and heating properties of the proposed mixture and traditional implant FILCT.

➢ Examination of lab-made nano-ferrofluid compared to commercial Resovist®

We examined the mixture of FILCT with the lab-made nano-ferrofluid instead of Resovist®. The samples prepared were (1) 0.5 g of FILCT; (2) 0.5 mL of Fe_3O_4 Nps; and (3) 0.5 g of FILCT dispersed in 0.5 mL of Fe_3O_4 Nps (volume fraction of nanoparticles to total volume was 0.65%). To compare Fe_3O_4 Nps to Resovist®, (2') 0.5 mL of Resovist®, and (3') 0.5 mL of FILCT dispersed in 0.5 mL of Resovist® were examined.

Figures 3-14 and 3-15 show the results obtained when using Fe_3O_4 Nps, whereas Figs. 3-16 and 3-17 show

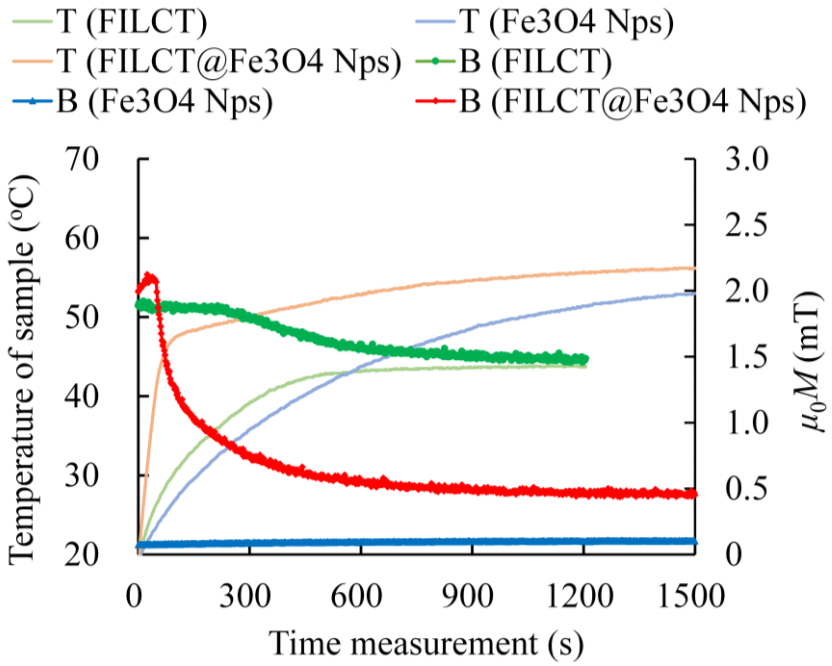

Fig. 3-14 Temporal change in sample temperature and magnetic flux density in pickup coil when using the lab-made nano-ferrofluid.

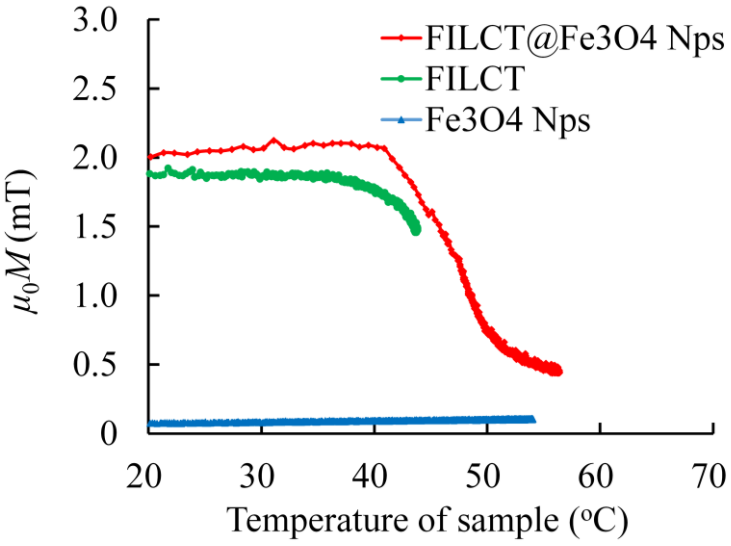

Fig. 3-15 Relationship between magnetic flux density calculated from pickup voltage and the sample temperature when using lab-made nano-ferrofluid.

the results when using Resovist®. We also confirmed that a similar tendency was obtained when the lab-made nano-ferrofluid Fe_3O_4 Nps was used instead of the commercial Resovist®. However, the improvement in thermal and permeability properties of the mixture using Fe_3O_4 Nps was slightly smaller compared to that of the mixture using Resovist®. This difference was probably due to the difference in their particle sizes, magnetic properties and coated agents.

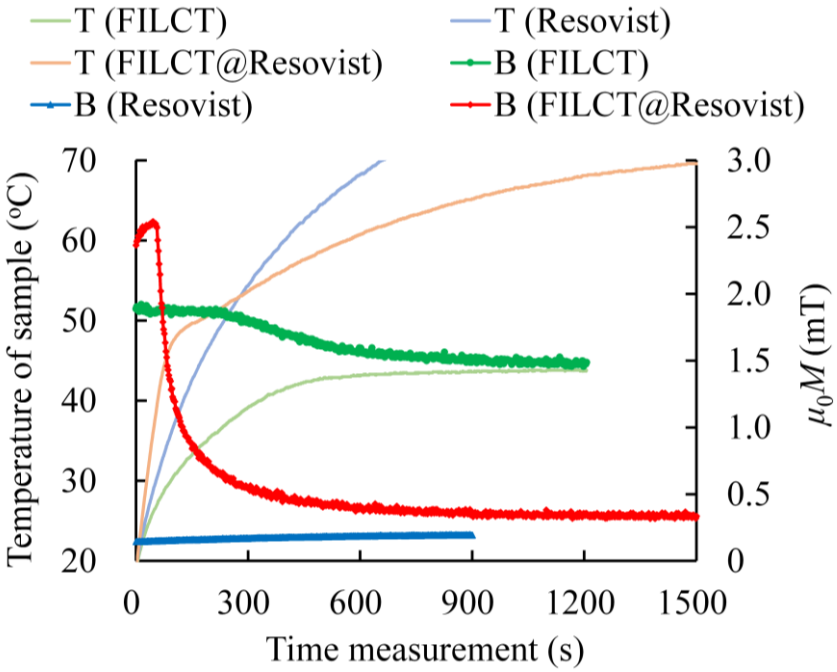

Fig. 3-16 Temporal change in sample temperature and magnetic flux density in pickup coil when using commercial nano-ferrofluid.

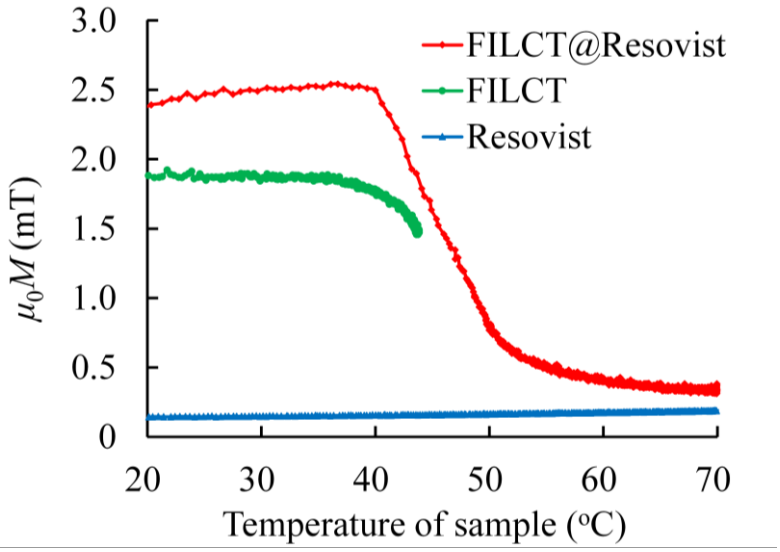

Fig. 3-17 Relationship between magnetic flux density calculated from pickup voltage and the sample temperature when using commercial nano-ferrofluid.

3.5 Summary

As an alternative approach to the gold coating of our previously developed implant (FILCT), we attempted to use nano-magnetic particles to improve the heating efficiency of FILCT. A commercially available nano-ferrofluid named Resovist® consisting of maghemite particles with average diameter of 3.6 nm was used for the examination. The results obtained indicate that the proposed mixture was more superior compared to FILCT and Au-FILCT as a thermosensitive implant for hyperthermia. Furthermore, the results also suggest that by mixing magnetic nanoparticles in Resovist® with FILCT at a volume fraction of nanoparticles of 0.5%, the resulting mixture will have high heating efficiency and permeability besides being easily controllable around the therapeutic temperature. We hypothesized that the magnetic nanoparticles in Resovist® can fill the gaps between the magnetic microparticles in FILCT, thereby reducing the demagnetizing field of magnetic microparticles, thus improving the permeability of FILCT in the mixture. In addition, a similar tendency was obtained when using a lab-made nano-ferrofluid consisting of magnetite particles with average diameter of 13.9 nm. With the proposed mixture, the signal detected can be enhanced significantly compared to the traditional implants, thereby increasing the treatable depth through our wireless temperature measurement and heating system.

Chapter 4

Development of localization technique of hyperthermia implant

4.1 Introduction

In clinical settings, the implant which cannot be seen from the body surface of the patient is expected to deviate from the central axis of MFSD unit (hereinafter, referred to as ‘central axis’). When the implant separates from the central axis, the magnetic flux density applied on the implant decreases, resulting in a decrease in heating efficiency of the implant. Moreover, a problem arises when the signal-to-noise ratio for detecting the temperature of the implant reduces due to a decrease in pickup voltage. Therefore, it is necessary to localize the position of the implant and adjust the MFSD unit to be directly above the implant before the implant is inductively heated (i.e. before applying a sufficiently high magnetic flux density to heat the implant at therapeutic temperature).

Figure 4-1 shows the magnetic behavior of magnetic material (below its Curie point) under applied magnetic field. Magnetic material with high magnetic permeability attracts magnetic flux density around it. The electromotive force induced in pickup coil depends on the position of the material. By utilizing this feature, we proposed a position adjustment method for adjusting the MFSD unit to be directly above the implant. This is done by using three pickup voltages induced in three pickup coils symmetrically installed inside drive coil.

In this chapter, we describe the principle of position adjustment method, and the evaluation experiment of the constructed automatic adjustment system based on the proposed method.

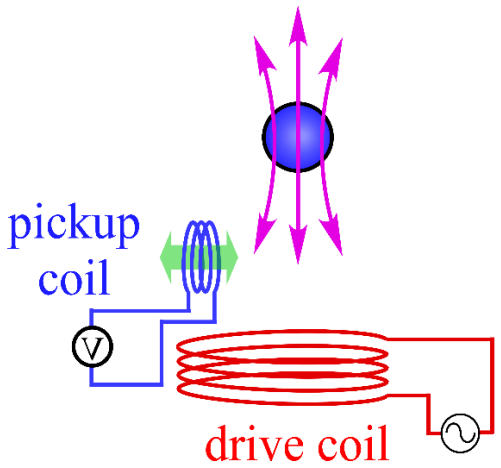

Fig. 4-1 Electromotive force induced in pickup coil depending on the position of magnetic material.

4.2 Principle of localization technique of hyperthermia implant

➢ Induction heating including localization method of hyperthermia implant

Figure 4-2 shows a conceptual diagram of magnetic hyperthermia including position adjustment method [43]. A patient lies in bed when injected with the implant into the affected part. A magnetic field with sufficiently low magnetic flux density is applied to maintain the implant constant at body temperature. Under this condition, pickup voltage changes depending on the position of the implant. Then, the MFSD unit is automatically adjusted by scanning device such as robot arm on the upper surface of the body. Then, the affected part is inductively heated while the temperature of the implant is simultaneously detected with the wireless temperature measurement method. As reference information is necessary to adjust the MFSD unit, measurement was done with the three pickup voltages induced in three pickup coils installed inside the drive coil with the same number of turns and diameter. Specifically, the pickup coils are installed at the same

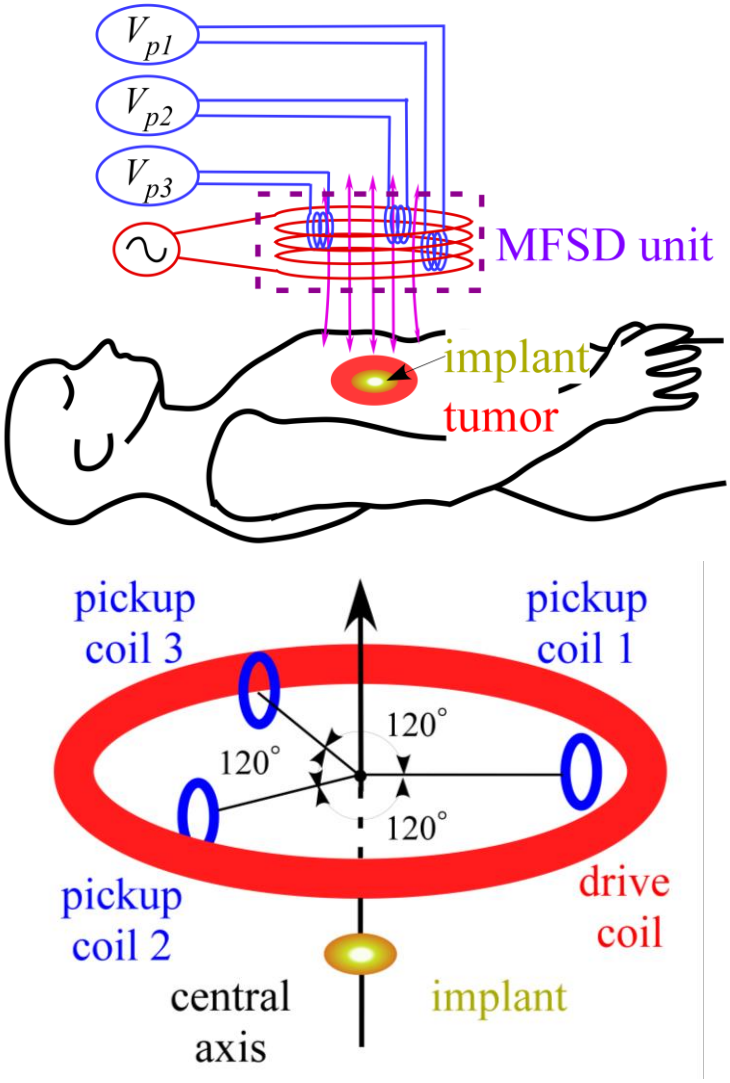

Fig. 4-2 Induction heating including localization method of magnetic implant using three pickup coils.

distance from the central axis and at 120° intervals. The orientation of pickup coils are adjusted in a parallel direction to the applied magnetic field so that the initial electromotive forces are not induced in the three pickup coils when the implant is not installed. After adjusting the position and orientation of the three pickup coils, the drive coil and the pickup coils are integrated as an MFSD unit. As a result, when the implant is located on the central axis, the three pickup voltages become equal. In summary, it is possible to examine whether the implant deviates from the central axis by referring to the three pickup voltages.

➢ Principle of localization method

Figure 4-3 shows a conceptual diagram for position adjustment method. Figures 4-3(a) and 4-3(b) shows a coordinate system of the top and side views of MFSD unit, respectively. Figures 4-3(c) and 4-3(d) shows a schematic view for coarse adjustment and fine-tuned adjustment. Firstly, the MFSD unit is coarsely scanned over the whole existence possibility area of the implant and then moved to a position close to the implant. Next, MFSD unit is finely adjusted by moving it linearly so that the central axis penetrates the implant.

In Fig. 4-3(c), the black circle represents the relative orbit of the implant as seen from MFSD unit when MFSD unit is circularly scanned (i.e., the orbit represented at the local coordinate system of MFSD unit, hereinafter, referred to as 'relative circular orbit'). At one rotation scan (one trial) during circular scanning, we focus on the pickup coil whereby the distance from the coil to the center of relative circular orbit is the farthest among the three pickup coils (hereinafter, referred to as 'farthest coil'). The farthest coil may change among pickup coils 1, 2 and 3. At one trial, the pickup voltage becomes the maximum value (V_{p_max}) at the position (D_{min}) closest to the pickup coil, and becomes the minimum value (V_{p_min}) at the position (D_{max}) farthest to the pickup coil. In the process of circular scanning the whole area, the maximum voltage (V_{p_max}) of the farthest coil increases when the central axis approaches the implant. Therefore, by extracting only the smallest voltage value among the maximum values (V_{p1_max}, V_{p2_max}, V_{p3_max}) of pickup coils 1, 2 and 3 in each trial, i.e., referring to the farthest coil, then comparing the extracted voltage values in all trials, the closest distance between the central axis and the implant can be determined by the largest value extracted. After moving the central axis into the relative circular orbit (the bold black circle in Fig. 4-3(c)), MFSD unit is adjusted more precisely.

As shown in Fig. 4-3(d) for fine-tuned adjustment, firstly the movement of MFSD unit parallel to the y-axis is repeated until the relative position of the implant is located on the symmetry xz-plane of pickup coils 2 and 3, i.e., until the difference between pickup voltages 2 and 3 becomes 0 V (see (1) of Fig. 4-3(d)). If the sign of the difference between (V_{p2}, V_{p3}) is reversed after moving the MFSD unit, i.e., the symmetry xz-plane passes the implant, then MFSD unit is moved in the reverse direction with half of its previous movement amount. After adjusting MFSD unit so that the implant is on the symmetry xz-plane, MFSD unit is adjusted so that the central axis penetrates the implant, i.e., the movement of MFSD unit parallel to the x-axis is repeated until the difference between pickup voltage 1 and the average of pickup voltages 2 and 3 becomes 0 V (see (2) of Fig. 4-3(d)).

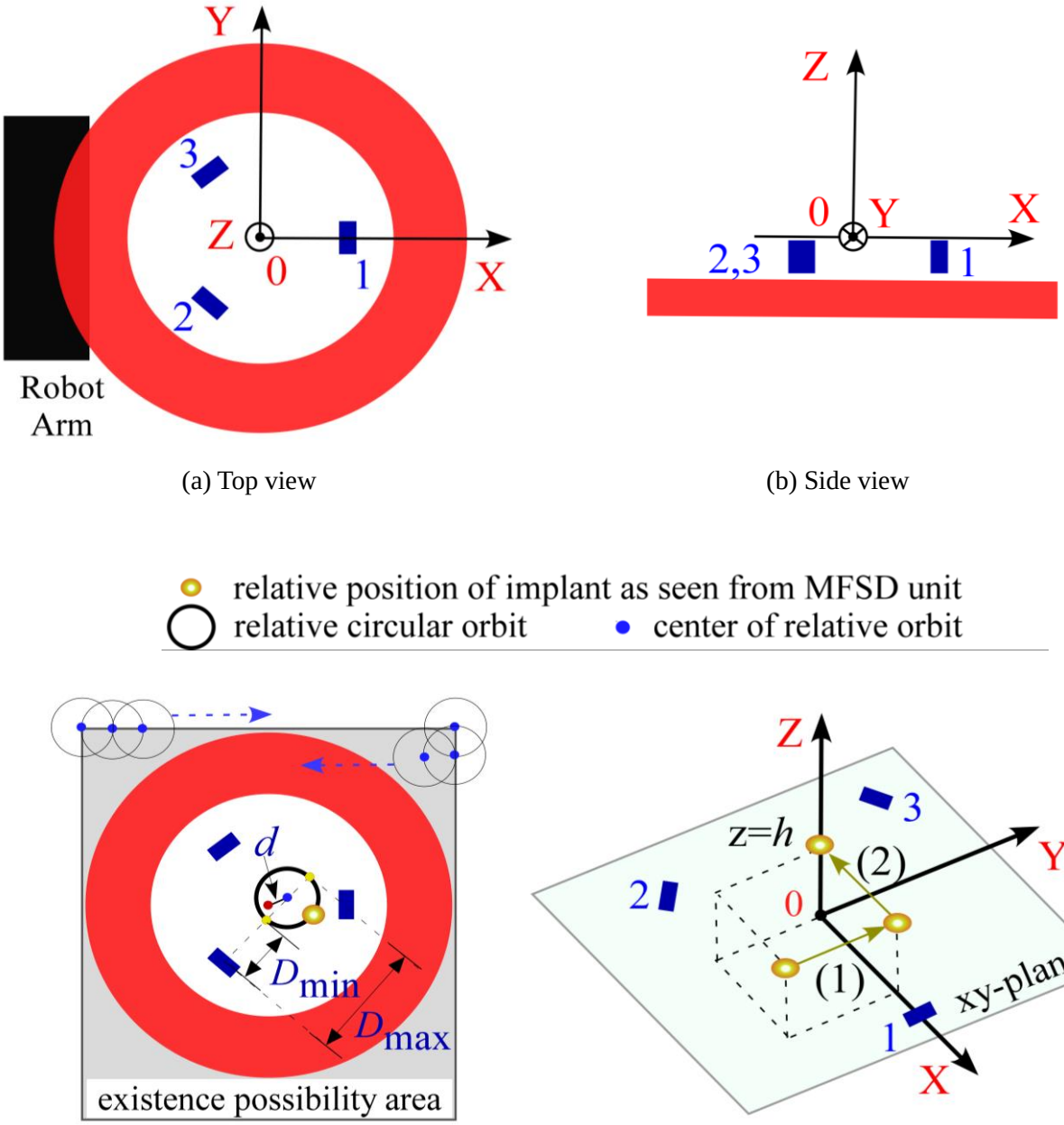

(a) Top view

(b) Side view

(c) Coarse adjustment

(d) Fine-tuned adjustment

Fig. 4-3 Conceptual diagram of position adjustment method.

4.3 Construction of localization system (experimental setup)

Figure 4-4 shows the block diagram and experimental landscape of the constructed automatic localization system of hyperthermia implant. In the following experiments, a sine wave alternating current of 2,560 Hz was generated by a function generator (WF1944A, NF Corp.). It was then amplified to 8.0 App by a bipolar amplifier (BP4610, NF Corp.), and was applied to the drive coil. The magnetic flux density at a position of 10 mm from the top surface of the MFSD unit (where the sample was initially placed) was 0.576 mT. The applied magnetic flux density was sufficiently low to maintain the sample constant at a room temperature of 25ºC.

The three pickup voltages, i.e. the shift in magnetic field brought about by the sample, were measured by three lock-in amplifiers (7265DSP, AMETEK Co.) which perform synchronous detection. A voltage between the ends of a non-inductive resistance of 0.5 Ω connected in series to the drive coil was used as reference signal required for the synchronous detection. The voltages detected by the three lock-in amplifiers via a GPIB cable and the position information of the MFSD unit transmitted from a robot arm control PC via a LAN cable were displayed and saved in real time on a measurement PC by using an automatic measurement program developed with LabVIEW2012 (National Instruments).

The drive coil (pickup coil) of the MFSD unit had an external diameter of 118 mm (12.5 mm), internal diameter of 76 mm (10 mm), thickness of 9 mm (5 mm), and a turn number of 20 turns (10 turns), respectively.

The sample used consisted of Au-FILCT (1.0 g) dispersed in deionized water (1.0 g). When there was no sample, under the condition of the magnetic field applied from the drive coil, the three pickup voltages were calibrated to 0 V by the auto-offset function of the lock-in amplifiers.

In this system, we utilized a robot arm (Motoman-SIA 10F, Yasukawa, positioning accuracy ± 0.1 mm) to produce precise movement of the MFSD unit. The position information of the MFSD unit was transmitted to LabVIEW through TCP/IP by using an automatic control program developed with Microsoft VC++ 2008. The installation position of the MFSD unit and the sample was turned upside down in contrast to the actual installation position in clinical settings. Here, the sample was placed in a test tube in a fixed position. Then, the MFSD unit was moved by the robot arm below. A sample holder was used to install the tube and position it initially on the central axis.

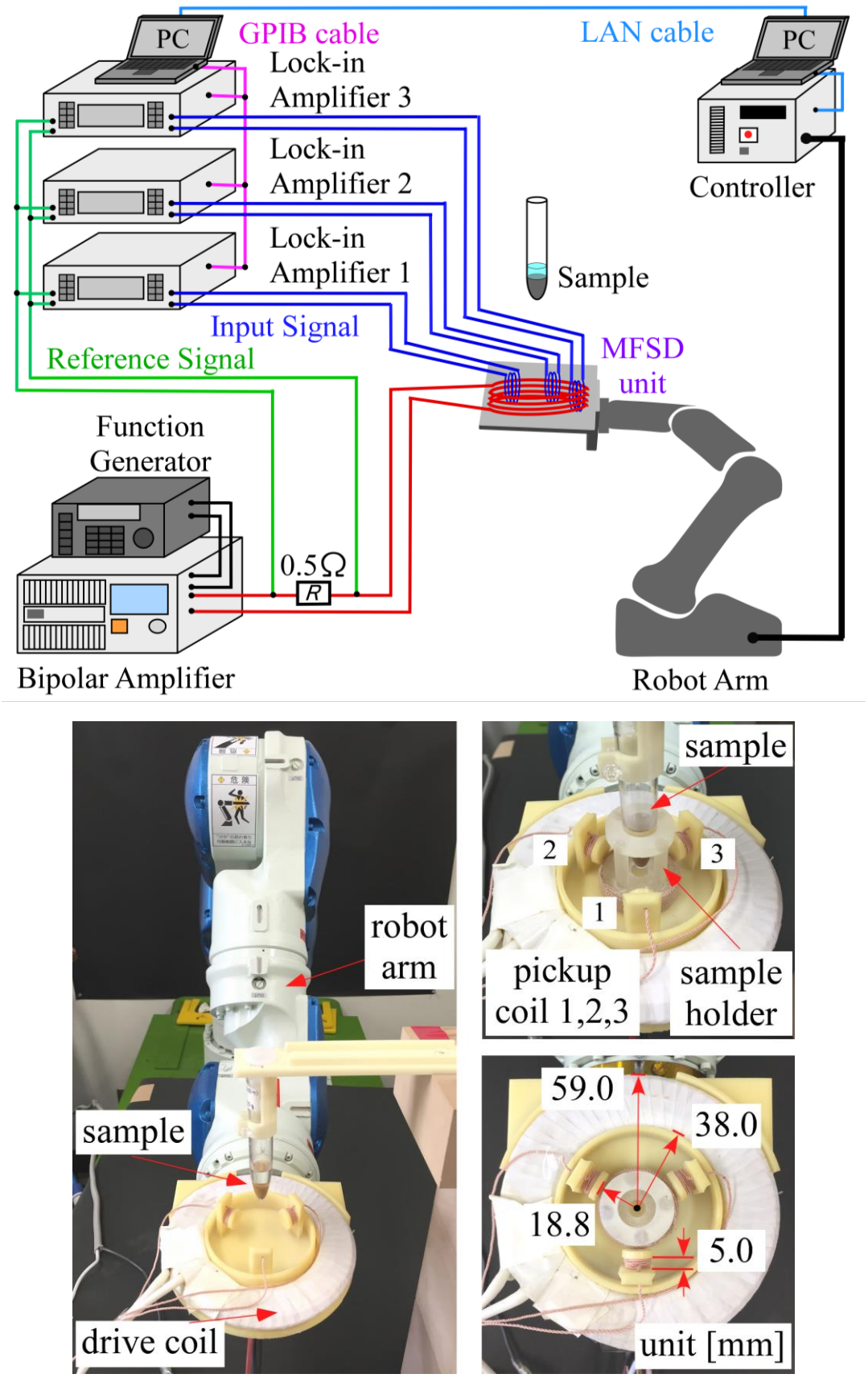

Fig. 4-4 Block diagram (above) and experimental landscape (below) of the constructed automatic localization system of hyperthermia implant.

4.4 Experimental method

The validity of the proposed method when the sample deviates from the central axis was examined by several evaluation experiments. First, to examine coarse adjustment, the sample was fixed at a position of 20 mm above MFSD unit, then MFSD unit was circularly scanned below, and the three pickup voltages were simultaneously measured. Here, the radius of circular scanning was 5 mm, while the distance between the center of relative circular orbit and the central axis was changed at four settings: 0, 10, 30, and 50 mm. Next, to examine fine-tuned adjustment, the three pickup voltages with respect to the position of the sample were measured every 1 mm from x = –10 mm to 10 mm on symmetry xz-plane of pickup coils 2 and 3 under the condition of treatment distance z = 10 mm and 20 mm. Subsequently, we constructed an automatic position adjustment system based on the proposed method and evaluated experimentally the constructed system.

4.5 Results and discussion

Figure 4-5 shows the relationship between the average and standard deviation (n = 5) of each pickup voltage and the position of the sample under the condition that MFSD unit is circularly scanned with a radius of 5 mm. Figures 4-5(a), 4-5(b), 4-5(c) and 4-5(d) show the results with the distances from the center of the relative circular orbit to the central axis being 0, 10, 30 and 50 mm, respectively. Here, the position of the sample is expressed as an angle on the relative circular orbit (clockwise direction +). The reference angle (0°) is the white dot on the enlarged relative circular orbit as shown in Fig. 4-5(a). When MFSD unit was circularly scanned, the relative distance between each pickup coil and the sample fluctuated periodically, thereby, each pickup voltage changed periodically. As the center of the relative circular orbit moved away from central axis, the maximum voltages of pickup coils 2 and 3 (the distance from the pickup coils to the center of relative circular orbit was the farthest among the three pickup coils) were decreasing. The absolute value of pickup voltage 1 became the maximum value when the sample was closest to pickup coil 1 (angle 0° in Figs. 4-5(a) and 4-5(b), and angle 180° in Fig. 4-5(d)), and the absolute value of pickup voltage 1 became the minimum value when the sample was farthest to pickup coil 1 (angle 180° in Figs. 4-5(a) and 4-5(b), and angle 0° in Fig. 4-5(d)). In contrast, as shown in Fig. 4-5(c), the absolute value of pickup coil 1 at angle 180° (the position was closest from pickup coil 1) was smaller than that of angle 0° (the position was farthest from pickup coil 1).

In Figs. 4-5(c) and 4-5(d), the maximum voltage of pickup coils 2 and 3 is larger than the maximum voltage of pickup coil 1, resulting in pickup coil 1 being determined as the farthest coil from the three pickup voltages measured (erroneous determination). However, even if the maximum voltage of pickup coil 1 was to be extracted in the trial of Figs. 4-5(c) and 4-5(d), it will still be smaller than the maximum voltage of pickup coils 2 and 3 extracted in the trial of Figs. 4-5(a) and 4-5(b) where the distance between MFSD unit and the sample is shorter. This means that since the trial became the maximum of the voltage values extracted by circular scanning on the whole area targeted, then even if an erroneous determination occurred in the trials of Figs. 4-5(c) and 4-5(d), this would not affect the result of the coarse adjustment.

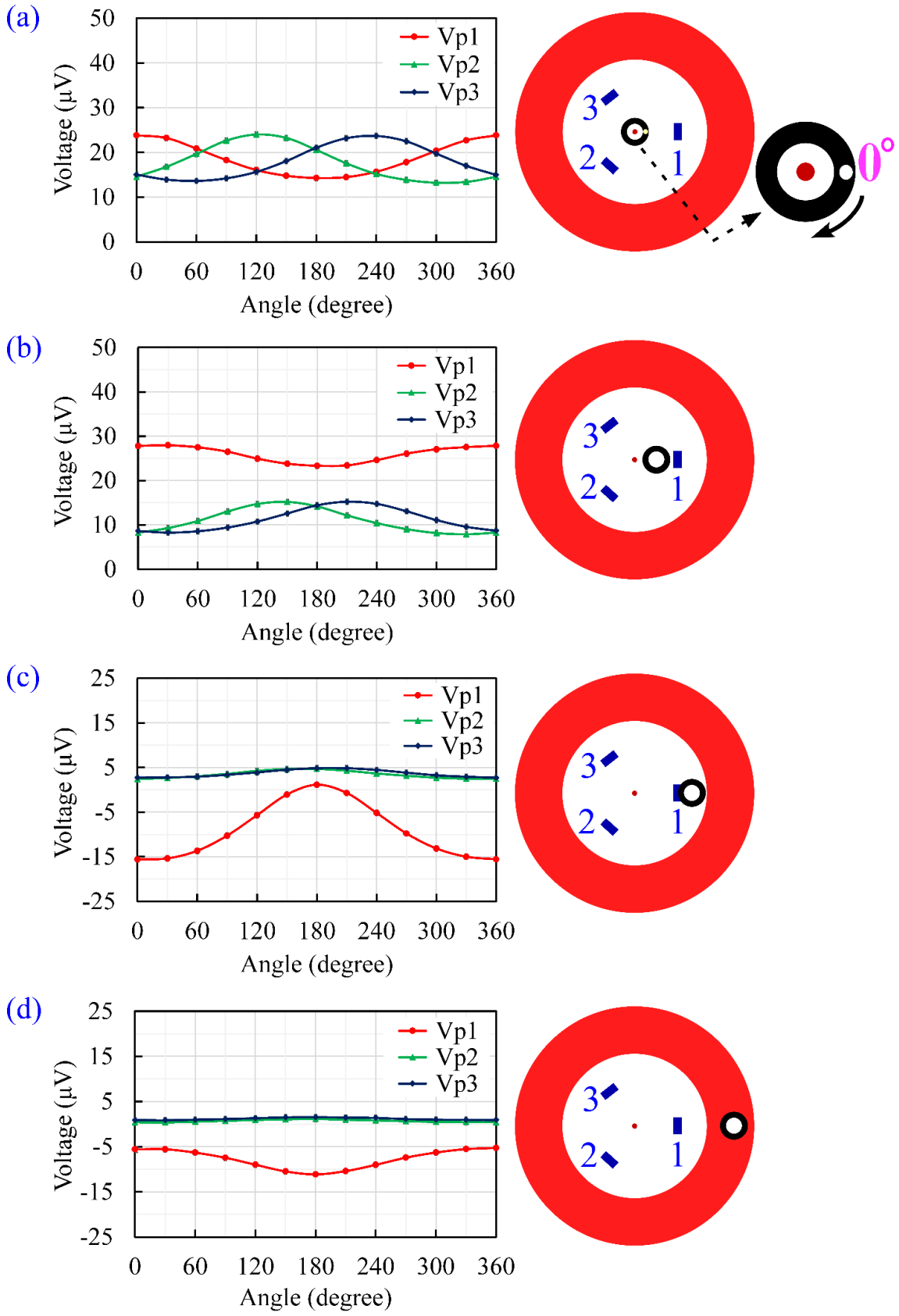

Fig. 4-5 Relationship between pickup voltages and position of sample during circular scanning for different distances between the center of the relative circular orbit and the central axis when treatment distance was 20 mm. (a) Distance at 0 mm, (b) distance at 10 mm, (c) distance at 30 mm, and (d) distance at 50 mm.

Figure 4-6 shows the relationship between the average and standard deviation (n = 5) of each pickup voltage and the position of the sample under the condition of the sample located on the symmetry xz-plane of pickup coils 2 and 3, which was moved in parallel to the x-axis. Figures 4-6(a) and 4-6(b) show the results of the treatment distance z = 10 mm and 20 mm, respectively. The black line passing through the center axis as shown in Fig. 4-6(a) is the relative orbit of the sample seen from MFSD unit. Pickup voltages 2 and 3 matched and the three pickup voltages had a tendency to match when the sample approaches the central axis (x = 0 mm). The same tendency was obtained under the condition of the treatment distance z = 20 mm, but the three pickup voltages decreased compared to the treatment distance z = 10 mm.

Moreover, it was also confirmed that pickup voltages 2 and 3 had a tendency to match when the sample approached their symmetry plane (e.g., V_{p2} = 22.6 μV, V_{p3} = 14.2 μV at angle 90°, V_{p2} = 13.8 μV, V_{p3} = 22.5 μV at angle 270° in Fig. 4-5(a), and V_{p2} = 18.8 μV, V_{p3} = 18.6 μV at position x = 0 mm in Fig. 4-6(a)). The above results confirmed that it is possible to adjust MFSD unit to be directly above Au-FILCT using the three pickup voltages as clues.

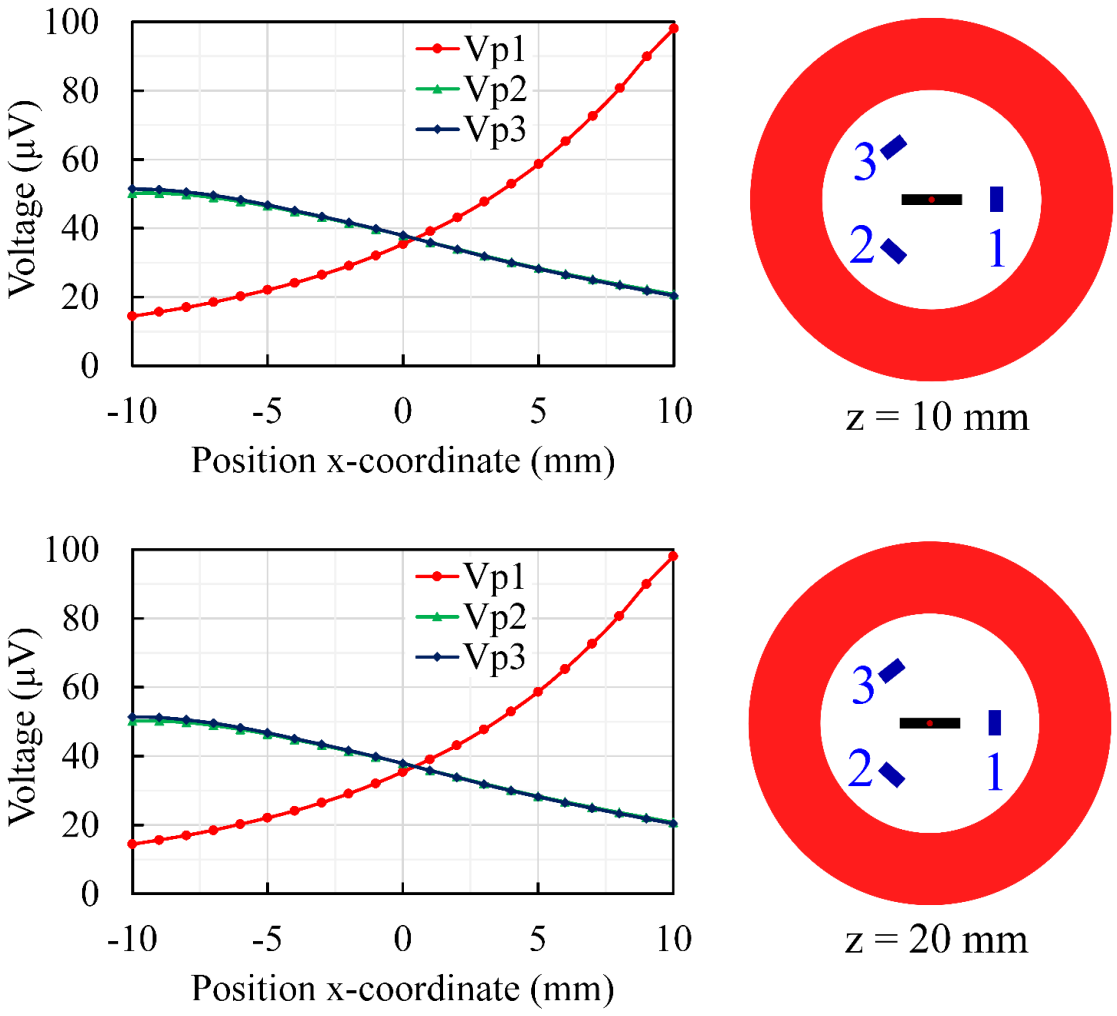

Fig. 4-6 Relationship between pickup voltages and position of sample during linear movement.

The following shows evaluation of the changes in the pickup voltage with respect to the position of the sample in the existence possibility area of the sample. Using the measurement results in Fig. 4-5 (angle 0° and 180°) and Fig. 4-6(b), the three pickup voltages are as plotted in Fig. 4-7. Here, the position of the sample ranges from x = –10 mm to 55 mm on the symmetry xz-plane of pickup coils 2 and 3. The blue area shown in Fig. 4-7 represents the position of pickup coil 1 as seen from the side view of MFSD unit. It was confirmed that when the sample located in area (a) was closer to pickup coil 1, the number of magnetic flux interlinking across pickup coil 1 increased. However, when located in area (b), the number of magnetic flux decreased when the sample was closer to pickup coil 1. When the sample passed through pickup coil 1 as shown in area (c), the orientation of the magnetic flux with respect to pickup coil 1 was reversed.

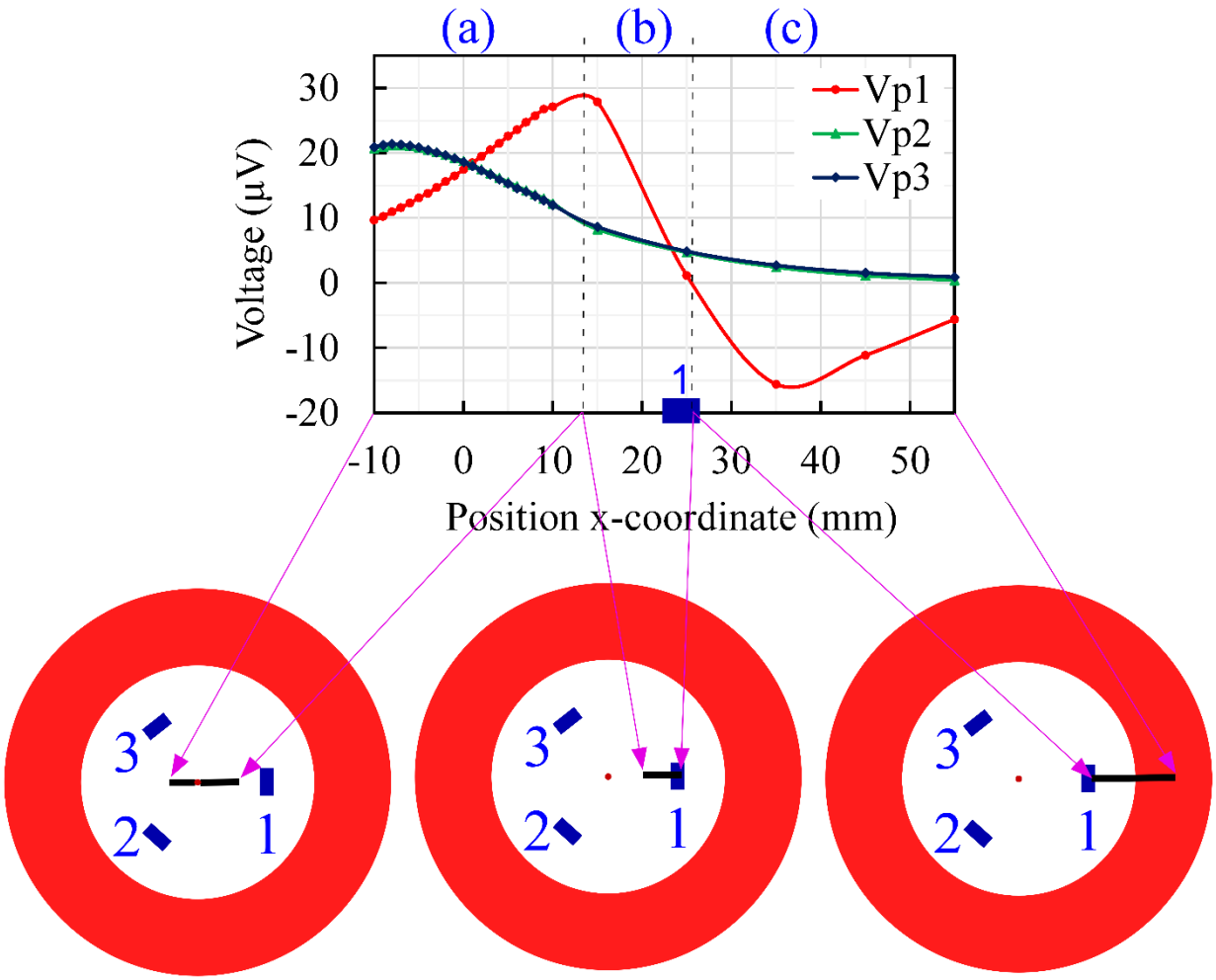

Fig. 4-7 Relationship between voltages and position of sample on xz-plane (treatment distance = 20 mm).

Figure 4-8 shows the relationship between the average and standard deviation (n = 5) of each pickup voltage and the treatment distance between MFSD unit and the sample. When the sample was located on the central axis, the three pickup voltages almost matched with each other and decreased as MFSD unit moved away from the sample. Furthermore, after calculating the average of the three pickup voltages at an arbitrary distance, a high coefficient of determination (R^2 = 0.998) was obtained when using an exponential approximation of the relationship between the average voltage and the treatment distance. We also confirmed that the average value of the three pickup voltages changes in inverse proportion to the distance between MFSD unit and the sample located on the central axis. Therefore, it is possible to estimate the treatment distance via the average measured value.

Since the pickup voltage depends on the mass of the sample, it is also necessary to carry out further studies on the effect of other factors such as the mass of the sample and its distribution in the treatment area on the approximation expression in Fig. 4-8 to improve the accuracy of the proposed method. Furthermore, the distance estimation becomes more difficult when MFSD unit moves away from the sample. We found that the voltage induced in the pickup coil changes greatly depending on the position of the sample even under the same treatment distance (see Fig. 4-7). Therefore, the treatment distance can also be improved by investigating the optimal installation position of the pickup coils inside the drive coil.

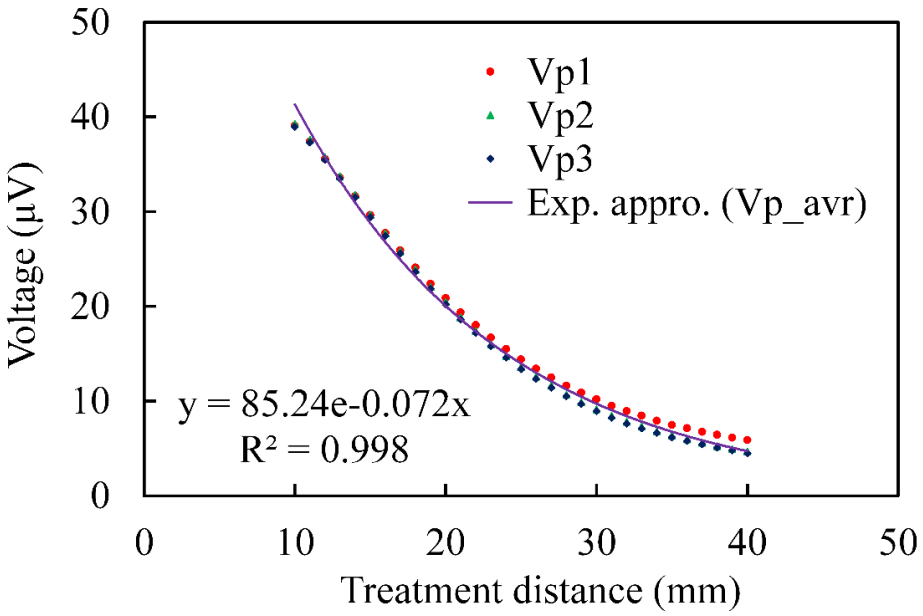

Fig. 4-8 Relationship between pickup voltages and the distance between MFSD unit and sample.

➢ Evaluation of the constructed automatic position adjustment system

In this section, we evaluated the constructed automatic adjustment system. In this experiment, a sine wave of 2,560 Hz was generated by a function generator, then amplified to 8.0 Ap-p by a bipolar amplifier and applied to drive coil. The applied magnetic field at a position of 15 mm (initial setting sample) from the top surface of MFSD unit was 0.520 mT.

Before starting adjustment, the position of the central axis of MFSD unit as seen from the implant is (i.e., x = –12 mm, y = –12 mm) as shown in Fig. 4-9. In this experiment, settings for coarse adjustment, the radius was r = 5 mm, scanning area was 25×25 mm. For fine-tuned adjustment, initial movement was d = 2 mm and the end conditions were d <= 0.5 mm or ΔV <= 0.5 V.

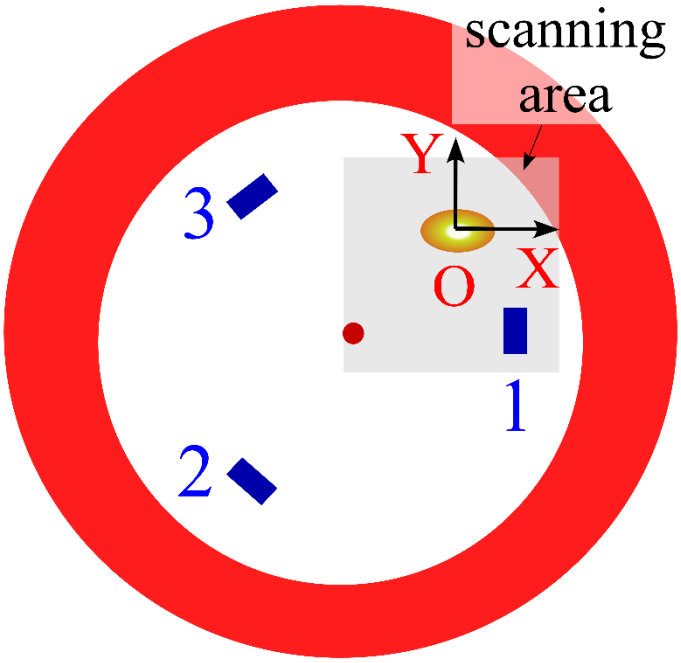

Fig. 4-9 Position of sample and MFSD unit before adjustment.

Figures 4-10 and 4-11 shows the position of the central axis of MFSD unit as can be seen from the sample which was fixed, and the temporal change in pickup voltages when MFSD unit was circularly scanned, respectively. In Fig. 4-10, the blue dot represented the initial position of central axis of MFSD unit, and the black dot represented the position of the sample. As shown in Fig. 4-10, the radius of each circle scan (each trial) was set with 5 mm, and the total of the trials for scanning area of 25×25 mm was 16. During circular scanning, the pickup voltages at each position of central axis (12 points for each trial) were plotted in Fig. 4-11. The maximum voltages of pickup coils 1, 2, and 3 in each trial were plotted in Fig. 4-12. Here, (Vp1,2,3_max)min is the minimum voltage of the three maximum voltages in each trial (i.e. referring to the farthest coil). It was confirmed that as the central axis got close to the sample, the value of (Vp1,2,3_max)min became larger. The sixth trial (red circle in Fig. 4-10) where the value of (Vp1,2,3_max)min was maximized, indicates that this trial was the closet to the sample. As a result, MFSD unit was moved to the center of the sixth trial (x = –2 mm, y = – 2 mm).

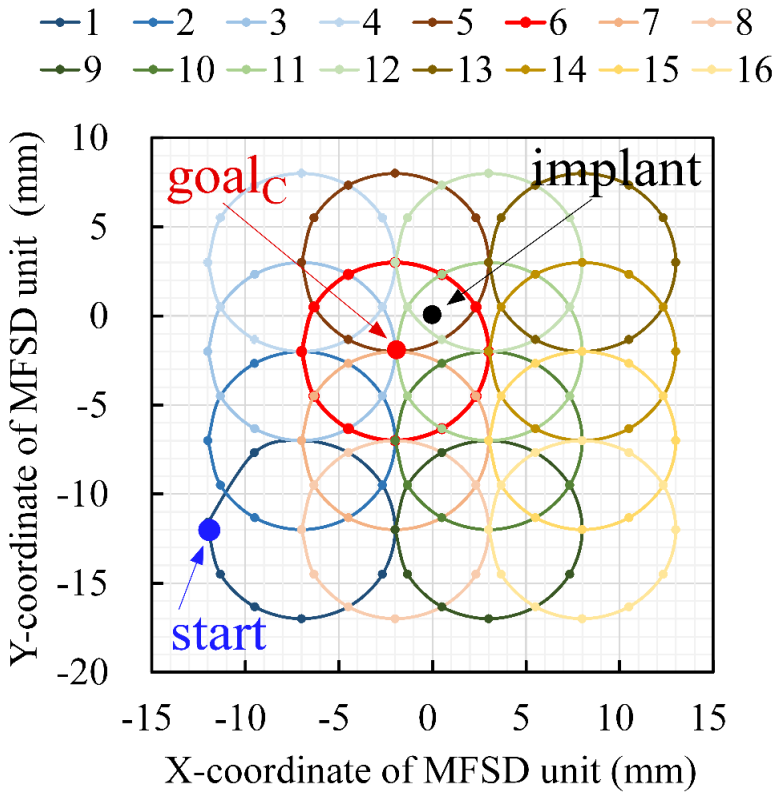

Fig. 4-10 The position of central axis as can be seen from the fixed sample (x = 0, y = 0) when MFSD unit was circularly scanned with the radius of 5 mm.

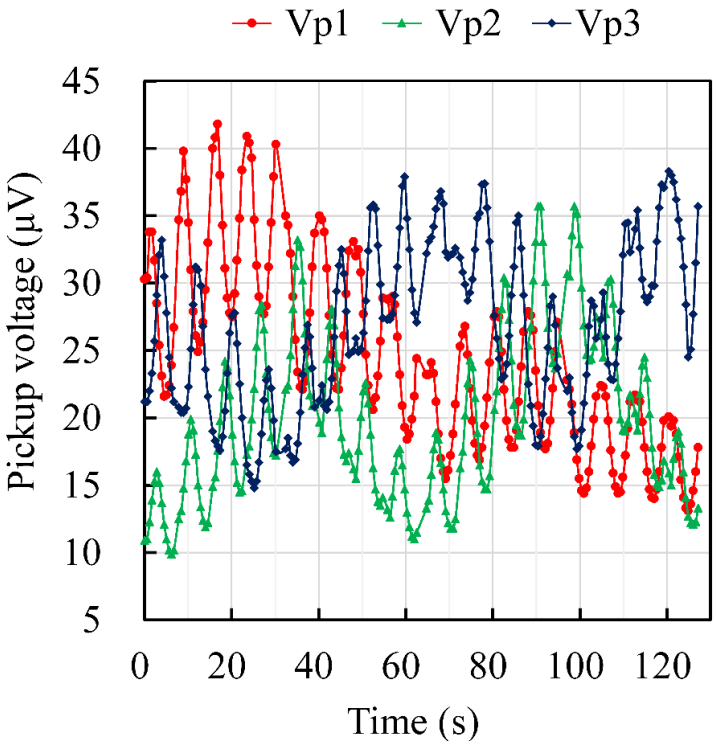

Fig. 4-11 The temporal change in pickup voltages when MFSD unit was circularly scanned.

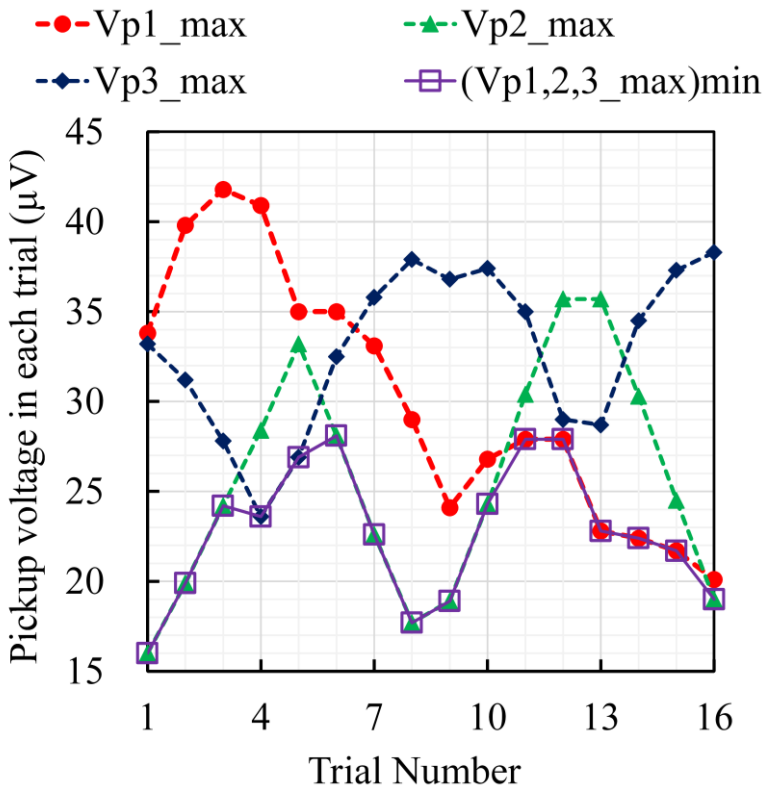

Fig. 4-12 The maximum voltage of each pickup coil in each trial and the minimum of the three maximum voltages in each trial (coarse adjustment).

Figure 4-13 shows the result of the fine-tuned adjustment after coarse adjustment above. When pickup voltages 2 and 3 had a tendency to match, the sample got close to the symmetry plane of pickup coils 2 and 3 as shown in (1) of Fig. 4-13, i.e. the y-coordinate of the central axis was close to 0. Subsequently, as shown in (2) of Fig. 4-13, when pickup voltages 1 and the average of pickup voltages 2 and 3 was close to 0 V, the x-coordinate of the central axis was close to 0. In summary, using the developed system, the adjustment time of MFSD unit to the sample can attain an accuracy of below 1 mm.

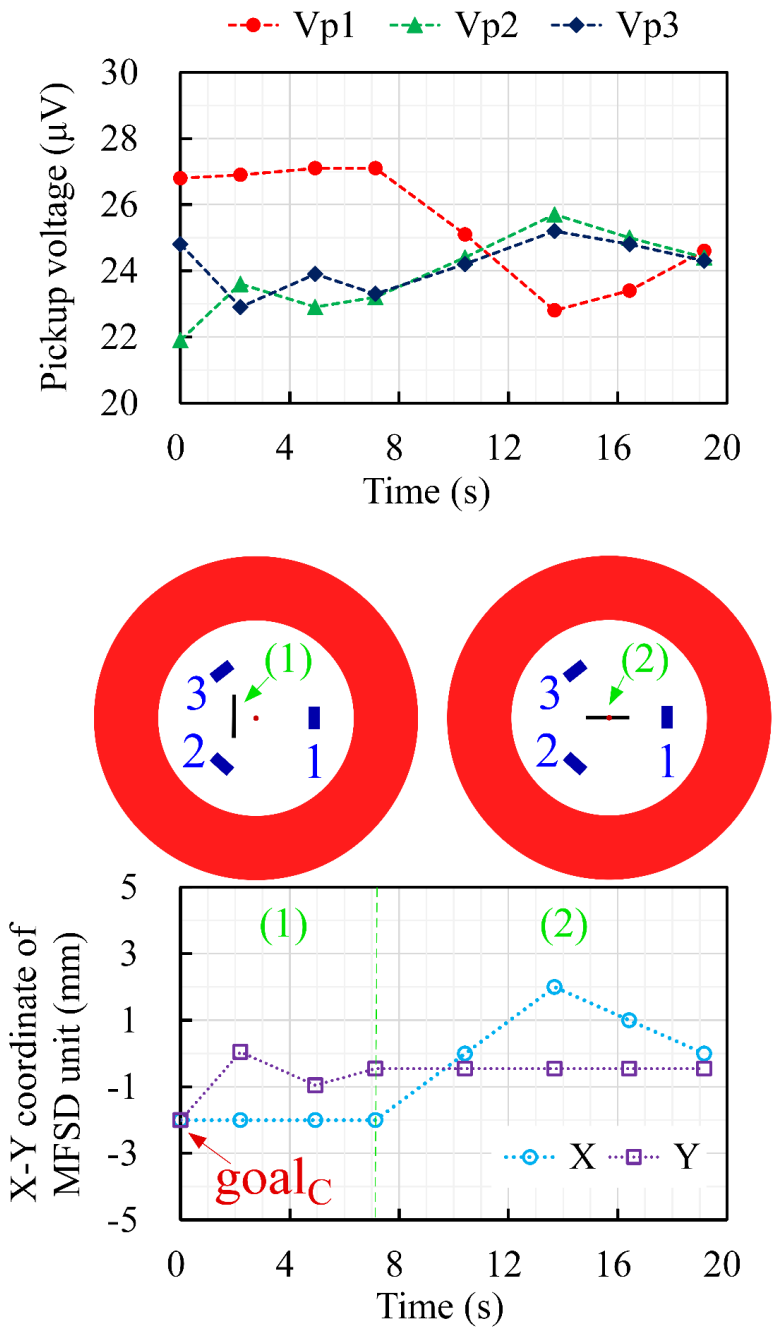

Fig. 4-13 The voltage of each pickup coil and the position of the central axis of MFSD unit when MFSD unit was linearly moved (fine-tuned adjustment).

4.6 Summary

In this study, we proposed a position adjustment method to solve the challenge of providing both accuracy in temperature detection and maintaining the heating effectiveness of treatment, which decreases as the implant injected into the affected part deviates from MFSD unit. MFSD unit was automatically adjusted to be directly above the implant by using the voltages induced in three pickup coils symmetrically installed inside the drive coil. Using the constructed position adjustment system, it was possible to automatically locate the position of the implant with accuracy below 1 mm. The proposed methods can be used in magnetic hyperthermia using heating elements such as in a bulk magnetic material and magnetic nanoparticles. These techniques can be used together with existing magnetic hyperthermia.

In the future, we plan to investigate the optimal installation position of the pickup coils inside the drive coil as well as investigate how distribution of the implant in affected part affects the accuracy of the proposed method. Moreover, it will be better if the time required for the position adjustment is shorter. Therefore, we are considering that the existence possibility area of the implant can be reduced from the signs and the magnitude relationship of the three pickup voltages measured before circular scanning. Furthermore, the time changes depending on the setting of the radius of circular scanning and the amount of linear movement can be further considered. Therefore, it is also necessary to investigate optimal parameters for the radius and the amount of movement.

Chapter 5

Development of rotary scanning technique of motion artifact reduction

5.1 Introduction

Human heart rate variability includes high frequency components (0.15–0.4 Hz) synchronized with respiration, low frequency components (0.04–0.15 Hz) due to baroreceptor reflex related to blood pressure regulator, and very low frequency components (≤0.04 Hz) [44]. Respiration is not limited to the frequency range of 0.15 to 0.4 Hz, e.g., it is as low as 0.1 Hz during rest and as high as 0.7 Hz during exercise. As a method of reducing the artifacts, methods such as respiratory arrest method by breath holding or respiration/heart rate synchronization method for periodic motion are performed.

In previous studies, we proposed a wireless temperature method using the thermosensitive implant as a probe. However, during treatment the relative position between MFSD unit and the implant is considered to fluctuate by the periodic physiological motions such as respiration and heartbeat-induced artifact. When the fluctuation of the implant is large, it cannot distinguish whether the change in pickup voltage is caused by the change in the temperature of the implant around therapeutic temperature, or by the change in distance between MFSD unit and the implant by the artifact. It is thus of paramount importance to reduce the artifact to improve the accuracy of wireless temperature measurement for clinical settings.

In this chapter, we proposed a motion artifact reduction method by rotating scanning technique of reducing the effects of periodic physiological motions such as respiration and heartbeat.

5.2 Principle of rotary scanning technique of motion artifact reduction

We focused on the periodic physical motions artifacts. MFSD unit is circularly scanned in a different period cycle from the motion artifacts, the spectrum component synchronized with the rotary scanning and the spectrum components of the motion artifacts are separated by Fourier transform, and only the target component (signal) is extracted for temperature measurement [45, 46].

Figure 5-1 shows an image of therapeutic system by rotary scanning. Figure 5-2 shows a conceptual of motion artifact reduction method. Here, Fig. 5-2(a) shows the results of power spectrum analysis in the case where there is no artifact, whereas Fig. 5-2(b) shows the case of artifact, and Fig. 5-2(c) shows the result of power spectrum analysis in the case of artifact. The left side of the figure shows the case where the temperature of the implant is below the Curie point, whereas the right shows the case where the temperature is above the Curie point. Since the relative distance between the pickup coil and the magnetic material

periodically varies by rotational scanning, the pickup voltage periodically varies in synchronization with the rotation period. When the temperature rise of the implant is above the Curie point, the permeability of the implant significantly decrease, thereby the amplitude value of the pickup voltage also decreases. As a result, it is possible to detect whether or not the implant has reached the Curie point from the change in the power of the spectral component synchronized with the rotary scanning, even if there is a motion artifact.

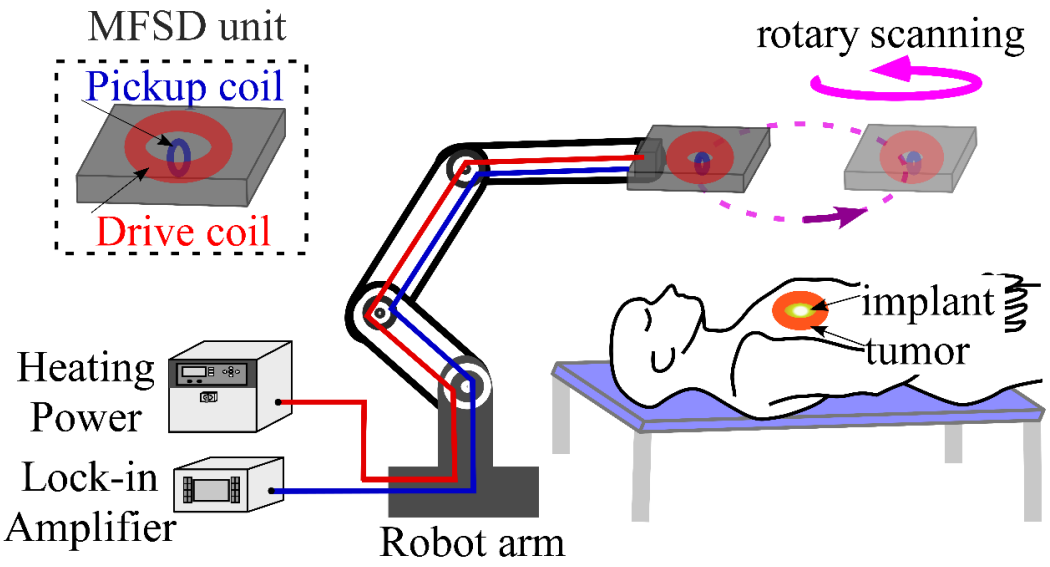

Fig. 5-1 Image of a therapeutic system by rotational scanning.

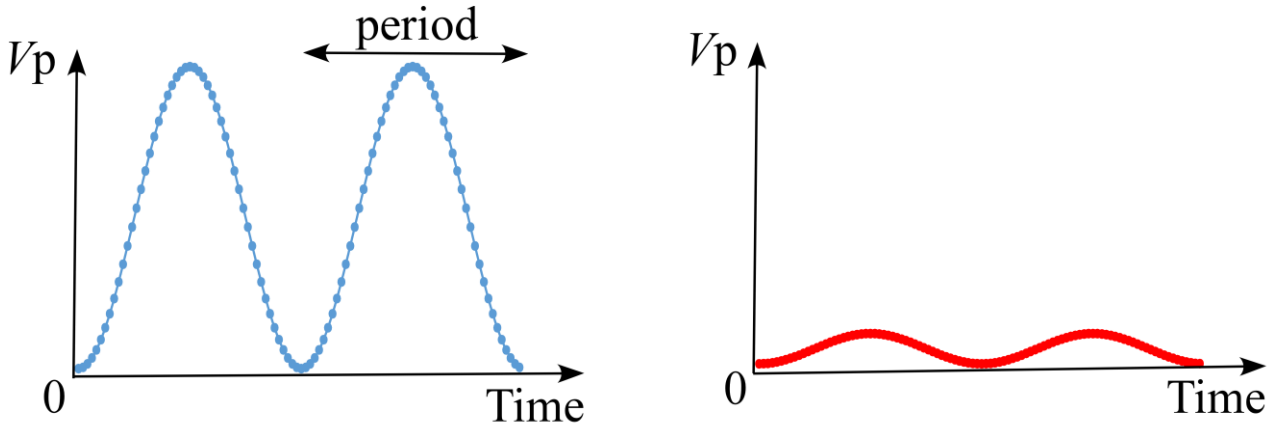

(a) Pickup voltage without motion artifact

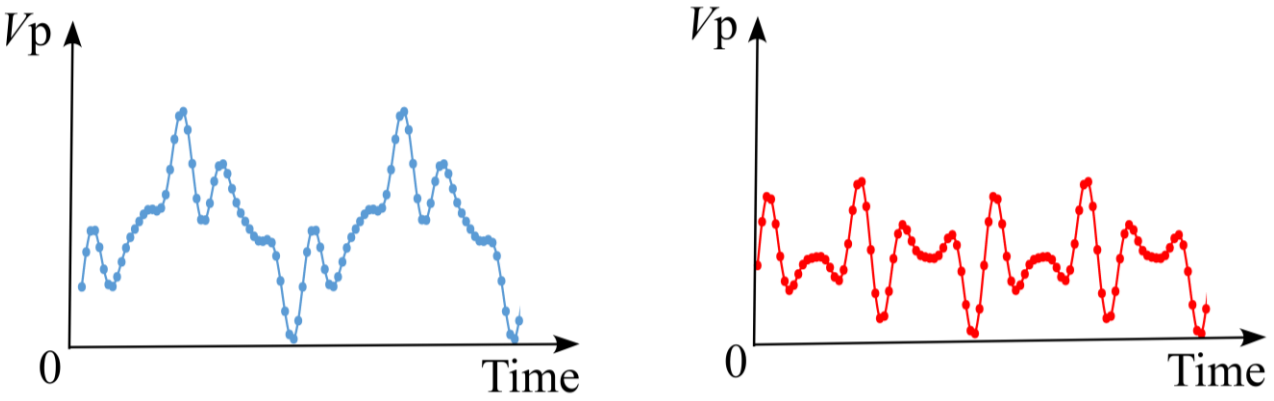

(b) Pickup voltage with motion artifact

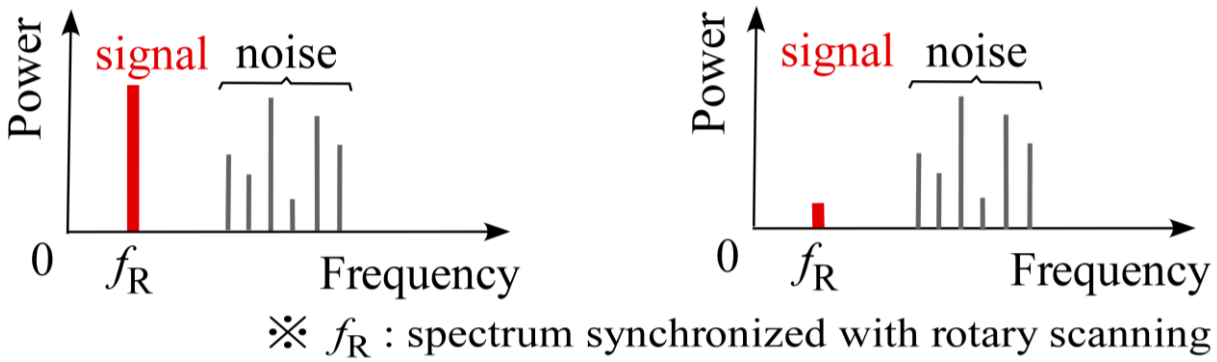

(c) Spectrum analysis of pickup voltage

Fig. 5-2 Concept of motion artifact reduction method by rotating scanning technique. The left side of the figure shows the case below Curie point, whereas the right side shows the case above Curie point.

5.3 Construction of rotary scanning system (experimental setup)

Figure 5-3 shows the block diagram of the constructed system to verify the validity of the proposed artifact reduction method. Figure 5-4 shows the top and side view of the experimental landscape. In clinical settings, a large capacity of induction heating power supply is used to generate a high frequency and strength of magnetic field enough to heat magnetic particles up to therapeutic temperature. To verify the validity of the proposed method, a small capacity of bipolar amplifier (BP4610, NF Corp.) was used to generate a magnetic field, so the sample was not inductively heated. In this system, a sinusoidal current was generated by a function generator (WF1944A, NF Corp.) which was amplified by bipolar amplifier and applied to drive coil, and a magnetic field (8 Ap-p, 2560 Hz) was generated around it. The magnetic flux density at the position of the sample was 0.55 mT. Pickup voltage which varies depending on the permeability of the sample was synchronously detected by a lock-in amplifier (7265DSP, AMETEK Co.). For the reference signal of lock-in amplifier, the voltage across the resistor of 0.39 Ω connected in series with drive coil was used. The real time voltage waveform was displayed and the voltage value was saved by automatic measurement program developed with LabVIEW 2012 to the computer via the GPIB interface. With low magnetic field applied by the bipolar amplifier, sample (1.0 g of Au-FILCT dispersed in 1.0 g of deionized water) cannot be inductively heated. Therefore, a sample heated to 70°C with a hot plate was then placed at a position 10 mm away from MFSD unit, naturally cooled until it decreased below the Curie point, and pickup voltage at that time was measured. At the same time, as reference data for evaluating the validity of this method, the center temperature of sample was measured by optical fiber thermometer (FL-2000, Anritsu-meter) and recorded on PC.

Before scanning MFSD unit, the pickup voltage was calibrated to 0 V by the offset function of lock-in amplifier in a state where a magnetic field was applied from drive coil without setting sample so that pickup voltage was minimized. MFSD unit was composed of drive coil and pickup coil which had an outer diameter of 118 mm and 12.5 mm, an inner diameter of 76 mm and 10 mm, a thickness of 9 mm and 5 mm, and turn number of 20 and 20 turns, respectively.

In the clinical setting, MFSD unit is assumed to rotationally scan on the body surface closest to the implant. In this experiment, the sample was fixed upward in the test tube and MFSD unit was rotationally scanned by a robot arm (Motoman-SIA 10F, Yasukawa) below the sample. In this experiment, the motion artifact was simulated by the vertical movement of MFSD unit by the robot arm. In particular, in the condition where there is no artifact, MFSD unit was circularly rotated with the robot arm. On the other hand, in the condition with periodic physiological motion artifact, MFSD unit was spirally rotated in which the vertical movement simulating the artifact was added to the circular rotation when there was no the artifact.

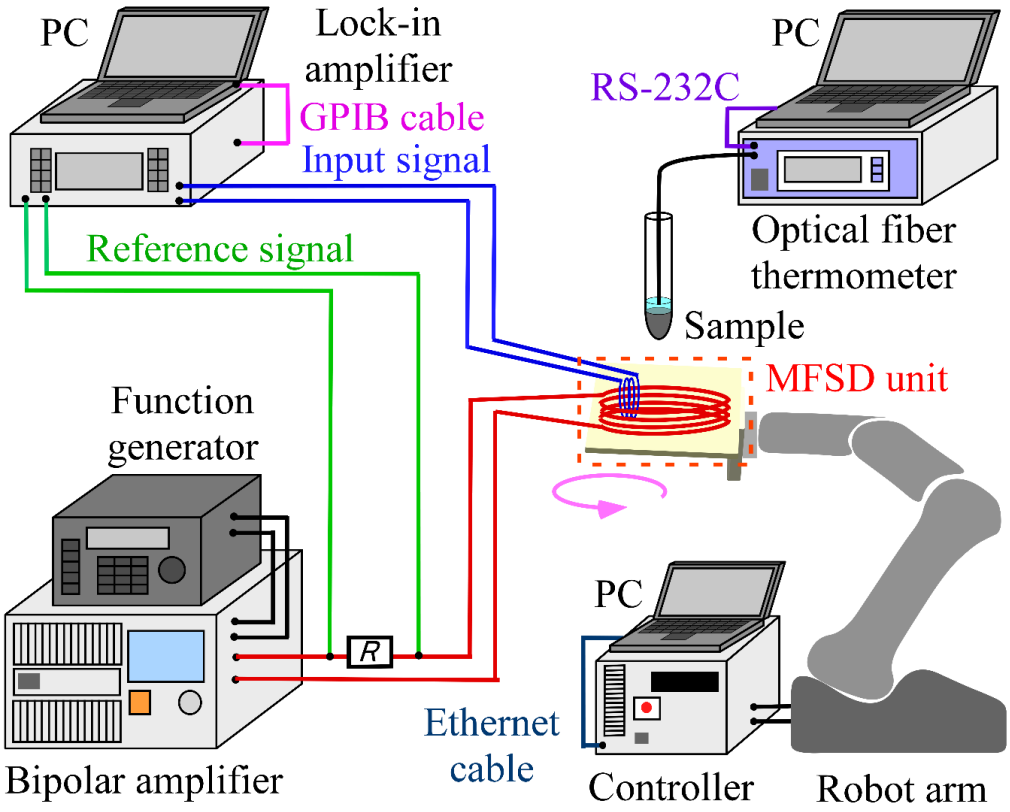

Fig. 5-3 Configuration diagram of experimental setup of motion artifact reduction method.

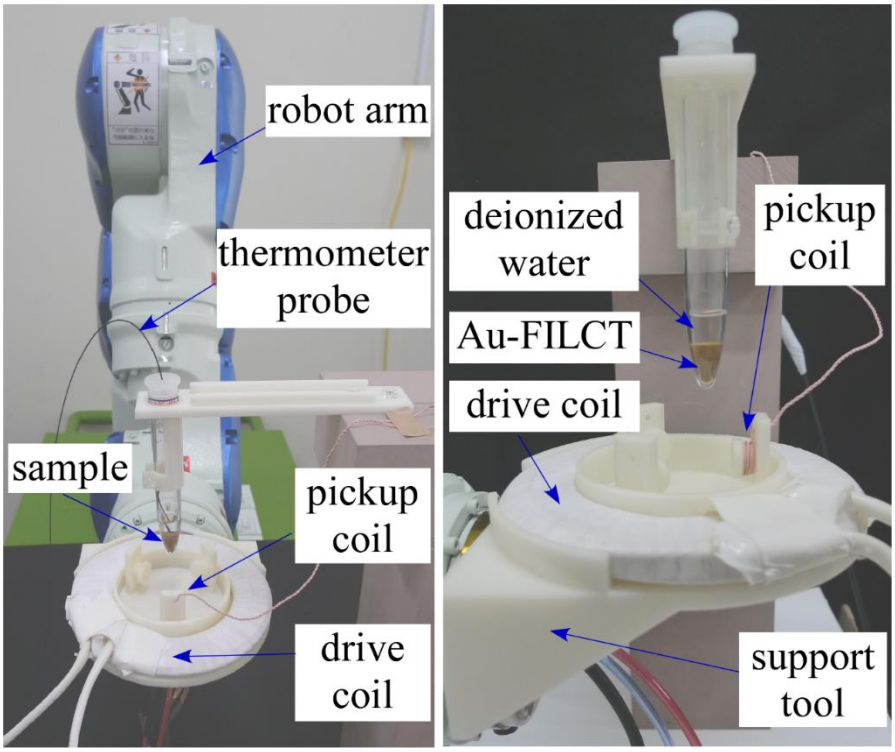

Fig. 5-4 The top view (a) and (b) side view of experimental landscape.

5.4 Experimental method

In the condition when there was no artifact, MFSD unit was circularly rotated with a period of 2s and a radius of 13 mm. In the condition with artifact, MFSD unit was expressed by spiral scan in which the vertical movement simulating the artifact was added to the circular scan when there was no the artifact. The amplitude of vertical movement of the simulated artifact was fixed at 10 mm and the periods were 5, 11 and 19s which were generated randomly so that they corresponded to the high, low frequency component and ultra-low frequency component of the human heart rate variability. The change in pickup voltage around the Curie point was measured.

5.5 Results and discussion

Figure 5-5 shows the temporal change in pickup voltage and the temperature of the sample when the MFSD unit was circularly scanned on the plane 1 cm from the sample. Here, the horizontal axis represents the measurement time, the first vertical axis represents pickup voltage, and the second vertical axis represents the temperature of the sample. As the temperature of the sample which was heated to 70°C beforehand decreased below the Curie point, the amplitude value of pickup voltage synchronized with the period of rotary scanning increased. Furthermore, the amplitude value did not change and became constant when the temperature of the sample decreased below Curie point. Figure 5-6 shows the partial waveform in the range from 350 to 385s of Fig. 5-5. It was confirmed that pickup voltage with an accurate period (2s) synchronized with the cycle of MFSD unit. Here, the amplitude value of each period of the induced electromotive force generated in pickup coil was at the position where pickup coil was closest to the sample, and the minimum value was at the position where pickup coil was farthest to the sample. The change in the permeability of the sample due to the change in its temperature could be expressed as the amplitude value of pickup voltage. The amplitude value of

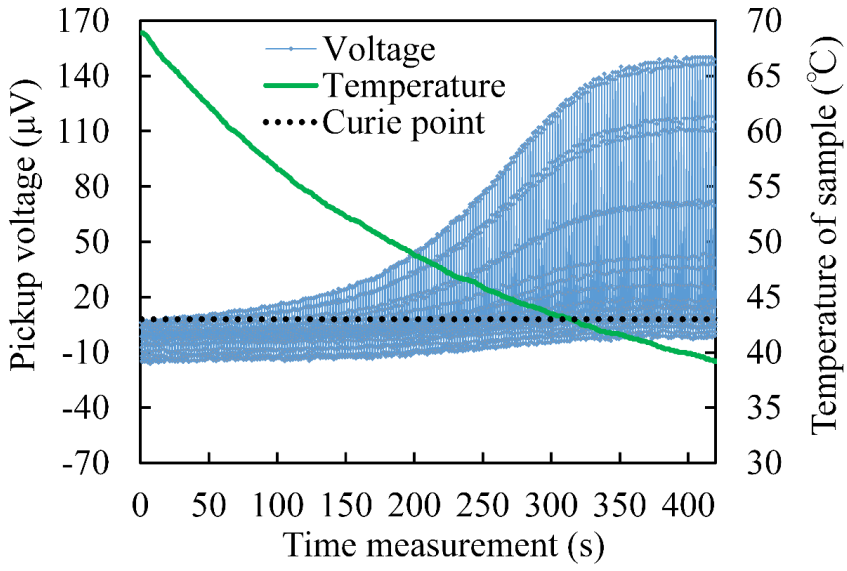

Fig. 5-5 Temporal change in pickup voltage and temperature of sample (without artifact).

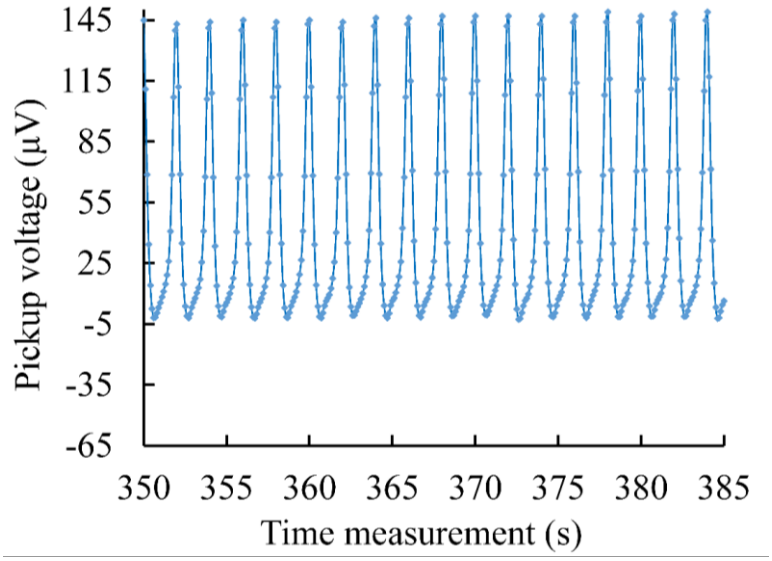

Fig. 5-6 A partial waveform (Fig. 5-5) of the temporal change of pickup voltage.

pickup voltage obtained changed clearly around the Curie point, and it is possible to detect whether the temperature of the implant has reached Curie point from the change in the amplitude value of pickup voltage.

Figure 5-7 shows the temporal change in pickup voltage and the temperature of the sample when MFSD unit was spirally rotated. It was confirmed that when the temperature of the sample heated to 70°C beforehand decreased below the Curie point, pickup voltage synchronized with the period of rotational scanning was influenced by the artifacts, resulting in the high disturbance in the amplitude value. Figure 5-8 shows the partial waveform in the range from 350s to 385s of Figure 5-7. It was confirmed that the signal synchronized with the rotary scan was buried in the noise due to the artifact when vertical motion simulating the artifact was added.

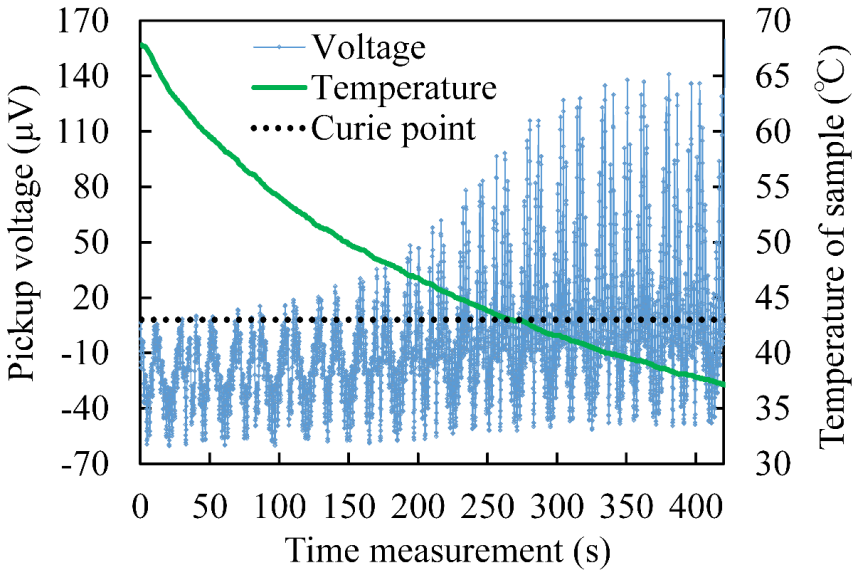

Fig. 5-7 Temporal change in pickup voltage and temperature of sample (with artifact).

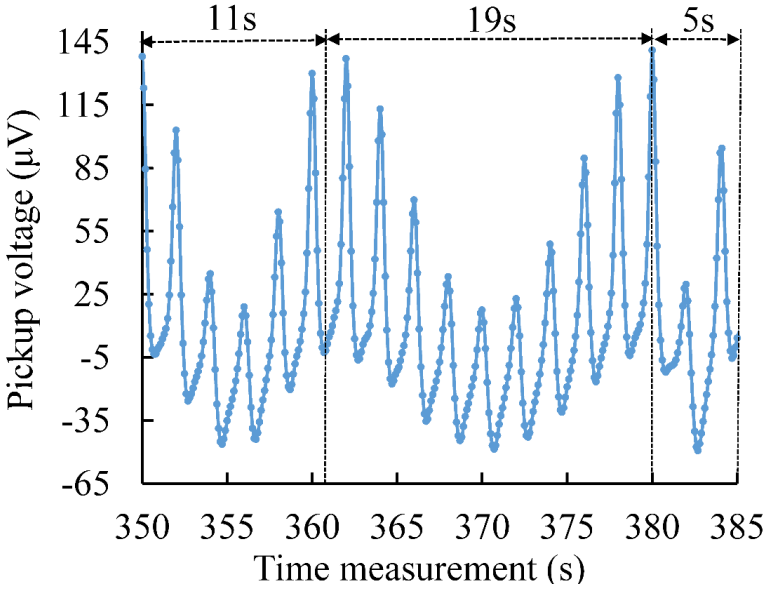

Fig. 5-8 A partial waveform (Fig. 5-7) of the temporal change of pickup voltage.

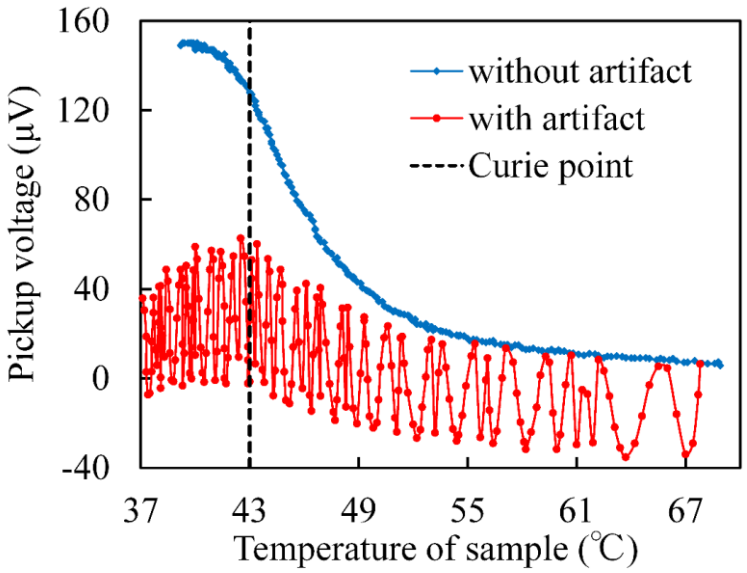

Fig. 5-9 Relationship between pickup voltage and the temperature without rotary scanning.

The relationship between pickup voltage which was extracted from the result in Figs. 5-5 and 5-7 at intervals of rotary scan cycle (2s) and the temperature of the sample are plotted in Figure 5-9. In the case without the artifact, pickup voltage obtained changed clearly around Curie point, and it was possible to detect whether or not the implant has reached Curie point from the change in the voltage around Curie point. On the other hand, the voltage was greatly disturbed in the case with the artifact, and it was not possible to detect the temperature of the implant. Therefore, an analysis method to extract only spectrum component synchronized with rotary scanning is necessary to reduce the effect of the artifact.

➢ Power spectrum analysis

In order to investigate the change in the power of the spectrum synchronized with the rotary scanning with respect to the temperature of the sample, pickup voltage obtained was divided into frame lengths of N = 2^n points for Fast Fourier Transform while shifting at M points interval (M < N), the power spectrum was analyzed. Figure 5-10 shows a conceptual diagram of frame movement for power spectrum analysis using the waveform in the case with the artifact. The overlap amount between adjacent frames was given by the following equation.

$$overlap = \frac{N - M}{N} \times 100\%$$

Before the implement of Fast Fourier Transform, each frame was applied with moving average (L = 5 points), then the frame was applied by Hanning window to suppress the harmonic components due to sudden changes near both ends of the frame. The frequency characteristic (cut-off frequency) of simple moving average is given by the following equation.

$$fc = 0.443 \times \frac{fs}{L}$$

where f_c is cut-off frequency, L is moving average point and f_s is the sampling frequency.

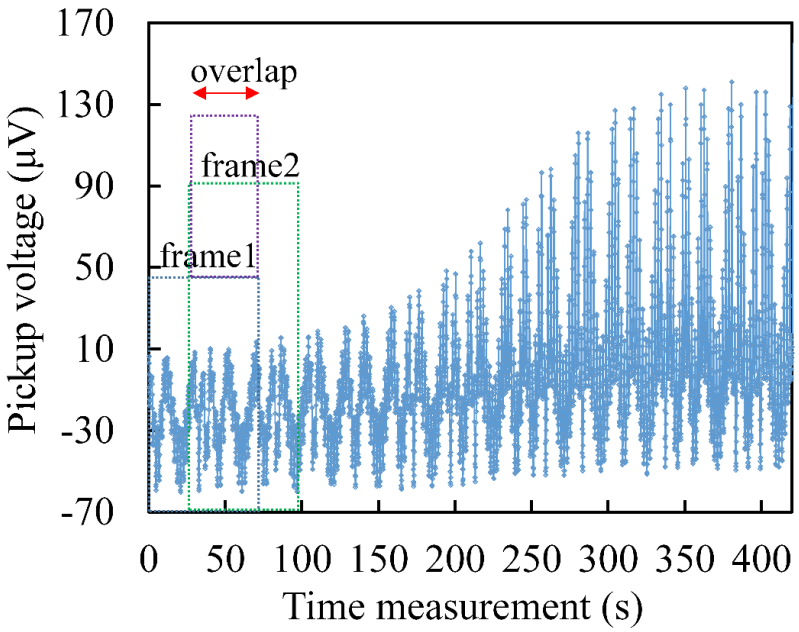

Fig. 5-10 Conceptual diagram of power spectrum analysis.

Figure 5-11 shows the relationship between the power of the frequency of 0 to 1 Hz and the temperature of the sample in the case of each frame N = 2^9 = 512 points (51.2s) and M = 32 points (3.2s, overlap 93.75%). Fig. 5-11(a) shows the case without the artifact, whereas Fig. 5-11(b) shows the case with artifact. The horizontal axis represents the frequency, the vertical axis represents the power of each frequency, and the depth axis represents the temperature of the sample. The direct-current component (0 Hz), the harmonic

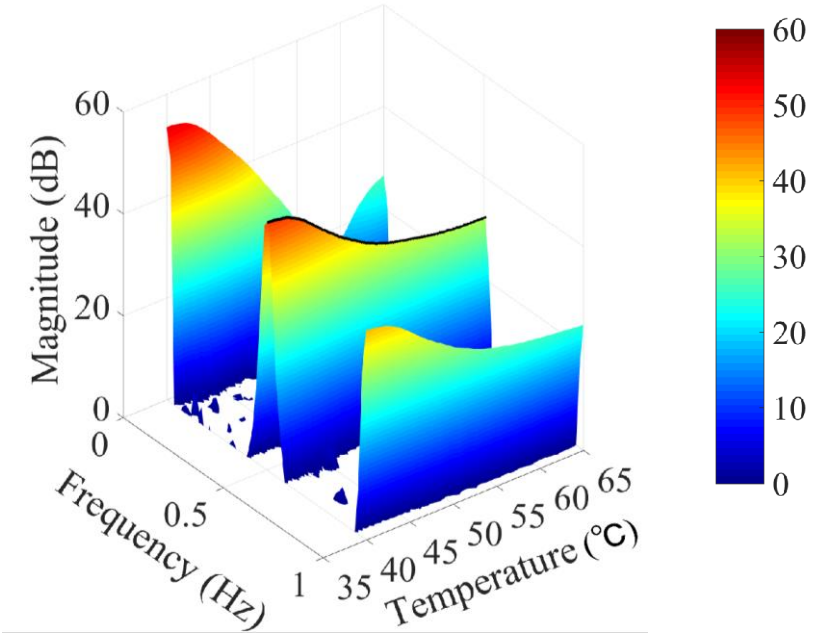

(a) Without the artifact

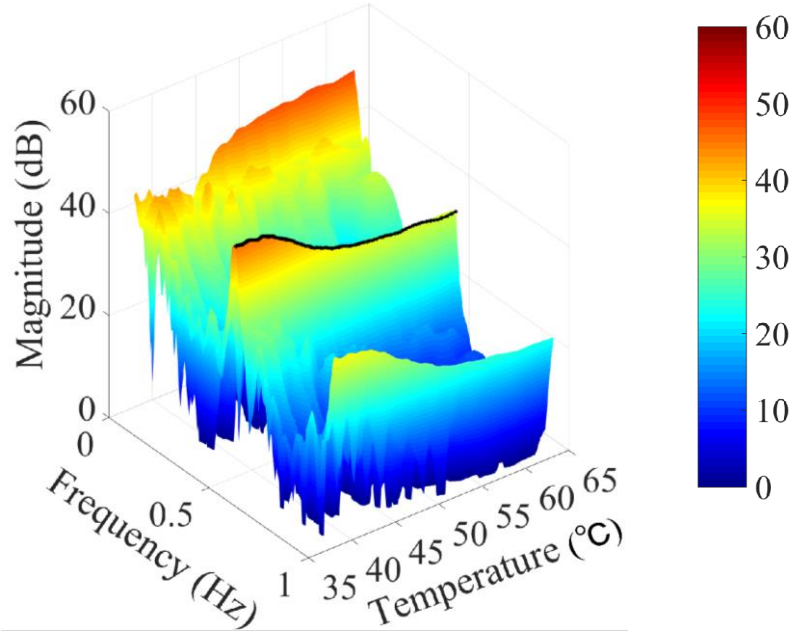

(b) With the artifact

Fig. 5-11 Change in the power of each frequency component due to the temperature of the sample (black solid line shows the relationship between the power of 0.5 Hz and the temperature).

component (0.5 Hz × 2 = 1 Hz), and the 0.5 Hz component (black solid line) synchronized with the rotary scanning were confirmed. Also, it was confirmed that the superimposition of the frequency component simulating the artifact as shown in Fig. 5-11(b).

Figure 5-12 shows the relationship between the power spectrum synchronized with rotary scanning (0.5 Hz) and the temperature of the sample which was extracted from Fig. 5-11. The result indicates that regardless of the presence or absence of the artifact, it was confirmed that the power greatly changed around Curie point. However, the change in the power around Curie point decreased due to the influence of the artifact compared to that of the case without the artifact. It was considered that it is possible to detect whether the implant has reached Curie point from the change in the power synchronized with rotary scanning. Therefore, even if the periodic physiological motion artifacts such as respiration or heartbeat occur, by focusing on only spectrum component synchronized with rotary scanning the influence of the artifacts can be reduced.

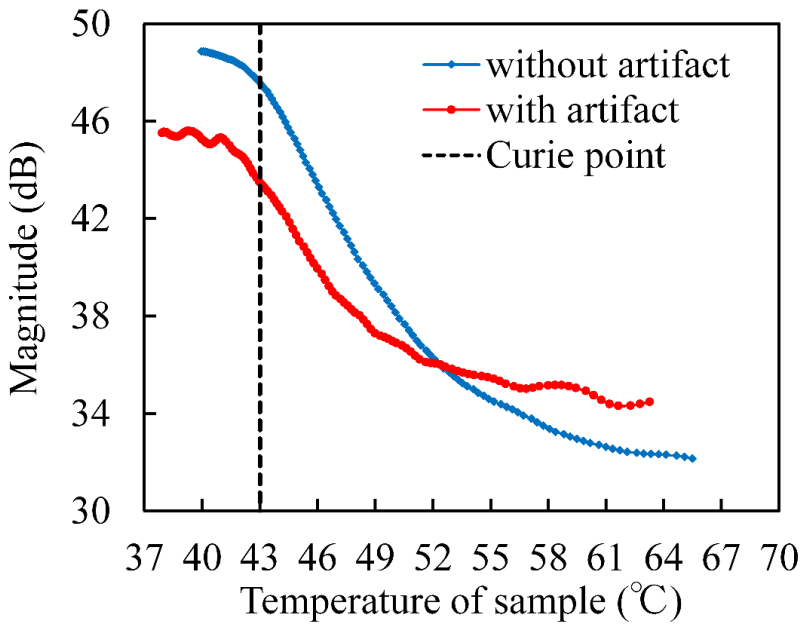

Fig. 5-12 Relationship between the power spectrum of rotary scanning and the temperature of the sample.

➢ Quantitative evaluation method

Next, we quantitatively evaluated the conventional method (Fig. 5-9) and the proposed method (Fig. 5-12) using signal to noise ratio index. Here, signal was the change in the maximum value and the minimum value of the cubic approximation curve of the voltage versus temperature in the range of 40–50°C, noise was the maximum value of the absolute value of the difference between the measured value and the approximate value, the SN ratio of the pickup voltage in the conventional method was represented by the following equation.

$$SNR = 10 \times \log_{10}\left(\frac{Signal^2}{Noise^2}\right)$$

Similarly, the SN ratio by the proposed method of the power versus temperature (Fig. 5-12) was calculated. Figure 5-13 shows the average value of SN ratios in the conventional method and the proposed method (n = 5). Here, the frame length for fast Fourier transform was set to 6.4 s, 12.8 s, 25.6 s, 51.2 s, and 102.4 s (overlap 93.75% in all frames) to examine the influence of frame length on the power versus temperature. It was confirmed that the SN ratio improves with the proposed method compared to the conventional method, regardless of presence or absence of the artifact. In particular, in the case of the artifact the SN ratio was –3.1 dB in the conventional method, whereas in the proposed method the SN ratios were 7.7, 9.2, 18.5, 30.4 and 38.7 dB which were improved by increasing the frame length, thereby the influence of body movement could be also reduced. The longer the measured waveform (frame length) was from the period of the target signal in Fourier transform, the higher the frequency resolution (sampling frequency/N) can be improved, and the spectrum can be extracted with high accuracy. However, the disadvantage was that the longer time required for collection and calculation of the data. In our system that needs real time detection for temperature control, the delay time should be as short as possible.

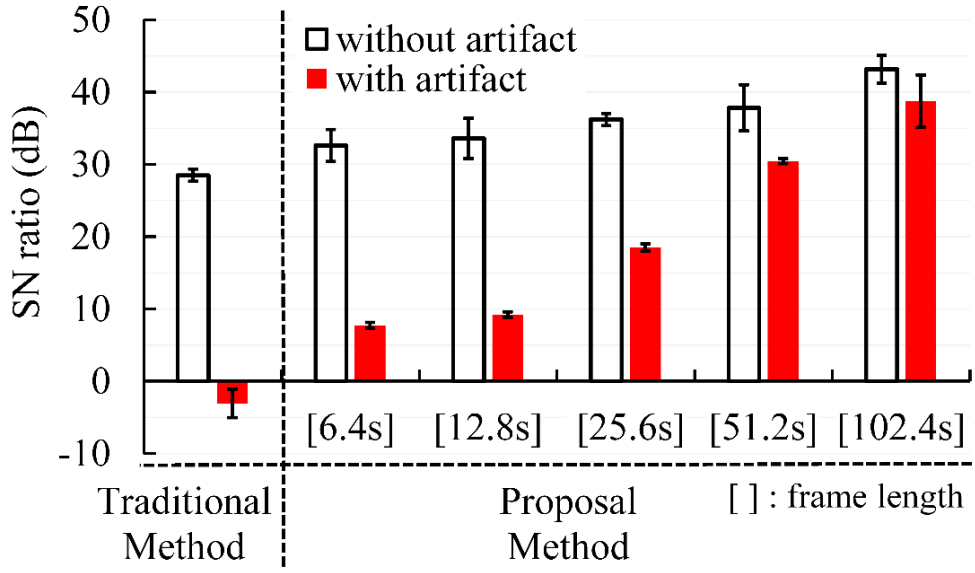

Fig. 5-13 The SN ratio of traditional method and rotary scanning method (n=5).

5.6 Summary

In this chapter, in order to reduce the effects of periodic physiological motion artifact such as respiration and heartbeat, we proposed the rotary scanning technique and validated the proposed method using the constructed system. In this method, MFSD unit is circularly scanned in a different period cycle from the motion artifacts, the spectrum component synchronized with the rotary scanning and the spectrum components of the motion artifacts are separated by Fourier transform, and only the target component (signal) is extracted for temperature measurement. From the result obtained, a clear change in the amplitude of pickup voltage around Curie point that it was possible to detect whether or not the temperature of the implant has reached Curie point. On the other hand, in the case with the artifact, pickup voltage was greatly disturbed, and it was not possible to detect the temperature. After extracting only the target signal (i.e. power spectrum synchronized with the rotary scanning), it was possible to detect the temperature even if the periodic physiological motion artifacts such as respiration or heartbeat occurred. Furthermore, it was confirmed that the SN ratio for temperature measurement was significantly improved with the proposed method compared to the conventional method, regardless of presence or absence of the artifact. Also, the SN ratio improved as the frame length increased.

Chapter 6

Conclusions and future works

6.1 Conclusions

Magnetic hyperthermia is a promising cancer therapy which has been gaining more attention in recent years owing to fewer side effects compared to chemotherapy and less invasive than surgical therapy. In previous studies, we succeeded in developing a microsize thermosensitive ferromagnetic implant with low Curie temperature (FILCT) as a self-controlled heating element and coating it for improving its heating efficiency (Au-FILCT). Furthermore, a wireless temperature measurement method has been proposed for monitoring the temperature of the tumor by using the thermosensitive implant as a thermal probe.

There are still challenges remaining to make our system feasible in clinical settings. Firstly, due to the gold coating layer a part of the applied magnetic field was shielded ascribed to the conductive coating around FILCT. As a result, the change in the detected pickup voltage induced in pickup coil was reduced by half, thereby the accuracy of the proposed wireless temperature measurement was significantly lowered compared to that of FILCT. Secondly, in the case that the implant deviates from the central axis of the magnetic field supply and detection unit composed of drive coil and pickup coil the magnetic flux density applied on the implant decreases, it results in a decrease in its heating efficiency as well as the accuracy of the proposed wireless temperature measurement. Thirdly, due to the periodic physiological motions such as respiration and heartbeat during treatment, it could not distinguish whether the change in pickup voltage was caused by the change in the temperature of the implant around therapeutic temperature, or by the change in distance between MFSD unit and the implant by the artifact.

In this study, we proposed solutions for the three problems above as below.

(1) Development of hyperthermia implant with high heating efficiency and high permeability

As an alternative approach to the gold coating, we proposed to mix FILCT with a high heating-efficient magnetic nanofluid. In the case of using a commercial nanofluid named Resovist® (MRI contrast agent) consisting of maghemite particles with average diameter of 3.6 nm, the heating efficiency of the proposed mixture of micro/nano-magnetic particles was improved 4.3 times, and the accuracy of the thermometry was improved 1.3 times compared to that of FILCT under a magnetic field of 500 kHz, 4.95 kA/m. A similar tendency was obtained when using a lab-made nanofluid consisting of magnetite particles with average diameter of 13.9 nm. Furthermore, the results also suggest that by mixing magnetic nanoparticles in Resovist® with FILCT at a volume fraction of nanoparticles of 0.5%, the resulting mixture will have high heating efficiency and permeability besides being easily controllable around the therapeutic temperature. We hypothesized that the magnetic nanoparticles in Resovist® can fill the gaps between the magnetic

microparticles in FILCT, thereby reducing the demagnetizing field of magnetic microparticles, thus improving the permeability of FILCT in the mixture.

(2) Development of localization technique of hyperthermia implant

To localize the position of the implant, we devised a position adjustment method in which the central axis is aligned directly above the implant by referring to three voltages induced in three pickup coils symmetrically installed inside drive coil. Using the constructed position adjustment system, it was possible to automatically locate the position of the implant with accuracy below 1 mm by operating MFSD unit in two modes of coarse adjustment (rotary scanning) and fine adjustment (linear scanning).

(3) Development of rotary scanning technique of body motion artifact reduction method

To overcome the periodic physiological motions such as respiration and heartbeat induced artifact during treatment, we proposed an artifact reduction method by using rotary scanning technique on MFSD unit in a different period cycle from the periodic respiration and heartbeat. We utilized the difference in the frequency domain of spectral component of rotary scanning (signal) and that of the artifact (noise), and extracted only the target signal needed for temperature measurement. Using the constructed verification system, we confirmed that regardless of the presence of the artifact, the change of the extracted power around the Curie point is sufficiently large to detect whether the temperature of the implant has reached the therapeutic temperature. In particular, in the case with the artifact the SN for temperature measurement was –3.1 dB, whereas the SN after reducing the artifact using the proposed method was enhanced significantly 38.7 dB, which was sufficient to estimate the temperature of the implant.

With the proposed implant and techniques above, the signal detected from pickup coil can be enhanced significantly, thereby increasing the treatable depth through our treatment system.

6.2 Future work

At present, using our constructed treatment system, it is possible to treat the tumor up to 5 cm from the body surface. However, to extend the treatable distance for deeper tumor, the optimal design of pickup coils and drive coil, the clarification of heating mechanism in micro/nanomagnetic particles, and the construction of automatic temperature control technique are needed.

Acknowledgements

First and foremost, I would like to thank my supervisor Professor Kazutaka Mitobe for his continuous guidance and encouragements during my research from bachelor to doctor degree.

My special thanks to the dissertation committee members: Professor Yoichi Kageyama, Professor Masatoshi Arikawa for their insightful comments and suggestions.

I would like to thank Associate Professor Yoshiyuki Yamamoto for his assistances in various experiments in his laboratory and insightful advices in magnetic material area.

I am deeply grateful to Professor Hajime Saito, Iwate Medical University for his helpful advices in medical area and allowing me to observe cancer surgery at hospital.

I would like to show my appreciation to Professor Yasushi Takemura, Yokohama National University for his helpful advices and assistances in various experiments in his laboratory.

I would also like to express my gratitude to the staffs of Mitobe laboratory: Lecturer Katsuya Fujiwara, Assistant Professor Sawako Nakajima, and Technical Specialist Masachika Saito for their numerous supports, as well as the present and past members in the laboratory for their assistance.

I am indebted to Japan Society for Promotion Science (JSPS) for financial support as a JSPS Research Fellowship for Young Scientist DC1. This study was supported in part by JSPS KAKENHI Numbers 16J09640, 15K01277 and 18H03545.

Finally, I would like to show my appreciation to my family for their continuous support and encouragement.

References

[1] World Health Organization, “Cancer” http://www.who.int/en/news-room/fact-sheets/detail/cancer (accessed Nov. 19, 2018)

[2] Ministry of Health, Labour and Welfare Japan, “Summary Report of Vital Statics of Japan 2017” https://www.mhlw.go.jp/toukei/saikin/hw/jinkou/geppo/nengai17/dl/kekka.pdf (accessed Nov. 19, 2018)

[3] G. Eduardo, “Physics of Thermal Therapy: Fundamentals and Clinical Applications,” 1st ed., CRC Press, pp. 139–158, 2012.

[4] H. Matsuki, K. Murakami, and H. Niizuma, “Soft Heating – A New Method of Heating Using Temperature-Sensitive Magnetic Materials,” *IEEE Trans. Magn.*, Vol. 18, No. 6, pp. 1788–1790, 1982.

[5] R.K. Gilchrist *et al.*, “Selective inductive heating of lymph nodes,” *Ann. Surg.*, Vol. 146, No. 4, pp. 596–606, 1957.

[6] H. Saito *et al.*, “Self-regulating hyperthermia induced using thermosensitive ferromagnetic material having a low Curie temperature,” *Cancer Science*, Vol. 99, pp. 805–809, 2008.

[7] A. Ito *et al.*, “Inhibition of heat shock protein 90 sensitizes melanoma cells to thermosensitive ferromagnetic particle-mediated hyperthermia with low Curie temperature,” *Cancer Science*, Vol. 100, pp. 558–564, 2009.

[8] T. Miyagawa *et al.*, “Inhibition of Hsp90 and 70 sensitizes melanoma cells to hyperthermia using ferromagnetic particles with a low Curie temperature,” *Int. J. Clin. Oncol.*, Vol. 19, No. 4, pp. 722–730, 2014.

[9] K. Mitobe and N. Yoshimura, “Low-invasive Heating and Temperature Measurement Method for Hyperthermia Treatment using The Metal Coated Ferromagnetic Implant with Low Curie Temperature,” *Proc. of Biodevices 2011*, pp. 341–344, 2011.

[10] K. Mitobe and N. Yoshimura, “Noninvasive Temperature Measurement Method for Hyperthermia Treatment using Ferromagnetic Implant with Low Curie Temperature,” *Proc. of 30th Annu. Inter. Conf. IEEE EMBS*, pp. 4384–4386, 2008.

[11] Japanese Society for Thermal Medicine, “Haipasamia gan onnetsuryoho gaidobukku,” 1st ed., Mainichi Kenko Salon, pp. 154–175, 2008.

[12] A. Ito *et al.*, “Medical Application of Functionalized Magnetic Nanoparticles,” *Journal of Bioscience and Bioengineering*, Vol. 100, No. 1, pp. 1–11, 2005.

[13] U. Jeong *et al.*, “Superparamagnetic colloids: Controlled synthesis and niche applications,” *Adv. Mater.*, Vol. 19, pp. 33–60, 2007.

[14] W. J. Minkowycz *et al.*, "Nanoparticle Heat Transfer and Fluid Flow," CRC Press, pp. 97–122, 2012.

[15] R. Rosensweig, "Heating magnetic fluid with alternating magnetic field," *J. Magn. Magn. Mater.*, Vol. 252, pp. 370–374, 2002.

[16] R. Miyamoto *et al.*, "Accuracy improvement of low-invasive temperature measurement for hyperthermia treatment using ferromagnetic implant with low curie temperature," *IEEJ Trans FM.*, Vol. 134, pp. 436–441, 2014.

[17] F. Aki *et al.*, "Examination of the Influence on Precision of the Wireless Temperature Measurement Induction Heating System by 37°C Constant Temperature Environment," *IEEJ Trans. Fund. Mater.*, Vol. 54, No. 6, pp. 2800303-1–2800303-3, 2018.

[18] F. Aki *et al.*, "Study of wireless temperature measurement induction heating system using magnetic properties of au-coated ferromagnetic implant with low curie temperature," *Electron Comm Jpn.*, Vol. 101, pp. 58–66, 2018.

[19] F. Aki *et al.*, "Study on Wireless Temperature Measurement Induction Heating System using Magnetic Properties of Mixture of Resovist® and Ferromagnetic Implant with Low Curie Temperature," *IEEJ Trans. Fund. Mater.*, Vol. 139, No. 1, pp. 38–44, 2019.

[20] S. Dutz and R. Hergt, "Magnetic particle hyperthermia – a promising tumour therapy?," *Nanotechnology*, Vol. 25, No. 45, pp. 1–28, 2014.

[21] T. Sasayama *et al.*, "Three-dimensional magnetic nanoparticle imaging using small field gradient and multiple pickup coils," *J. Magn. Magn. Mater.*, Vol. 427, pp. 143–149, 2017.

[22] T. Kuboyabu *et al.*, "Magnetic Particle Imaging for Magnetic Hyperthermia Treatment: Visualization and Quantification of the Intratumoral Distribution and Temporal Change of Magnetic Nanoparticles in Vivo," *Open Journal of Medical Imaging*, Vol. 6, No. 1, pp. 1–15, 2016.

[23] H. Nagae *et al.*, "Study on Cancer Treatment using Magnetic Fluid for Medicine and Induction Heating Device," *IEEJ Trans. Fund. Mater.*, Vol. 133, No. 6, pp. 366–371, 2013.

[24] T. Aoto *et al.*, "Specific Loss Power of Magnetic Particles for Hyperthermia Excited by Pancake-type Applicator," *IEEJ Trans. Fund. Mater.*, Vol. 137, No. 8, pp. 476–480, 2017.

[25] L. Tonthat *et al.*, "Thermosensitive Ferromagnetic Implant for Hyperthermia Using a Mixture of Magnetic Micro-/nanoparticles," *IEEE Trans. Magn.*, Vol. 54, No. 7, pp. 5400506-1–5400506-6, 2018.

[26] L. Tonthat *et al.*, "Thermosensitive Implant for Magnetic Hyperthermia by Mixing Micromagnetic and Nanomagnetic Particles," *IEEE Trans. Magn.*, Vol. 54, No. 6, pp. 5400104-1–5400104-4, 2018.

[27] H. Yang *et al.*, "Synthesis and magnetic properties of monodisperse magnetite nanocubes," *J. Appl. Phys.*, Vol. 103, pp. 07D526-1–07D526-3, 2008.

[28] Y. Huh *et al.*, "In Vivo Magnetic Resonance Detection of Cancer by Using Multifunctional Magnetic Nanocrystals," *J. Am. Chem. Soc.*, Vol. 127, No. 35, pp. 12387–12391, 2005.

[29] Y. Yamamoto *et al.*, "Size dependence study on magnetic heating properties of superparamagnetic iron oxide nanoparticles suspension," *J. Appl. Phys.*, Vol. 116, No. 12, pp. 123906-1–123906-7, 2014.

[30] Y. Yamamoto *et al.*, "Effects of coating molecules on the magnetic heating properties of Au-Fe_3O_4 heterodimer nanoparticles," *Appl. Phys. Lett.*, Vol. 109, No. 14, pp. 142406-1–142406-4, 2016.

[31] S. Gudoshnikov *et al.*, "Hysteresis losses in a dense superparamagnetic nanoparticle assembly," *AIP Adv.*, Vol. 2, pp. 012143-1–012143-6, 2012.

[32] S. Gudoshnikov *et al.*, "AC Magnetic Technique to Measure Specific Absorption Rate of Magnetic Nanoparticles," *J. Supercond. Nov. Magn.*, Vol. 26, No. 4, pp. 857–860, 2013.

[33] E. Garaio *et al.*, "A wide-frequency range AC magnetometer to measure the specific absorption rate in nanoparticles for magnetic hyperthermia," *J. Magn. Magn. Mater.*, Vol. 368, pp. 432–437, 2014.

[34] E. Garaio *et al.*, "Harmonic phases of the nanoparticle magnetization: An intrinsic temperature probe," *Appl. Phys. Lett.*, Vol. 107, No. 12, pp. 123103-1–123103-5, 2015.

[35] V. Connord *et al.*, "An air-cooled Litz wire coil for measuring the high frequency hysteresis loops of magnetic samples – A useful setup for magnetic hyperthermia applications," *Rev. Sci. Instrum.*, Vol. 85, No. 9, pp. 093904, 2014.

[36] C. Guibert *et al.*, "Magnetic fluid hyperthermia probed by both calorimetric and dynamic hysteresis measurements," *J. Magn. Magn. Mater.*, Vol. 421, pp. 384–392, 2017.

[37] E. Abenojar *et al.*, "Structural effects on the magnetic hyperthermia properties of iron oxide nanoparticles," *Prog. Nat. Sci. Mat. Int.*, Vol. 26, No. 5, pp. 440–448, 2016.

[38] E. Natividad *et al.*, "Adiabatic vs. non-adiabatic determination of specific absorption rate of ferrofluids," *J. Magn. Magn. Mater.*, Vol. 321, No. 10, pp. 1497–1500, 2009.

[39] Kado *et al.*, "Estimation of Specific Power Loss of Heating Mediator (La-Sr-Mn-Cu perovskite) for Magnetic Hyperthermia under 1 MHz Magnetic Field at Different Temperatures," *J. Magn. Soc. Jpn.*, Vol. 39, pp. 126–129, 2015.

[40] T. Kuboyabu *et al.*, "Magnetic Particle Imaging for Magnetic Hyperthermia Treatment: Visualization and Quantification of the Intratumoral Distribution and Temporal Change of Magnetic Nanoparticles *in Vivo*," *Open Journal of Medical Imaging*, Vol. 6, pp. 1–15, 2016.

[41] Y. Shimada *et al.*, "Enhanced Initial Permeability of Composite Assembly of Ferromagnetic Particles," *J. Magn. Soc. Jpn.*, Vol. 30, pp. 540–544, 2006.

[42] T. Loi *et al.*, "Magnetic Field Dependence of Heating Property of Resovist® for Magnetic Hyperthermia," *IEEJ Trans. Electr. Electron. Eng.*, Vol. 14, No. 4 (in press, available online Dec. 3, 2018).

[43] T. Loi *et al.*, "Position Adjustment Method and Distance Estimation Method of Magnetic Field Supply and Detection Unit for Magnetic Hyperthermia," *IEEJ Trans. Electr. Electron. Eng.*, Vol. 12, No. S2, pp.

S3–S9, 2017.

[44] M. Malik *et al.*, “Heart rate variability. Standards of measurement, physiological interpretation, and clinical use,” *Eur. Heart J.*, Vol. 17, pp. 354–381, 1996.

[45] T. Loi *et al.*, “Rotary Scanning Wireless Temperature Measurement Method for Hyperthermia using Ferromagnetic Implants,” *IEEJ Trans. Electr. Electron. Eng.*, Vol. 10, pp. S1–S6, 2015.

[46] T. Loi *et al.*, “Body Motion Artifact Reduction Method using Rotary Scanning for Accuracy Improvement of Wireless Temperature Measurement,” *IEEJ Trans. Fund. Mater.*, Vol. 136, No. 8, pp. 529–534, 2016.

Achievements

Papers (peer review)

(1) Tonthat, L., Yamamoto, Y., Aki, F., Saito, H. and Mitobe, K.
Magnetic Field Dependence of Heating Property of Resovist® for Magnetic Hyperthermia
IEEJ Transactions on Electrical and Electronic Engineering, Vol. 14, No. 4, pp. 648–649 (2019)

(2) Aki, F., Tonthat, L., Saito, H., Yoshimura, N. and Mitobe, K.
Study on Wireless Temperature Measurement Induction Heating System using Magnetic Properties of Mixture of Resovist® and Ferromagnetic Implant with Low Curie Temperature
IEEJ Transactions on Fundamentals and Materials, Vol. 139, No. 1, pp. 38–44 (2019)

(3) Tonthat, L., Yamamoto, Y., Aki, F., Saito, H. and Mitobe, K.
Thermosensitive Ferromagnetic Implant for Hyperthermia Using a Mixture of Magnetic Micro-/nanoparticles
IEEE Transactions on Magnetics, Vol. 54, No. 7, pp. 5400506-1–5400506-6 (2018)

(4) Aki, F., Tonthat, L., Saito, H. and Mitobe, K.
Examination of the Influence on Precision of the Wireless Temperature Measurement Induction Heating System by 37°C Constant Temperature Environment
IEEE Transactions on Magnetics, Vol. 54, No. 6, pp. 2800303-1–2800303-3 (2018)

(5) Tonthat, L., Yamamoto, Y., Aki, F., Saito, H. and Mitobe, K.
Thermosensitive Implant for Magnetic Hyperthermia by Mixing Micromagnetic and Nanomagnetic Particles
IEEE Transactions on Magnetics, Vol. 54, No. 6, pp. 5400104-1–5400104-4 (2018)

(6) Aki, F., Tonthat, L., Saito, H., Yoshimura, N. and Mitobe, K.
Study of wireless temperature measurement induction heating system using magnetic properties of Au-coated Ferromagnetic Implant with Low Curie Temperature
IEEJ Transactions on Fundamentals and Materials, Vol. 138, No. 3, pp. 76–83 (2018)

(7) Aki, F., Tonthat, L., Saito, H., Yoshimura, N. and Mitobe, K.
Study of wireless temperature measurement induction heating system using magnetic properties of Au-coated Ferromagnetic Implant with Low Curie Temperature
IEEJ Electronics and Communications in Japan, Vol. 101, No. 6, pp. 58–66 (2018)
[English translation of Journal-selected Japanese article (6)]

(8) Tonthat, L., Aki, F., Matsuda, E., Saito, H., Yoshimura, N. and Mitobe, K.
Position Adjustment Method and Distance Estimation Method of Magnetic Field Supply and Detection Unit for Magnetic Hyperthermia

IEEJ Transactions on Electrical and Electronic Engineering, Vol. 12, No. S2, pp. S3–S9 (2017)

(9) Tonthat, L., Aki, F., Matsuda, E., Saito, H., Yoshimura, N. and Mitobe, K.
Body Motion Artifact Reduction Method using Rotary Scanning for Accuracy Improvement of Wireless Temperature Measurement
IEEJ Transactions on Fundamentals and Materials, Vol. 136, No. 8, pp. 529–534 (2016)

(10) Tonthat, L., Saito, H., Miyamoto, R., Suzuki, M., Yoshimura, N. and Mitobe, K.
Rotary Scanning Wireless Temperature Measurement Method for Hyperthermia using Ferromagnetic Implants
IEEJ Transactions on Electrical and Electronic Engineering, Vol. 10, No. S1, pp. S1–S6 (2015)

Patents

(1) 水戸部 一孝，トン タット ロイ，齊藤 元
磁性体の位置探索システム，及び位置探索方法
特開2018-185174（公開日 2018年11月22日）

(2) 水戸部 一孝，トン タット ロイ，山本 良之，齊藤 元
ハイパーサーミア用インプラント
特開2019-523（公開日 2019年1月10日）

International conferences

(1) Tonthat, L., Yamamoto, Y., Aki, F., Saito, H. and Mitobe, K.
Development of Wireless Temperature and Position Monitoring for Magnetic Hyperthermia using Pickup Coils
3rd International Workshop on Magnetic Bio-Sensing (IWMBS 2018), (Yokohama, Japan), (Nov. 5–6 2018)

(2) Tonthat, L., Yamamoto, Y., Saito, H. and Mitobe, K.
Effects of Magnetic Field on Permeability and Heating Properties of Hyperthermia Implant using Micro-/Nano-Magnetic Particles
40th Annual International Conference of the IEEE Engineering in Medicine and Biology Society (EMBC'18), (Hawaii, USA), (Jul. 17–21, 2018)

(3) Tonthat, L., Yamamoto, Y., Aki, F., Saito, H. and Mitobe, K.
Thermosensitive Implant for Magnetic Hyperthermia by Mixing Micromagnetic and Nanomagnetic Particles
4th International Symposium on Advanced Magnetic Materials and Applications (ISAMMA 2017), (Phu Quoc, Vietnam), (Dec. 10–13, 2017) (Papers (5) is a paper related to this conference)

(4) Aki, F., Tonthat, L., Saito, H. and Mitobe, K.

Examination of the Influence on Precision of the Wireless Temperature Measurement Induction Heating System by 37°C Constant Temperature Environment
4th International Symposium on Advanced Magnetic Materials and Applications (ISAMMA 2017), (Phu Quoc, Vietnam), (Dec. 10–13, 2017) (Papers (4) is a paper related to this conference)

(5) Tonthat, L., Yamamoto, Y., Aki, F., Saito, H. and Mitobe, K.
Improvement of Heating Efficiency and Magnetization Property of Ferromagnetic Implant with Low Curie Temperature for Hyperthermia using Nano-Magnetic Fluid
8th International Conference on Materials Engineering for Resources (ICMR 2017 AKITA), (Akita, Japan), (Oct. 25–27, 2017)

(6) Tonthat, L., Aki, F., Saito, H. and Mitobe, K.
Position Adjustment Method of Magnetic Field Supply and Detection Unit for Magnetic Hyperthermia using Ferromagnetic Implant
39th Annual International Conference of the IEEE Engineering in Medicine and Biology Society (EMBC'17), (Jeju Island, Korea), (Jul. 11–15, 2017)

(7) Tonthat, L., Saito, H. and Mitobe, K.
Study on Shortening Latency in Body Motion Artifact Reduction Method for Accuracy Improvement of Wireless Temperature Measurement by using Symmetrical Multi-pickup coils
International Conference on Electrical Engineering 2016 (ICEE2016), (Okinawa, Japan), (Jul. 3–7 2016)

(8) Aki, F., Saito, H., Tonthat, L., Matsuda, E. and Mitobe K.
Study of Induction Heating Approach with Wireless Temperature Measurement Technique for Hyperthermia
International Conference on Electrical Engineering 2016 (ICEE2016), (Okinawa, Japan), (Jul. 3–7 2016)

(9) Mitobe, K., Miyamoto, R., Tonthat, L., Aki, F. and Saito, H.
Noise suppression method for Wireless Temperature Measurement for Hyperthermia Treatment using FILCT
7th Biomedical Engineering International Conference (BMEiCON), (Fukuoka, Japan), (Nov. 26–28 2014)

Internal conferences

(1) トンタットロイ，高野 渚，安藝 史崇，齊藤 元，水戸部 一孝
ハイパーサーミア用感温性磁性体の検知可能距離延伸のための磁場印加検知ユニットの検討
第57回日本生体医工学会大会，（札幌，日本），（2018年6月19～21日）

(2) Tonthat, L., Yamamoto, Y., Aki, F., Saito, H. and Mitobe, K.
Magnetic Hyperthermia Implant: A Mixture of Micro/Nano Magnetic Particles

第51回日本生体医工学会東北支部大会，（秋田，日本），（2017年12月2日）

(3) 松田 瑛生，安藝 史崇，トンタットロイ，齋藤 元，水戸部 一孝
ハイパーサーミアのためのワイヤレス温度計測技術を用いた自動定温加熱制御システムの開発
第55回日本生体医工学会大会，（富山，日本），（2016年4月26～28日）

(4) トンタットロイ，齊藤 元，水戸部 一孝
ハイパーサーミア用ワイヤレス温度計測技術の精度向上のための回転走査による体動アーチファクト低減法
平成27年度情報処理学会東北支部研究会，（秋田，日本），（2015年12月1～2日）

(5) トンタットロイ，齊藤 元，鈴木 雅史，吉村 昇，水戸部 一孝
感温磁性体を利用したハイパーサーミアのための回転走査によるワイヤレス温度計測技術の精度向上
第29センサ工学研究会，（秋田，日本），（2015年9月28～29日）

(6) 安藝 史崇，トンタットロイ，松田 瑛生，齊藤 元，水戸部 一孝
感温磁性体を用いたハイパーサーミアにおける ワイヤレス温度計測技術のバイアス低減手法の提案
電気学会医用・生体工学研究会，（東京，日本），（2015年3月27日）

(7) Tonthat, L., Saito, H., Miyamoto, R., Suzuki, M., Yoshimura, N. and Mitobe K.
Accuracy Improvement of Wireless Temperature Measurement Technique by Rotary Scan for Hyperthermia using Ferromagnetic Implant
53rd Annual Conference of Japanese Society for Medical and Biological Engineering, (Sendai, Japan), (Jun. 24–26, 2014)

Awards

(1) 3rd International Workshop on Magnetic Bio-Sensing「Poster Presentation Award」, 2018年11月6日授与

(2) 平成29年度電気学会（東北支部）「優秀論文賞」，2018年4月17日授与

(3) 平成29年度秋田大学学生表彰「奨励賞（学術研究活動関係）」，2018年3月15日授与

(4) 第8回素材物性学国際会議「優秀論文賞」，2017年10月27日授与

(5) 平成30年度秋田大学学生表彰「優秀賞（学術研究活動関係）」，2019年3月18日授与

(6) 第57回日本生体医工学会大会「研究奨励賞・阿部賞」，2019年1月8日ノミネート，最終選考中